Cell Cycle Specific Recruitment of PKCε

Victoria Marian Crossland

University College London

and

Cancer Research UK London Research Institute

PhD Supervisor: Professor Peter Parker

A thesis submitted for the degree of

Doctor of Philosophy

University College London

July 2012

Declaration

I, Victoria Marian Crossland, confirm that the work presented in this thesis is my own. Where information has been derived from other sources, I confirm that this has been indicated in the thesis.

Abstract

Protein kinase C (PKC) comprises a family of serine/threonine kinases which play central roles in intracellular signal transduction typically triggered by recruitment to membraneous compartments. The epsilon isoform of PKC (PKCε) has been shown to localize to cell-cell contacts and to the cytokinetic furrow/midbody, indicative of a role in the cell cycle. Both recruitment patterns can be visualized under conditions of PKCε inhibition, which is selectively achieved using a gatekeeper mutant (PKCε-M486A) and the inhibitor NaPP1. Initial studies indicated that interphase and mitotic cells were not distinguished in their capacity for PKCε-M486A recruitment as evidenced by optical trapping experiments. I therefore assessed whether recruitment to the furrow/midbody is a general property reflecting the juxtaposition of two membranes and a cell-cell contact response. I have successfully used fluorescence recovery after photobleaching (FRAP) to distinguish between the localization at the furrow/midbody from that at cell-cell contacts by measuring PKCε-M486A turnover at these two compartments. It is demonstrated that PKCε-M486A has a slower turnover at the furrow/midbody.

The distinct kinetic behaviour of PKCε M486A at the furrow/midbody is indicative of other factors contributing to recruitment and/or retention. Sites and domains within PKCε-M486A were therefore assessed for their involvement in this process using a combination of mutagenesis and confocal microscopy. Through these studies I have identified a short motif in the regulatory domain of PKCε-M486A, the inter C1 domain (IC1D), that is in part required for the accumulation of PKCε-M486A at the furrow/midbody. The deletion of this domain (PKCε-ΔIC1D-M486A) prevents the kinase being recruited to the furrow/midbody despite, the recruitment and furrow/midbody localization of the co-expressed PKCε-M486A.

Given that the IC1D was previously identified as an actin-binding region, I have assessed the relationship between actin and PKCε-M486A recruitment by manipulating actin polymerization. Using latrunculinA, an inhibitor of F-actin assembly, I have shown that PKCε-M86A and RhoA colocalize and are stabilized in the same

compartment in conditions where F-actin is depolymerized. Importantly, the behaviour is observed for both active and inactive PKCε-M486A. This condition may be analogous to a stage in midbody biogenesis and may be evidence of the requirement of F-actin for normal PKCε and RhoA behaviour in cytokinesis.

These data show some progress towards understanding the unique behaviour of PKCε at the furrow/midbody and indicate a complex relationship between PKCε, actin and RhoA.

Acknowledgement

In my time at CRUK, I have had the privilege of working with some exceptional scientists, none more so than my supervisor, Peter Parker and so I wish to take this opportunity to express my sincerest thanks.

Peter, I am so very grateful for everything you have done for me and I can't thank you enough. As for Nicola Brownlow, you quite simply rock my world. To the other members of the Parker lab, thank you for making this experience an enjoyable one and to Fred Bollet-Quivogne, thank you for making frapping (almost) fun.

Finally, I dedicate this thesis to my parents, I love you both very much.

Table of Contents

Table of figures

List of tables

Abbreviations

Amino Acids

A	Alanine
D	Aspartic acid
E	Glutamic acid
G	Glycine
M	Methionine
R	Arginine
S	Serine

Ala	Alanine
Asp	Aspartic acid
Cys	Cysteine
His	Histidine
Lys	Lysine
Ser	Serine
Thr	Threonine
Tyr	Tyrosine
Trp	Tryptophan

APC/C	Anaphase-promoting complex
ATP	Adenosine triphosphate
BIM1	Bisindolylmaleimide-1
BSA	Bovine serum albumin
Cdc	Cell division cycle
Cdk	Cyclin dependent kinase
CPC	Chromosomal passenger complex
DAG	Diacylglycerol
DAP1	Diamidino-2-phenylindole
DMEM	Dulbecco's modified eagle medium
DNA	Deoxyribonucleic acid
DTT	Dithiothreitol
Ect2	Epithelial cell-transforming sequence 2
EGTA	Ethylene glycol tetraacetic acid
EtOH	Ethanol
F-actin	Filamentous actin
FCS	Foetal-calf serum
FIP3	Rab11-family interacting protein 3
FRAP	Fluorescence recovery after photobleaching

G1	Gap phase 1
G2	Gap phase 2
G-actin	Globular actin
GAP	GTPase activating protein
GDP	Guanosine diphosphate
GEF	Guanine nucleotide exchange factor
GFP	Green fluorescent protein
GTP	Guanosine triphosphate
H2B	Histone 2B
IC1D	Inter-C1 domain
latA	Latrunculin A
LB	Lysogeny broth
M	Mitosis
mDia	Mammalian homologues of Drosophila diaphanous
MeOH	Methanol
MgcRacGAP	Male germ cell Rac GTPase-activating protein
MKLP1	Mitotic kinesin-like protein
MOPS	3-(N-morpholino) propanesulfonic acid
mTOR	Mammalian target of rapamycin

NaPP1	4-amino-1-tert-butyl-3-(1'natphthyl)-pyrazolo[3,4-d] pyrimidine
PB1	Phox/Bem1
PH	Pleckstrin homology
Pdk1	3-phosphoinositide-dependent protein kinase-1
PI3K	Phosphatidylinositol 3-kinase
PIP_2	Phosphatidylinositol 4,5 bisphosphate
PKC	Protein Kinase C
aPKC	Atypical Protein Kinase C
cPKC	Conventional Protein Kinase C
nPKC	Novel Protein Kinase C
PKCε	Protein Kinase C epsilon
Plk1	Polo-like kinase 1
PMA	Phorbol 12-myristate 13 acetate
PI-PLC	Phosphatidylinositol-specific phospholipase C
Prc1	Protein regulator of cytokinesis 1
PS	Phosphatidylserine
Rb	Retinoblastoma
RFP	Red fluorescent protein
S	DNA synthesis

SAC	Spindle assembly checkpoint
SDS	Sodium dodecyl sulfate
TGN	Trans-golgi network
Tris	Tris(hydroxymethyl)aminomethane
WT	Wild-type

Chapter 1. Introduction

1.1 The Cell Cycle and Cancer

Human development from a single-cell zygote to a fertile adult, consisting of approximately 100,000 billion cells, requires many rounds of cell division, as does the continued renewal of many parts of the mature adult. While the formal definition of cell division came in 1855 with Rudolph Virchow's aphorism *"omnis cellula e cellula"* (every cell from a pre-existing cell) it is only during the last four decades that a molecular mechanism has emerged. During each division cells complete an ordered series of events, known collectively as the cell cycle (Figure 1.1), which consists of four distinct phases; a DNA synthesis (S) phase and a mitotic (M) phase separated by two 'gap' phases (G1 and G2). M is further subdivided into nuclear division (mitosis) and cytoplasmic division (cytokinesis). It is essential that the different phases of the cell cycle are precisely coordinated. The phases must follow in sequential order and one phase must be completed before the next phase can begin. Errors in coordination are associated with many human diseases, in particular inappropriate proliferation has been identified as one of the hallmarks of cancer (Hanahan and Weinberg, 2000, Hanahan and Weinberg, 2011). It is therefore not surprising that the cell cycle has become an active area of drug discovery.

Progression through the cell cycle is complex but tightly regulated by protein kinases in particular cyclin-dependent kinases (Cdks). Cdks are a family of small Ser/Thr kinases whose periodic activation is driven by forming bipartite complexes with different cyclins (reviewed in Suryadinata et al., 2010). When active, these complexes function by phosphorylating a multitude of downstream transducers that act on various components of the cell cycle apparatus. In *Schizosaccharomyces pombe* and *Saccharomyces cerevisiae* cell division cycles (Cdcs) are regulated by only a single Cdk, $p34^{cdc2}$ and Cdc28 respectively, coupled with several different cyclins that are expressed at different cell cycle phases. Higher eukaryotes also use a variety of different cyclins but in contrast, possess multiple Cdks.

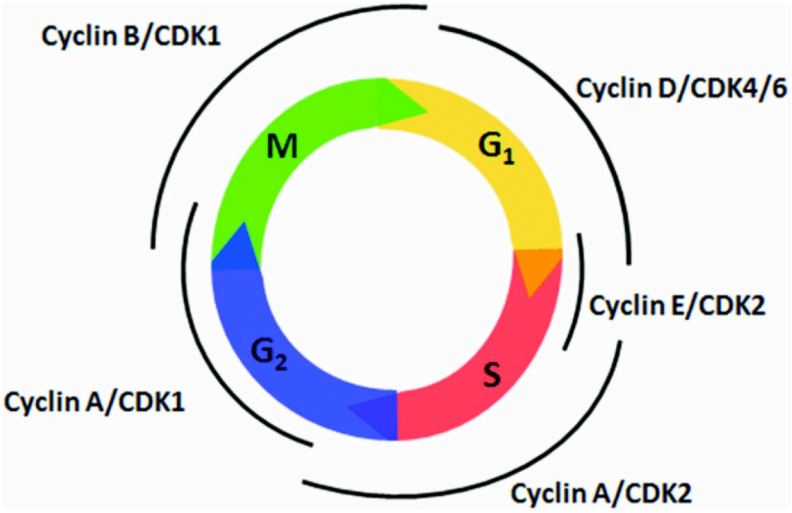

Figure 1-1 Progression through the mammalian cell cycle.
(Reproduced with permission from Suryadinata et al., 2010, Bioscience Reports, 30, p243-55, © the Biochemical Society). The cell cycle consists of four distinct phases; G1, S (DNA synthesis), G2 (together known as interphase) and M (mitosis/cytokinesis). Different cyclin-Cdk complexes regulate the progression of cells through the different phases.

Mammalian cell culture studies have led to the simplified but dogmatically accepted view that cyclin D-Cdk4/6 complexes are activated and important for progression during G1 (Matsushime et al., 1992, Meyerson and Harlow, 1994) the transition from G1 to S is mediated by cyclin E-Cdk2 (Ohtsubo et al., 1995) and Cdk2 and Cdk1 in association with A-type cyclins are important during S and G2 respectively (Pagano et al., 1992). Progression through mitosis is dependent on cyclin B-Cdk1 (King et al., 1994). In addition to the controlled oscillations in cyclin levels and phase specific combinatorial associations, Cdk activity is also modulated by specific inhibitors and by changes in the phosphorylation of the catalytic subunit. Furthermore, cell cycle checkpoints are also imposed to monitor the order and quality of the cell cycle events, with the option to halt the cell cycle if any perturbations are encountered (Hartwell and Weinert, 1989). Defects in parts of the checkpoint machinery are, unsurprisingly, found in cancer cells. Often the consequence of such deregulation results in a reliance on the remaining functional DNA damage process and this can be embraced therapeutically by chemically targeting the intact checkpoints resulting in synthetic lethality of cancer cells (reviewed in Garrett and Collins, 2011).

1.1.1 Basics of Cancer

As previously mentioned, the human body is comprised of billions of cells precisely arranged and working in concert. Normal, healthy cells divide on a regular basis for growth, repair and replacement purposes and this division is stringently controlled. In cancer however, control is lost and cells start to divide aberrantly thus paving the way for tumour formation. More specifically, the consecutive acquisition of a number of biological capabilities-the hallmarks of cancer-are necessary for tumour growth and progression. These include: self-sufficiency in growth signals, insensitivity to growth suppressors, evasion of apoptosis, limitless replicative potential, induced angiogenesis and tissue invasion and metastasis (Hanahan and Weinberg, 2000, Hanahan and Weinberg, 2011). Importantly, genomic instability has been suggested to explain the means by which these six capabilities are acquired.

1.1.1.1 Self-sufficiency in growth signals

Cancer cells must induce and maintain positively acting growth stimulatory signals to sustain chronic proliferation and are able to do so in number of alternative ways including: the production of extracellular growth signals, alterations in the receptor molecules (for example, PDGF and PDGF-R by glioblastomas, Westermark et al, 1995) and the constitutive activation of intracellular signalling pathways downstream of receptors (such as Ras activation, reviewed in Hanahan and Weinberg).

1.1.1.2 Insensitivity to growth suppressors

In contrast to the positively acting growth stimulatory signals, cancer cells also have the ability to circumvent negatively acting growth inhibitory signals. Tumour suppressor genes, that normally function to limit cell growth and proliferation, are inactivated in a multitude of cancers. In particular, defects in the Rb pathway (see below) are observed in the vast majority of human cancers (reviewed in Hanahan and Weinberg, 2011).

1.1.1.3 Evasion of apoptosis

Programmed cell death, triggered by various stresses including DNA damage as a consequence of chronic proliferation, is thought to serve as a natural barrier to cancer progression (Adams and Cory, 2007). However cancer cells have developed multiple strategies to avoid apoptosis and this includes inducing the expression of antiapoptotic regulators or by downregulating proapoptotic factors (reviewed in Hanahan and Weinberg, 2011).

1.1.1.4 Limitless replicative potential

While most types of healthy cells limit their replication to approximately 60-70 divisions by progressive telomere shortening, cancer cells are able to bypass this limit acquiring unlimited replicative potential (Blasco, 2005). They can achieve this by expressing telomerase, a DNA polymerase that functions by adding telomeric repeat segments to the ends of DNA thus opposing the telomere shortening that would otherwise occur.

1.1.1.5 Induced angiogenesis

All cells, including cancer cells, require the continued delivery of nutrients and oxygen for their survival. While the normal vasculature in adults is largely quiescent, in tumour

progression angiogenesis is almost always turned on (Hanahan and Folkman, 1996). At a molecular level, vascular endothelial growth factor (VEGF) is one known stimulator of angiogenesis initiation and Ras activation in cancer cells can induce its upregulation (Baeriswyl and Christofori, 2009).

1.1.1.6 Tissue invasion and metastasis

The multistep process of invasion and metastasis begins with local invasion of cancer cells into surrounding tissues (Talmadge and Fidler, 2010). The intravasation of said cells into nearby blood and lymphatic vessels then aids their transfer to distant sites. Extravasation and the formation of micrometastases follow. It is the growth of micrometastatic lesions into macroscopic tumours that accounts for approximately 90% of cancer deaths.

1.1.2 Interphase (G1, S, G2)

The G1 phase of the cell cycle serves as a 'time delay' not only to allow for cell growth but also to monitor the cell's external environment. If extracellular conditions are unfavourable, cells delay progress through G1 and may even enter a quiescent state, G0. If however, the cell receives the necessary growth signals it can pass through the restriction point (R, occurring between mid and late G1) and commit the cell to one round of division (Planas-Silva and Weinberg, 1997). At the molecular level, it is the cyclin D-Cdk complexes that act to integrate these extracellular signals. In early G1, the product of the retinoblastoma tumour suppressor gene, Rb exists in a hypophosphorylated state and prevents the premature entry into S phase by tightly binding and repressing the activity of transcription factors, such as E2F family member (Zhang et al., 1999, reviewed in Harbour and Dean, 2000). During G1, phosphorylation of Rb by cyclin D-Cdk4 and cyclin D-Cdk6 complexes, expressed in response to mitogenic growth signals, cancel this growth inhibitory effect and allow transcription to occur and cyclin E is synthesised (Harbour et al., 1999). When cyclin E is abundant and conditions are favourable, it interacts with Cdk2 and allows the progression from G1 to S phase. One of the most crucial targets of cyclin E-Cdk2 is Rb (Hinds et al., 1992),

which is able to completely dissociate from E2F and permit the transcription of genes required for S phase. As cells progress into S phase, cyclin A becomes the primary cyclin associated with Cdk2.

In order for two copies of the genome to be equally distributed to the daughter cells at M phase, DNA must be precisely replicated in the parental cell during S phase. DNA replication begins with the assembly of the pre-replication complex (pre-RC) during G1 (reviewed in Woo and Poon, 2003). Briefly, this complex consists of the origin recognition complex (ORC), Cdc6, chromosome licensing and DNA replication factor (Cdt1) and the mini-chromosome maintenance 2-7 (Mcm 2-7) (Santocanale and Diffley, 1996, Aparicio et al., 1997, Tanaka et al., 1997, Nishitani et al., 2000). Once the DNA is 'licensed' to replicate, pre-RCs are phosphorylated by cyclin-Cdk complexes, which in turn triggers the appropriate modifications required for replication initiation, including loading of DNA polymerases. Interestingly, cyclin A-Cdk2 appears to mediate elongation (Bashir et al., 2000) and phosphorylates several components of the replication machinery, including DNA polα (Nasheurer et al., 1991), DNA pol δ (Zeng et al., 1994) and proliferating cell nuclear antigen (PCNA, Prosperi et al., 1994). Furthermore, cyclin A-Cdk2 is also required to prevent re-replication as it phosphorylates Cdc6, sequestering the protein from the nucleus to the cytoplasm (Petersen et al., 1999). The resultant sister chromatids, are then physically linked as a results of cohesion loading by the cohesion complex (Uhlmann et al., 1999).

At the end of the S phase, A-type cyclins associate with Cdk1 and participate in the progression of G2. Much of G2 is spent growing into the size that is required for M phase. The activation of cyclinB-Cdk1 then allows entry of the cell into mitosis by promoting the phosphorylation of components which are involved in, for example, chromosome condensation, disassembly of the nuclear lamina and breakdown of the nuclear envelope (Nigg, 1995).

1.1.3 Mitosis

Prior to cytokinesis, mitosis is required to precisely regulate the segregation of replicated DNA so that when the two daughter cells are formed they will each inherit an identical set of chromosomes (reviewed in Walczak et al., 2010). The process of mitosis can be divided into distinct phases: prophase, pro-metaphase, metaphase, anaphase and telophase (Figure 1.2). First, during prophase, the chromosomes condense inside the nucleus and microtubule nucleation at centrosomes increases. Pro-metaphase follows and is marked by nuclear envelope breakdown and attachment of the kinetochores (specialised protein complexes that assemble on centromeric DNA) of individual sister chromatids to microtubles originating from the opposite poles. During this stage the spindle assembly checkpoint (SAC) operates to ensure correct chromosome alignment and biorientation on the mitotic spindle by sensing microtubule attachment and gain of spindle tension (Rieder et al., 1994, Li and Nicklas, 1995). By the action of the SAC proteins (including Mad2, Bub1 and BubR1, Chen et al., 1996, Li and Benezra, 1996, Taylor and McKeon, 1997, Skoufias et al., 2001) the function of Cdc20 is inhibited (Yu, 2007) and cyclin B is stabilized until all chromosomes are correctly attached to the mitotic spindle at metaphase. On achieving the latter, the anaphase-promoting complex (APC/C), a multisubunit E3 ubiquitin ligase, becomes activated by binding Cdc20 and marks cell cycle proteins, including cyclin B and securin, for degradation (reviewed in Pines, 2006, Holloway et al., 1993, Yu, 2007). Destruction of these mitotic regulators lead to the inactivation of Cdk1 and the cohesin complex (more specifically its subunit, scc1, Uhlmann et al., 1999) Scc1 cleavage destroys the link between sister chromatids and thereby promotes anaphase. Once each set of sister chromatids have reached the opposite spindle poles, the chromosomes decondense as the nuclear envelope reforms around the two daughter nuclei (telophase). Ingression of a cytokinetic cleavage furrow between the segregated chromosomes then partitions the remaining cellular material and is discussed in more detail below.

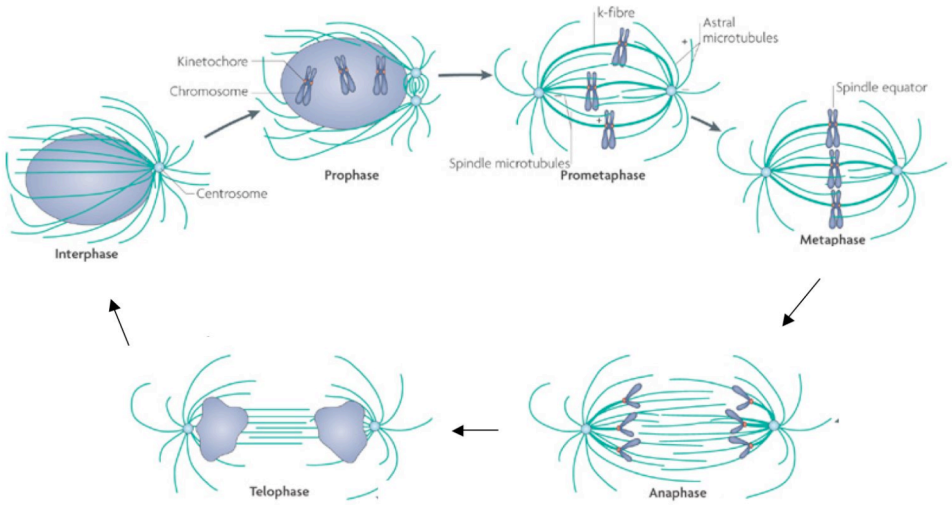

Figure 1-2 Progression through mitosis and re-entry into interphase.
(Reprinted with permission from Macmillan Publishers Ltd, Nature Reviews Molecular Cell Biology Walczak et al., 2010, 11, p91-102). Mitosis is subdivided into prophase, pro-metaphase, metaphase, anaphase and telophase, see text for details.

1.2 Cytokinesis

The final bifurcation of a 'pre-existing' cell, cytokinesis, is the concluding step in cell division. The process begins at anaphase onset when the mitotic spindle undergoes complex structural changes including the growth of astral microtubules towards the cell cortex and central spindle formation inbetween the segregating chromosomes. These anaphase spindle structures induce localized activation of the small GTPase RhoA (reviewed in Douglas and Mishima, 2010) which in turn triggers the formation of a contractile ring, a network of actin and myosin filaments. Contraction of the actomyosin ring forms a cleavage furrow typically around the middle of the cell and ingresses until the dividing cells are connected by a narrow, tubular intracellular bridge, containing the midbody. Dissolution of the bridge completes cytokinesis and two daughter cells are formed (reviewed in (Glotzer, 2005, Eggert et al., 2006, Barr and Gruneberg, 2007). Although less well understood than some of the earlier phases, it is by no means less critical and failure to complete cytokinesis can lead to genetically unstable tetraploid cells (Fujiwara et al., 2005), a prelude to aneuploidy, the most common characteristic of human solid tumours (reviewed in Kops et al., 2005). In order to be able to assess whether intervention might bring benefits in the treatment of cancer, a detailed understanding of the mechanisms involved are required.

1.2.1 Selecting the site of cell division

One of the first steps in cytokinesis is determining the site of cell division, ensuring that it is correctly positioned between separating chromosomes so that each daughter cell receives only one copy of the genome. For over forty years the mitotic spindle has been consistently associated with defining this position, however there has been much debate regarding the exact part of the spindle apparatus which is responsible. Classic experiments performed on marine invertebrate eggs established the importance of spindle asters (Rappaport, 1961) whereas in comparatively more recent studies, the

signalling potential has been reported to occur via the central spindle (Giansanti et al., 1998). Consequently, different models have been proposed to explain the induction of furrow positioning (see Figure 1.3 and corresponding figure legend for a detailed explanation). It has been suggested that all organisms have the potential to use both the aster-directed and central spindle pathway to initiate and execute cleavage furrow formation but the relative importance between the two differs between cell types and species (reviewed in Barr and Gruneberg, 2007). Although the molecular details of the aster-directed pathway are beginning to emerge, there is a much clearer understanding of those components involved in the central spindle pathway.

1.2.2 Central spindle assembly

The proteolytic degradation of cyclin B, as a consequence of APC activation following the satisfaction of the SAC (Holloway et al., 1993) inactivates Cdk1 and permits dephosphorylation and subsequent activation of proteins that are critical for the assembly of the central spindle. Factors that contribute to the central spindle assembly include; Prc1, a microtubule-associated protein with microtubule bundling activity (Mollinari et al., 2002) and the centralspindlin complex composed of the kinesin motor protein MKLP1 and the Rho-family GTPase activating protein (RhoGAP) MgcRacGAP (Mishima et al., 2002). Cdk1 phosphorylation sites have been mapped in both Prc1 and MKLP1 and consistent with their recruitment negatively regulated by Cdk1-cyclinB mediated phosphorylation, Ala substitutions of a subset of these sites cause the premature association of both to the central spindle (Mollinari et al., 2002, Mishima et al., 2004).

The stable localization of centralspindlin also depends on the chromosomal passenger complex (CPC) which includes the kinase aurora B and its coactivator the inner centromere protein, INCENP (Kaitna et al., 2000). Both MgcRacGAP and MKLP contain phosphorylation sites for aurora B. Whereas the phosphorylation of the N-terminal of MgcRacGAP has been proposed to affect binding to Prc1 (Ban et al., 2004), phosphorylation of the GAP domain has been reported to convert MgcRacGAP

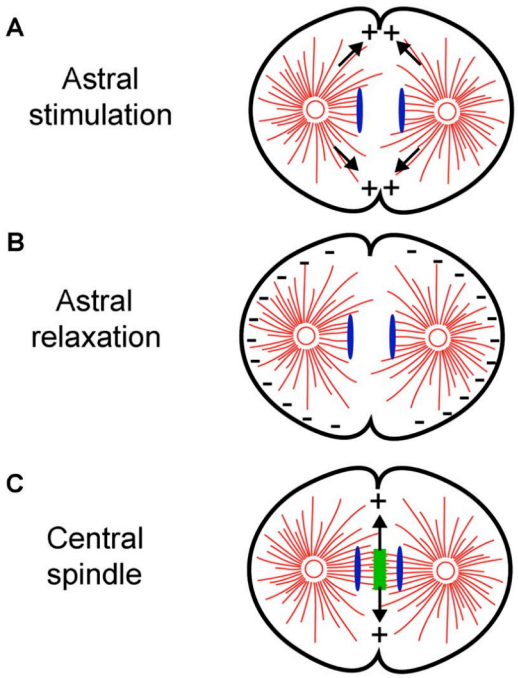

Figure 1-3 Three schematic models for the positioning of cleavage furrow. (Reproduced with permission from ©2004 Rockefeller University Press. Originally published in J.Cell Biol. 164:347-351). A) Astral stimulation model. According to this model, astral microtubules provide a cleavage furrow stimulus which is transported along astral microtubules. Given that microtubules from both poles project towards the equatorial cortex, it is assumed that the strength of the stimulus is maximal here. B) In contrast to A) the astral relaxation model assumes that the density of astral rays, is greater at the poles compared with at the equator causing these regions to be less contractile and consequently inducing equatorial furrowing. C) In the central spindle model, the overlapping microtubules between segregating chromosomes, provides a platform for which to recruit key regulators of RhoA. In turn they are able to function by signalling to the overlapping equatorial cortex.

into a RhoGAP (Minoshima et al., 2003). Aurora B mediated phosphorylation of MKLP1 further serves to assemble the central spindle by preventing 14.3.3 mediated sequestration of MKLP1 in the cytoplasm, instead promoting its association with aurora B at the central spindle (Douglas and Mishima, 2010).

1.2.3 Actomyosin contractile ring assembly

Once assembled the central spindle serves as a platform for the coordinated recruitment of numerous signalling proteins that regulate RhoA at the equatorial cortex and promote furrow ingression. RhoA is a central player in contractile ring assembly, which is attached to the plasma membrane to create a cleavage furrow that partitions the cell into two (reviewed in Glotzer, 2005). Like many of its fellow small GTPases, RhoA switches between an active GTP-bound form and an inactive GDP-form. The cycling of RhoA between these two states is regulated by guanine nucleotide-exchange factors (GEFs) and GTPase activating proteins (GAPs). GEFs activate RhoA by promoting the release of GDP and the consequent binding of GTP (which is present in an ~10-fold excess over GDP), whilst GAPs inactivate RhoA by increasing the intrinsic GTPase activity. Only in its active, GTP-bound state is RhoA able to interact with and activate downstream effector proteins (reviewed in Heasman and Ridley, 2008). However the precise mechanisms of RhoA localization at the equatorial cortex and its activation remain unclear. Interestingly, astral microtubules have been shown to be essential for localising RhoA and inducing contractile ring formation at the equatorial cortex in NRK-52E cells (Nishimura and Yonemura, 2006). In contrast, central spindle microtubules were shown only to recruit RhoA to the cortex when the central spindle microtubules were in close enough proximity (Nishimura and Yonemura, 2006).

The RhoA GEF Ect2 is a critical RhoGEF in cytokinesis. Overexpression of Ect2 lacking its GEF domain inhibits the completion of cytokinesis in mammalian cells (Tatsumoto et al., 1999) and depletion of the entire Ect2 prevents cytokinesis in human cells (Kim et al., 2005). Ect2 localizes to and becomes active at the central spindle by binding to MgcRacGAP. More specifically, through its association with Prc1,

mammalian Polo-like kinase (Plk1) is recruited to the central spindle where it functions to phosphorylate the N terminus of MgcRacGAP, generating a phospho-epitope recognised by the BRCA1 C-terminal (BRCT) domain of Ect2 (Petronczki et al., 2007, Wolfe et al., 2009). Complex formation between MgcRacGAP and Ect2 is thought to relieve Ect2 autoinhibition which then signals to the overlying equatorial cortex by activating a local pool of RhoA (Yuce et al., 2005). In contrast, Nishimura and Yoemura have proposed a model whereby localization of the centralspindlin complex to the tips of the astral microtubules localize Ect2 to the equatorial cortex and results in active RhoA accumulating there. They suggest that the role of the centralspindlin-Ect2 complex at the central spindle is merely to maintain active RhoA during furrow ingression. Interestingly, Ect2 has also been shown to localize to the cortex through a mechanism that depends on its C-terminal pleckstrin homology (PH) domain binding phosphatidylinositol lipids PI(4,5)P_2 (Chalamalasetty et al., 2006). Nonetheless, once active RhoA then acts on downstream effectors including Rho kinase (ROCK), citron kinase and mammalian homolog of Drosophila diaphanous (mDia) that in combination lead to myosin II activation and actin polymerization (Madaule et al., 1998, Kosako et al., 2000, Watanabe et al., 2008).

1.2.4 Furrow ingression and midbody formation

Once the filaments are assembled into contractile bundles around the equator, the progressive sliding of anti-parallel actin filaments along myosin II, in a manner similar to the contraction of the sarcomere, causes the bundles to shorten. This tightening ‘purse string’ in turn is believed to provide the contractile force necessary to drive furrow ingression (reviewed in Wang, 2005). While this contractile ring hypothesis dominates current thinking, the exact mechanism of force generation remains widely debated. Alternative theories of force generation include the involvement of a subcortical cytoskeleton and spindle axis forces ‘pulling’ daughter cells away from one another.

The RhoA activated furrow continues to ingress until the dividing cell remains connected by an intracellular bridge (Figure 1.4). The intracellular bridge contains dense bundles of antiparallel microtubules and the region where they overlap is now referred to as the midbody. Most of the central spindle components and RhoA specifically localize here, collectively serving as a platform for the recruitment of factors essential for the completion of cytokinesis. For example, the sequential binding of MgcRacGAP to Ect2 and Rab11-FIP3/Eferin/arfophillin (FIP3) regulates the targeting of recycling endosomes to the midbody (Simon et al., 2008), which has been shown previously to be required for abscission (Wilson et al., 2005). Interestingly, evidence has also emerged in support of a role for membrane traffic at the furrow stage. Specifically, vesicles from the trans-golgi network (TGN) have been found to mediate furrow ingression (Hill et al., 2000). However, the exact role of vesicles in cytokinesis is yet to be resolved. In principle, vesicle fusion with the plasma membrane might act to trigger plasma membrane fission by suddenly increasing the membrane surface at the abscission site. However, the gradual reduction in TGN vesicles during furrow ingression perhaps suggests a more preparatory role rather than directly promoting abscission.

1.2.5 Abscission

Following its rapid assembly, the intracellular bridge can persist for up to several hours, ensuring the complete clearance of chromatin from the cleavage plane (Steigemann and Gerlich, 2009a), after which the cell finally undergoes abscission, the process that leads

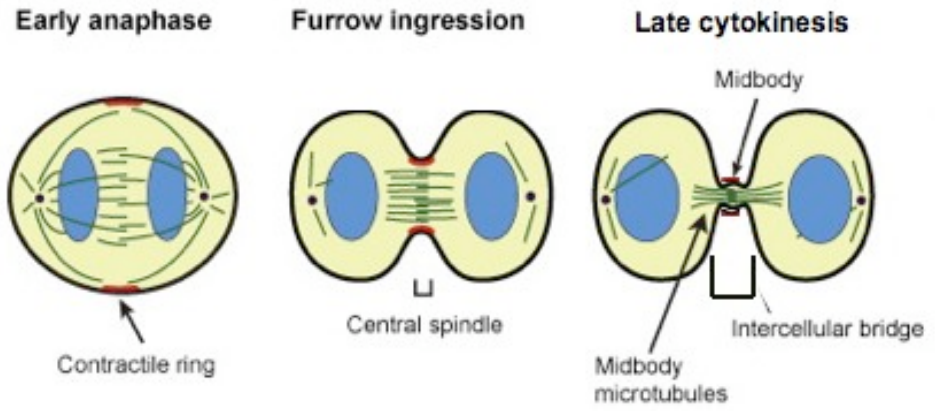

Figure 1-4 Progression through cytokinesis.
(Reprinted from Seminars in Cell and Developmental Biology, 21, Guizetti and Gerlich, Cytokinetic abscission in animal cells, p909-916, 2010, with permission from Elsevier). In early anaphase the components of the contractile ring have assembled. Contraction of the actomyosin ring is thought to provide the necessary force for furrow ingression. Once fully ingressed, in late cytokinesis, compression of the central spindle creates an intracellular bridge containing the midbody.

to its irreversible severing (reviewed in Guizetti and Gerlich, 2010, Steigemann and Gerlich, 2009b). Currently, both the regulation and mechanism of abscission are poorly defined. With regards to its regulation, animal cells are thought in part to be dependent on aurora B (Steigemann et al., 2009). It is thought that aurora B is part of an undefined sensor that responds to unsegregated chromatin at the cleavage site by delaying abscission. Maintenance of aurora B in an active state is sufficient to induce its relocalization to a narrow-ring at the intercellular canal where it functions to stabilize the structure and delay abscission. Subsequent dephosphorylation then correlates with abscission. In terms of mechanics, the evidence indicates asymmetric midbody disassembly coinciding with either i) mechanical rupture and subsequent would healing; ii) targeted vesicle secretion and subsequent fusion or iii) plasma membrane ingression and subsequent fission (see Figure 1.5 and the corresponding figure legend for a more detailed explanation).

It has been proposed that the removal of actin is also a prerequisite for this terminal step and could be controlled by the inactivation of RhoA. This loss of RhoA-GTP may be driven by control of a RhoGEF, a RhoGAP, a physical relocation of either of these regulators or of RhoA itself. Interestingly, recent work has uncovered the epsilon (ε) isoform of the protein kinase C family (PKC) acting as a key regulator at this end stage of cytokinesis to trigger RhoA inactivation (Saurin et al., 2008). How this particular control is exerted will be addressed throughout this thesis.

1.2.6 Cytokinesis Failure

Given that cytokinesis is such a highly ordered process it is not surprising that it can sometimes fail. Cytokinesis failure leads to both centrosome amplification and production of tetraploid cells (reviewed in Storchova and Pellman, 2004). These 4N cells can then undergo chaotic mitosis causing extensive genomic instability, leading the way to aneuploidy and ultimately tumour growth. Endoscopic biopsies of patients with Barrett's oesophagus have, arguably, provided the most direct evidence for the

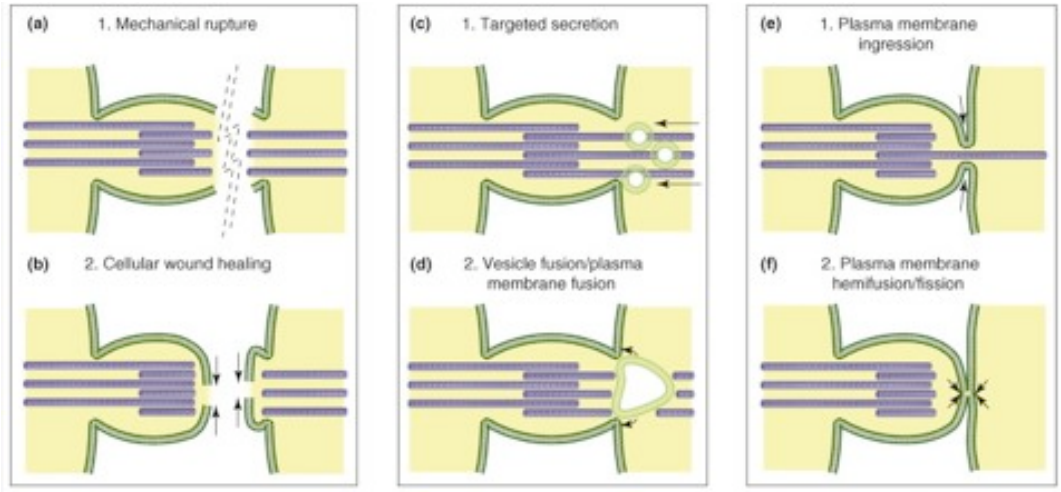

Figure 1-5 Schematic models for the process of abscission
(Reprinted from Trends in Cell Biology, 19, Steigemann and Gerlich, Cytokinetic abscission: cellular dynamics at the midbody, p606-616, 2009, with permission from Elsevier) (a,b) Following destabilisation of the intercellular bridge, it is suggested that the frictional force of sister cells could induce rupturing. The holes made would then be filled using a process similar to that of wound healing. (c,d) Targeted secretion and membrane fusion model. TGN or endosome derived vesicles have been suggested to accumulate close to the midbody. Vesicle fuse with one another and the plasma membrane to support the splitting of cells. (e,f) Plasma membrane ingression for fission model. An alternative model proposes that disassembly of the intercellular bridge permits the direct fission of ingression plasma membranes.

tetraploid hypothesis for carcinogenesis. The progressive analysis of these patients has revealed a striking correlation between the early loss of p53 (a gene required for the tetraploid checkpoint), the acquisition of a population of tetraploid cells and the development of aneuploidy (Reid et al., 1996, Margolis et al,. 2003). However, given the genetic complexity of aneuploid cells, it still remains widely debated as to whether aneuploidy is a causative effect or merely a consequence of transformation. It is therefore important to conclusively prove whether a tetraploid intermediate, occurring as a result of cytokinetic failure, has a role in genomic instability in tumours.

1.3 Protein Kinases

Mammalian protein kinases are key regulators of almost every aspect of eukaryotic cellular behaviour, including cell cycle progression, metabolism, apoptosis and differentiation. They constitute one of the largest and most functionally diverse gene families and catalyse the rapid and reversible transfer of γ-phosphate from adenosine triphosphate (ATP) to protein hydroxyl groups on Ser, Thr and Tyr residues (Hanks and Hunter, 1995, Manning et al., 2002).

1.3.1 AGC kinases

PK**C** belongs to the AGC superfamily of Ser/Thr protein kinases and based on the sequence alignment of its kinase domain was one of the three defining subfamilies, along with cAMP-dependent protein kinase 1 (PK**A**) and cGMP-dependent protein kinase (PK**G**). It is now held in wide regard that the AGC family contains sixty out of the five hundred and eighteen human protein kinases identified by the human genome project (reviewed in Pearce et al., 2010). Currently, fourteen AGC kinase domain structures have been solved, all of which exemplify the prototypical bilobal kinase fold initially described for PKA (Knighton et al., 1991). In the bilobal kinase fold, an amino-

terminal small lobe (N-lobe) and a carboxyl-terminal large lobe (C-lobe) surround one molecule of ATP and a deep cleft, between the two, forms an active site. While the N-lobe is associated with nucleotide binding, the C-lobe is primarily involved in substrate binding and catalysis. The αC helix, located in the N-lobe and a C-terminal tail are also critical for regulatory interactions between the two.

In addition to the high degree of primary sequence conservation within the kinase domain, AGC protein kinases share a conserved system for regulating the intrinsic activity of these domains. Generally, this involves phosphorylation at three conserved priming sites; the activation loop (found in the C-lobe), the hydrophobic motif and the turn motif (both located in the C-terminal tail).

While phosphorylation of the activation loop typically involves phosphoinositide-dependent kinase 1 (PDK1, Alessi et al., 1997), accumulating data indicate that the mammalian target of rapamycin (mTOR) mediate the phosphorylation of the hydrophobic motif and turn motif of several AGC kinases (reviewed in Jacinto and Lorberg, 2008). There are two distinct mTOR protein complexes, mTORC1 and mTORC2, differing in their molecular composition and sensitivity to rapamycin. In mTORC1, mTOR forms a complex with regulatory associated protein of mTOR (Raptor) and mammalian lethal with sec thirteen (mLST8) and mediates the rapamycin sensitive function of mTOR (Kim et al., 2002). In contrast, mTORC2 signalling is rapamycin insensitive and mTOR forms a complex with rapamyicin-insensitive companion of mTOR (Rictor), stress-activated protein kinase interacting protein 1 (Sin1) and mLST8 (Pearce et al., 2007, Yang et al., 2006).

Apart, from the kinase domain the AGC kinases show little similarity and not surprisingly are activated downstream of a wide range of extracellular stimuli by distinct mechanisms. For example, PKB, p70 ribosomal S6 kinase (S6K) and serum and glucocorticoid induced protein kinase (SGK) are downstream mediators of phosphoinositide 3-kinase (PI3K, Ming et al., 1994, Franke et al., 1995, Kobayashi and Cohen, 1999). PKA is subject to control by cAMP (Taylor and Young, 1990) and p90 ribosomal kinase (RSK) and mitogen and stress activated protein kinase (MSK) are effectors of extracellular signal-regulated kinase (ERK) and ERK/p38 mitogen-

activated protein kinases (p38 MAPK) respectively (Dalby et al., 1998, Deak et al., 1998). In the case of PKC, the subject of this thesis, activation is generally downstream of phospholipase C (PLC).

1.3.2 Protein Kinase C

PKCs contribute a significant number of members to the AGC superfamily and currently, nine PKC isoforms have been identified unequivocally (reviewed in Mellor and Parker, 1998, Steinberg, 2008). In addition to the highly conserved carboxyl-terminal catalytic kinase domain, PKCs contain an amino-terminal regulatory domain. Both structures are composed of a number of conserved regions (C1-C4) interspersed by regions of lower homology, termed variable domains (V0-V5). Structural differences within the regulatory domain confer variations in cofactor requirement and consequently subdivide the family into three groups (Figure 1.6). The best characterized and first discovered are the conventional PKCs (cPKC): α, the βI/βII splice variants and γ subtypes, which are all DAG and Ca^{2+} dependent; in this case a duplicated Cys-rich motif (the C1 domain) binds DAG, while the C2 domain contains a Ca^{2+} binding site. The second best characterized PKCs are the novel PKCs (nPKC): δ, ε, η and θ subtypes. These isoforms are structurally similar to the cPKCs, except that the C2 domain does not contain the functional Asp residues that appear to mediate Ca^{2+} binding, nPKCs are therefore classified as Ca^{2+} independent but DAG dependent. The least understood isoforms are the atypical PKCs (aPKC): ζ and λ/ι subtypes. They contain a variant of the C1 domain with an impaired ligand-binding pocket that does not bind DAG and the C2 domain is replaced by a Phox/Bem1 (PB1; protein interaction domain). Consequently, aPKCs are DAG and Ca^{2+} independent and regulation occurs in part through the N-terminal Phox/Bem1 (PB1) domain and protein interactions.

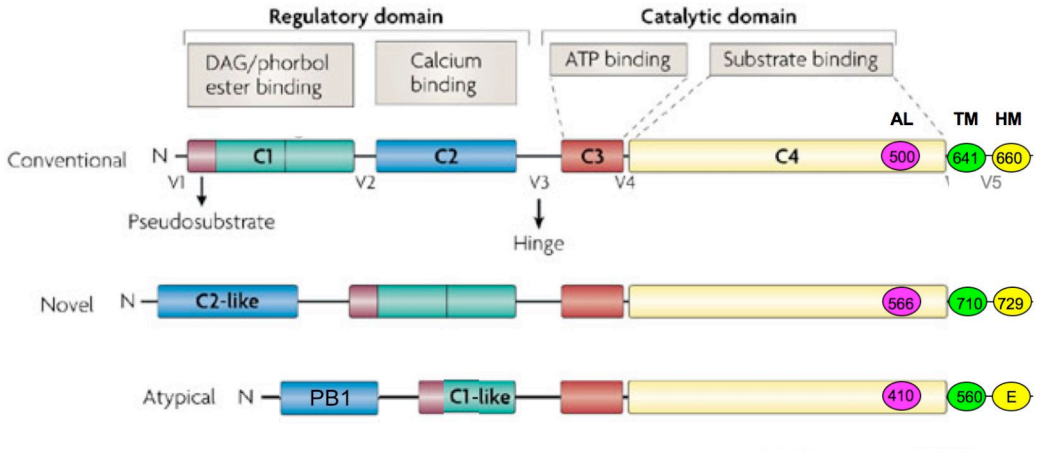

Figure 1-6 PKC structure and classification
(Reprinted with permission from Macmillan Publishers Ltd, Nature Reviews Cancer, Mackay and Twelves, 7, 554-562, 2007). PKC has four conserved domains (C1-C4) located within two regions (regulatory and catalytic). Schematic includes the pseudosubstrate (burgundy rectangle), C1 domain and C1-like (green rectangle), C2 domain and PB1 (blue rectangle), the connecting variable regions and kinase domain (red and cream rectangles). The 3 priming phosphorylations for PKCβII, PKCε and PKCζ are shown also.

1.3.3 Protein Kinase C and Cancer

PKCs have been linked to cancer progression ever since the 1980s when it was discovered that tumour promoting phorbol esters were PKC activators in 2 stage carcinogenesis models (Castagna et al., 1982, Kikkawa et al., 1983, Leach et al., 1983). Extensive research since has indeed established key roles for PKC isoforms in malignant transformation. Although mutations and chromosomal rearrangements are rare, alterations in the expression of PKC in human cancers are regularly displayed (Table 1.1), the profile of which is dependent upon the particular cancer type (reviewed in Griner and Kazanietz, 2007). Currently, little is known as to whether changes in PKC expression are a consequence of genetic and/or epigenetic effects.

1.3.4 PKC regulation-priming site phosphorylation

In common with other members of the AGC kinase superfamily, PKC activity typically requires phosphorylation at three conserved priming sites (two for ζ and λ/ι); the activation loop, the hydrophobic motif and the turn motif (in aPKCs a phosphomimetic is present at the hydrophobic motif). In the absence of phosphorylation at one or more of these sites, catalytic activation is impaired or enzyme stability is compromised (reviewed in Newton, 2009, Freeley et al., 2011).

Phosphorylation of the activation loop in most PKC isoforms is critical for catalysis. Moreover, it likely represents the first phosphorylation event in the processing series, as substitution of the activation loop Thr of cPKCs with a neutral or non-phosphorylable residue abolishes activity and prevents the subsequent phosphorylations on the C-

PKC isoform	Tumour type	Expression	Correlation
α	Bladder	Increased	With tumour grade
	Brain	Decrease	Level of cellular differentiation
	Brain	Increased	With tumour grade
	Breast	Decreased	With tumour grade
	Ovarian	Decreased	With tumour grade
	Renal	Decreased	ND
	Colon	Decreased	ND
	T- cell leukaemia	Decreased	ND
β	Bladder	Decreased	With tumour grade
	Colon	Decreased	ND
	Prostate	Decreased	Implicated in early stage tumour development
	T-cell leukaemia	Decreased	ND
	Melanoma	Decreased	ND
δ	Bladder	Decreased	With tumour grade
	Brain	Decreased	With tumour grade
	Colon	Increased	ND
	SCC	Decreased	ND
ε	Bladder	Increased	With tumour grade
	Brain	Increased	With tumour grade
	Breast	Increased	With tumour grade, poor survival, negative correlation with ER status
	Colon	Decreased	ND
	Prostate	Increased	Implicated in early stage tumour development
	Thyroid	Decreased	ND
η	Breast	Decreased	With tumour grade; expression of MDR genes
	Colon	Decreased	Level of cellular differentiation
	Renal	Increased	With tumour grade
θ	GIST	Increased	Diagnostic marker of tumour type

Table 1-1 Expression of PKC isoforms in human tumours
(Reprinted by permission from Macmilan Publishers Ltd: Nat Rev Cancer, Griner and Kazanietz, 7, 281-294, 2007). ND, not determined; ER, oestrogen receptor; GIST, gastrointestinal stromal tumour; MDR, multidrug resistance

terminal tail sites (Cazaubon et al., 1994, Orr and Newton, 1994). The molecular detail of this regulation has been provided by the publication of PKC kinase domain crystal structures including the cPKC PKCβII (Grodsky et al., 2006). The activation loop is located in the C-lobe and lies adjacent to the nucleotide binding site when arranged in the bilobal fold. It is connected to the N-lobe through the αC helix and its phosphorylation leads to a conformational change which coordinates the formation of a hydrogen bond network that is required for catalytic activity. It is now appreciated that activation loop phosphorylation is mediated by PDK1 and in cells that are deficient in PDK1, PKC levels and/or activation loop phosphorylation are significantly reduced (Balendran et al., 2000). Both the hydrophobic motif and turn motif are located outside of the kinase domain and instead they are found on the C-terminal tail. While the turn motif is conserved in all PKC isoforms, the hydrophobic motif is only found in cPKCs and nPKCs (the aPKCs instead have an acidic residue present). Structural and modeling studies on the kinase domains have demonstrated that the phosphorylated turn motif serves to stabilize the kinase core by assisting the C-terminal tail in finding its way around the N-lobe and helping to position the αC helix in an active conformation. However, there are discrepancies between the data as to the importance of this site for catalytic activity, whereas phosphorylation is required for PKCβI and PKCβII activity (Zhang et al., 1994, Edwards et al., 1999) it is found to be dispensable for PKCα, PKCθ and PKCι (Bornancin and Parker, 1996, Liu et al., 2002, Hauge et al., 2007). Whilst the turn motif site of PKCβII was initially described as an autophosphorylation site (Behn-Krappa and Newton, 1999), recent studies have demonstrated that autophosphorylation is not necessarily required (Cameron et al., 2011). Rather, a subset of PKC isoforms have been identified as downstream targets of mTOR. Specifically, mTORC2 has been implicated in turn motif phosphorylation of cPKCs and PKCε. However whether mTORC2 controls the phosphorylation of this site either directly or indirectly is unclear. More importantly perhaps is that in murine embryonic fibroblasts (MEFs) lacking critical components of mTORC2, the levels of cPKCs and PKCε are vastly reduced (Ikenoue et al., 2008).

mTORC2 has also been implicated in the hydrophobic motif of some cPKCs and nPKCs. Interestingly, in human embryonic kidney cells (HEK 293), PKCε at the hydrophobic motif is sensitive to rapamycin (Ziegler et al., 1999), which is indicative of an involvement of mTORC1 rather than mTORC2 in phosphorylation. Similar to the turn motif, the effects of this site on catalytic activity are inconsistent but are very much supportive of a role in stabilizing the enzyme. From structural studies, it is demonstrated that phosphorylation of the hydrophobic motif is required for an interaction between the C-terminal tail with the hydrophobic pocket in the N-lobe, formed in part by the αC helix. Like the turn motif, the hydrophobic motif helps position the αC helix in an active conformation.

Collectively, theses results have led to a model (Figure 1.7) in which: 1) unphosphorylated PKCs are in a catalytically-incompetent open conformation, probably constitutively on the membrane; 2) PDK1 phosphorylates the activation loop at the membrane; 3) PDK1 dissociates from PKC, allowing phosphorylation at the turn motif and hydrophobic motif by mTORC1/mTORC2 dependent pathways; 4) PKC adopts an activity-competent but autoinhibited conformation, once dissociated from the membrane. The enzyme is now in a closed configuration but access to the active site is sterically hindered through the binding of the pseudosubstrate sequence. The pseudosubstrate sequence is composed of highly conserved residues and found juxtaposed to the N-terminus of the C1 domain of all PKC isoforms (House and Kemp, 1987). Activation of PKC is accompanied by its removal from occupation of the substrate site and is mediated by the recruitment to cell membranes or binding of accessory proteins.

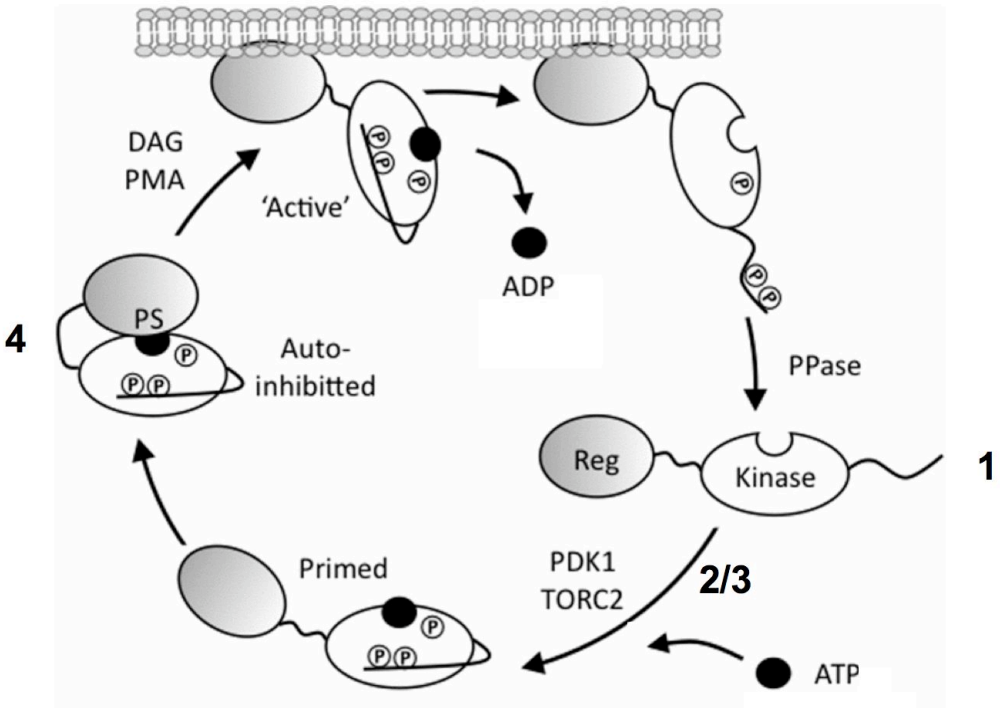

Figure 1-7 A schematic outlining the cycle of generic c/n PKC activation
(This figure was originally published in Biochemical Society Transactions, Cameron, Occupational hazards: allosteric regulation of protein kinases through the nucleotide-binding pocket, 2011, 39, 472-6, © the Biochemical Society). See text for details.

1.3.5 PKC activation-recruitment to cell membranes

DAG is produced acutely in response to phosphoinositide-specific phospholipase C (PI-PLC) hydrolysis of PIP_2 and functions to reversibly recruit cPKCs and nPKCs to the membrane via their C1 domains (reviewed in Newton, 2009). Specifically, the duplicated Cys-rich regions (HX12CX2CXnCX2CX4HX2CX7C) denoted C1A and C1B, are the binding sites for both DAG and the tumour-promoting phorbol esters such as phorbol-12-myristate-13-acetate (PMA, Castagna et al., 1982). Membrane phosphatidylserine (PS) also plays a critical role in this interaction and its binding is facilitated by a ring of positive charges around the middle of the domain. This particular electrostatic interaction positions the C1 domain to penetrate the membrane bilayer and bind the more deeply located DAG/PMA. Whereas, nearly all C1 domains have been shown to bind PS with equal affinity, their interaction with DAG/PMA varies. The C1 domain of nPKCs has an affinity for DAG two orders of magnitude higher than that of the C1 domain of cPKCs (Giorgione et al., 2006). Recently, this has been attributed to a single residue in the C1B domain. A Trp residue in the lipid-binding surface of nPKCs is replaced by a Tyr at an equivalent position in cPKCs and appears to bind DAG-containing membranes with lower affinity (Dries et al., 2007). Consequently, cPKCs must be pre-targeted to membranes by their C2 domains, in response to an increase in intracellular Ca^{2+}, where they bind anionic phospholipids, with selectivity for PIP_2. Detailed structural studies have revealed that the C2 domain assumes a compact β sandwich fold with flexible loops on the top and bottom. Functional Asp residues, responsible for Ca^{2+} binding, are located in the flexible top loops and bind two-three Ca^{2+} ions and also interacts with PS (Ochoa et al., 2002). A Lys-rich cluster located in the β3 and β4 sheets is suggested to specifically bind PIP_2 (Corbalan-Garcia et al., 2003). Once engaged on the membrane, the C1 domain can then bind PS and DAG as previously described. The binding of the C1 domain, or the coordinated binding of the C1 and C2 domains, to membranes provides the energy to release the autoinhibitory pseudosubstrate from the active site and thus allows efficient substrate phosphorylation.

1.3.6 PKC activation-binding accessory proteins

The removal of the pseudosubstrate sequence from the active site in aPKCs is allosterically regulated by the binding of proteins. Despite the molecular detail of this regulation remaining unclear, a wealth of genetic data has been reported in which components involved have been identified (Rosse et al., 2010). One such protein-mediated pathway involves partition defective 6 (Par6, one of the evolutionarily conserved polarity proteins first identified in *Caenorhabditis elegans*). Par6 has been found to associate with the N-terminal PB1 domain in aPKCs, forming a stable heterodimer which is then activated by members of the Rho family GTPases, Rac1 and Cdc42 (Suzuki et al., 2003). Consistent with the latter, Yamanaka et al showed that kinase activity of aPKC in the Par6 complex is enhanced by the addition of recombinant Cdc42 preloaded with GTP (Yamanaka et al., 2001).

1.3.7 PKC degradation

cPKCs and nPKCs reversibly translocate on and off membranes in response to second messengers and are constitutively phosphorylated. However, prolonged activation, as is the case with phorbol esters, results in the dephosphorylation and subsequent degradation of PKC (reviewed in Newton, 2009). More specifically, it has been proposed that the PH domain leucine-rich repeat protein phosphatase (PHLPP) selectively dephosphorylates the hydrophobic motif at the membrane and then shunts PKC to the detergent-insoluble fraction of the cell for subsequent desphosphorylation at the remaining sites (Gao et al., 2008). The dephosphorylated species then undergoes ubiquitination and proteolytic degradation by the 26 S proteasome, a large multicatalyic protease complex (Lee et al., 1996). Dephosphorylation, however, is not necessarily a prerequisite for degradation, a second pathway can coexist in which phosphorylated PKC is also ubiquinated and degraded (Leontieva and Black 2004). Interestingly, recent studies have added a layer of complexity with regards to the phosphorylated/dephosphorylated balance of PKC levels within the cell. Occupation of

the ATP binding site with inhibitors results in an increase in phosphorylation of a kinase-inactive ATP binding mutant (that is not normally phosphorylated) and protects PKCs from dephosphorylation (Cameron et al., 2009, Gould et al., 2011).

1.4 PKCε in Cytokinesis

1.4.1 Specific functioning of PKC isoforms

PKC isoforms are widely distributed in mammalian tissues and while some are tissue specific (PKCγ is restricted mainly to the central nervous system and spinal cord, PKCθ is present in skeletal muscle and hematopoietic cells and PKCβ is found in pancreatic islet cells, monocytes, brain and vascular tissue, reviewed in (Way et al., 2000) many are found within the same cell and *in-vitro* have broadly overlapping substrate specificities. It has, therefore, been suggested that substrate specificity could be mediated by the localization of individual isoforms to specific subcellular compartments. Since there is a high sequence conservation within the C-terminal kinase domain it has been proposed that relatively small sequence motifs or signal patches found in the N-terminal regulatory domain and variable regions contribute to the isoform specific interactions and consequent signal diversity. Consistent with this hypothesis, kinase domain swapping experiments in Drosophila show that the kinase domain of PKC53E can functionally substitute for the kinase domain of protein kinase C-related, Pkn (the most closely related AGC kinase, (Palmer et al., 1994, Kitagawa et al., 1995) suggesting that it is the N-terminus of Pkn that localizes the PKC53E kinase domain to a particular subcellular region and that the kinase domain simply does its job there (Betson and Settleman, 2007).

Even so, how can the specific function of each PKC isoform be determined unequivocally? Currently, the most exquisitely specific approach employed for perturbing kinase activity is that of a chemical genetic approach, pioneered by the Shokat laboratory (Bishop et al., 1998, Bishop et al., 2000, Alaimo et al., 2001). A

conserved residue that sits in the bottom of the ATP-binding pocket and termed the 'gatekeeper' can be exploited to generate mutants that are specifically inhibited by kinase inhibitor analogues (Figure 1.8). Point mutation of the bulky gatekeeper to a small residue such as Gly or Ala renders the kinase almost uniquely sensitive to sterically bulky analogues of naturally occurring kinase inhibitors. Wild type kinases, which retain their bulky gatekeeper residues, are resistant to such inhibition. Indeed this strategy has been useful in determining the physiological role of the regulated PKCε-14.3.3 complex assembly, see below (Saurin et al., 2008). It is notable, however, that a mutation of this kind can impair the activity or ATP binding potential of the kinase. A reduced affinity for ATP in the gatekeeper mutant PKCε-M486Ais reflected in the relative instability of the priming phosphorylations. In contrast to PKCε-WT, PKCε-M486A exposure to PMA induces substantial dephosphorylation of all three priming sites within 30 minutes (Cameron et al., 2009).

A chemical genetic approach using Src kinase inhibitor analog, 4-amino-1-tert-butyl-3-(1'naphthyl)-pyrazolo[3,4-d] pyrimidine, NaPP1 (Qi et al., 2007, Durgan et al., 2008) to target mutant, PKCε-M486A provided the opportunity to confirm a role for PKCε in cytokinesis (which was initially identified in 14.3.3 binding defective and kinase defective mutants) and also permitted the monitoring of the localization of GFP-PKCε-M486A. Under conditions of selective inhibition, PKCε-M486A was shown to localize at the cytokinetic furrow/midbody with polymerized actin, active RhoA and an accompanying delay in cytokinesis. Indeed accumulated PKCε-M486A was shown to persist for several hours after which time the cells either separated or failed and instead formed a single binucleate cell (Saurin et al., 2008). Furthermore, the retention of RhoA-GTP on treatment of GFP-PKCε-M486A cells with NaPP1 is indicative of a role in RhoA inactivation and consequent control of actin depolymerization (Saurin et al., 2008).

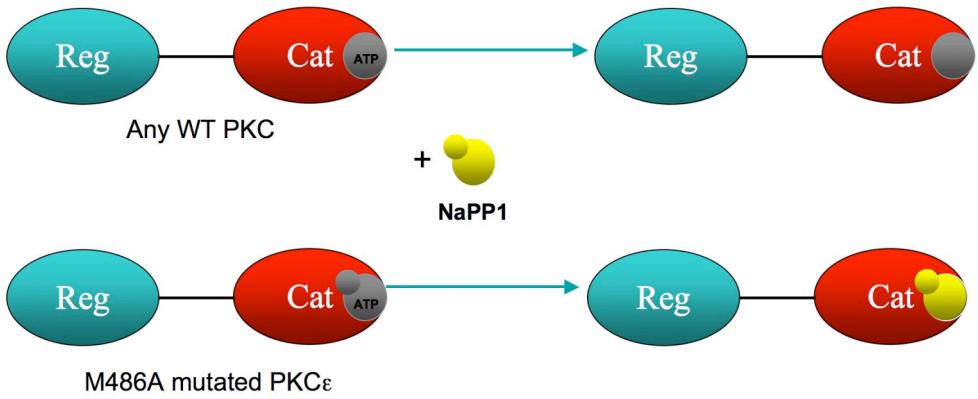

Figure 1-8 A chemical genetic approach for selectively inhibiting PKCε
WT kinases generally have a hydrophobic gatekeeper residue making inhibition difficult. Point mutation of M486A in PKCε renders the kinase almost uniquely sensitive to a sterically bulky analogue of ATP, in this case NaPP1. Although the schematic is shown depicting the inhibition of PKCε, this strategy is applicable to most protein kinases.

As previously mentioned, PKCε could mediate its function here by driving the control of a Rho GEF/GAP or RhoA itself. Alternatively, PKCε may contribute to the aurora B undefined sensor complex that responds to unsegregated chromatin at the cleavage site by delaying abscission (Steigemann et al., 2009). Consistent with a function of PKCε in mediating checkpoint control, recent work in the laboratory has shown that PKCε plays an important role in a metaphase to anaphase surveillance mechanism that is sensitive to unresolved metaphase catenation (Brownlow et al In Preparation), whether this is an extension of the SAC or precedes that of the aurora B mediated cytokinesis checkpoint however, remains to be defined. Interestingly, loss of PKCε function results in a large number of lagging chromosomes in anaphase, in principle the inhibition of PKCε-M486A by NaPP1 might act to induce a similar response that then becomes evident only at the point of RhoA inactivation. In view of the critical role of PKCε in cell division it is, however, intriguing that a PKCε knockout mouse is viable. This is perhaps reflective of the redundant behaviour of PKC isoforms. In the absence of PKCε, it is plausible that the related PKCδ performs the appropriate function instead and this is consistent with the embryonic lethality of a PKCε/δ double knockouts (unpublished).

In an attempt to resolve how PKCε control is exerted during cytokinesis it is imperative that we define a detailed molecular pathway which would include the signal input required for PKCε action and its consequent associations, the mechanism by which PKCε is localized and retained at the furrow/midbody and whether it controls RhoA-GTP loading and the mechanism by which it does so.

1.4.2 PKCε localization at the cytokinetic furrow/midbody

With regards to PKCε localization at the furrow/midbody, there are several motifs located within the N-terminal region of PKCε which may mediate this accumulation (Figure 1.9). Potential candidates include the V3 hinge region motifs responsible for binding 14.3.3 and selective targeting to cell-cell contacts (Quittau-Prevostel et al., 2004). In view of the role of actin in cytokinesis, the unique actin binding motif,

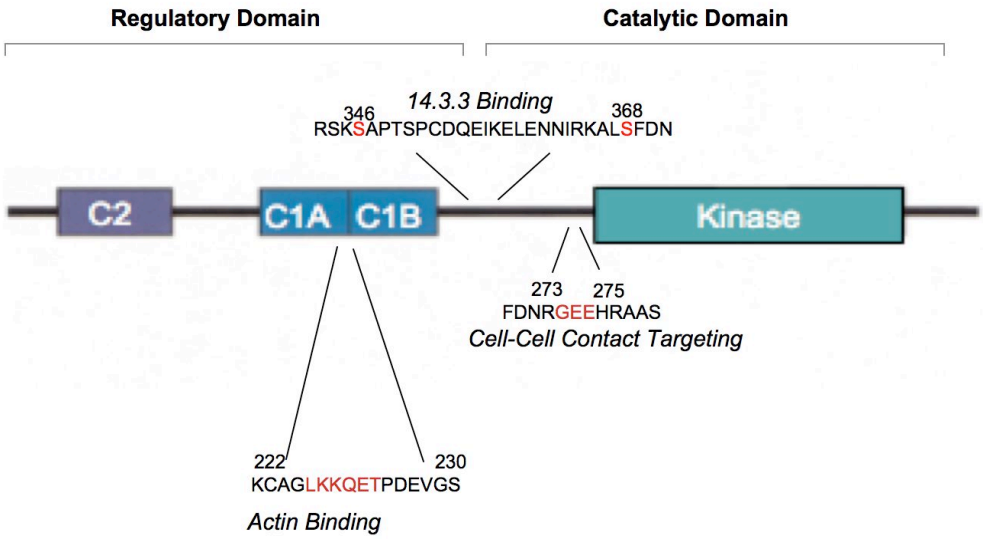

Figure 1-9 Schematic of PKCε showing domains and post-translational modifications
Critical residues highlighted in red, see main text.

LKKQET (Prekeris et al., 1996, Prekeris et al., 1998) located in the region between the C1A and C1B domains (herein referred to as the inter-C1 domain, IC1D) is also a plausible candidate.

1.4.3 PKCε and 14.3.3 binding

14.3.3 proteins are an abundant family of 28-33kDa proteins that exist as homo-or in hetero-dimers prior to interaction with a diverse array of cellular proteins (Morrison, 2009). At least 100 proteins have been found to interact with 14.3.3 isoforms including PKCs, Raf family members and receptor proteins (glucocorticoid receptor and insulin-like growth factor I receptor). In mammalian cells, seven isoforms (β, ε, γ, η,σ, τ and ξ) have been identified (Yaffe et al., 1997). All actions of 14.3.3 involve binding to target proteins, which typically involves recognizing the phosphorylation of specific Ser or Thr residues within either a mode I motif (RSXpSXP) or a mode II motif (RXXXpSXP, Yaffe et al., 1997). Successful binding has been shown to affect protein localization (Lo et al., 2004, Douglas et al., 2010), stability (LeBron et al., 2006) and/or activity (Obsil et al., 2001) thereby influencing cell adhesion (Han et al., 2001), cell polarity (Benton et al., 2002), cell survival (LeBron et al., 2006) and cell cycle (Douglas et al., 2010). Recently, it has been described that 14.3.3 functions during the late stages of mitosis, where its association with PKCε is required for the completion of cytokinesis (Saurin et al., 2008). Whether this particular control relates to the earlier 14.3.3 inhibition of centralspindlin remains to be determined (Douglas et al., 2010).

The defined PKCε-14.3.3 interaction is dependent on PKCε phosphorylation at 3 distinct V3 domain sites (situated between the regulatory and catalytic domains). Specifically; a glycogen synthase kinase-3 (GSK3) site (S346) matching the consensus 14.3.3 mode I site, an autophosphorylation site (S368) that is related to a mode II binding motif and a priming phosphorylation on PKCε targeted by p38 MAPkinase at S350 (required for the phosphorylation at S346,(Saurin et al., 2008). The structure of this phosphorylated V3 domain complexed to 14.3.3 has also been solved and shows a

1:2 hetero-trimer formation (Kostelecky et al., 2009). The authors propose that the binding of 14.3.3 to the V3 hinge region of PKCε acts as a conformational clamp to lock the enzyme in an active open conformation and this is consistent with data displaying constitutive lipid-independent activity. With regards to its physiological role, the 14.3.3 interaction is required for the exit from cytokinesis as exemplified by the PKCε mutant S346/368A, which unlike the wild-type protein does not rescue cytokinetic defects after PKCε knockdown (Saurin et al., 2008).

1.4.4 PKCε and selective targeting to cell-cell contacts

Cells are connected to their neighbours in a highly ordered manner mediated by well-organized macromolecular structures. The components of these adhesion complexes include a transmembrane protein (a cadherin) and numerous cytoplasmic proteins (α, β and γ-catenins Ozawa et al., 1989, Aberle et al., 1996), vinculin (Hazan et al., 1997) and α-actinin (Knudsen et al., 1995). The most common type of intercellular adhesion involves E-cadherin, which in the presence of Ca^{2+} can establish homophilic interactions at the site of cell-cell contacts (Takeichi, 1991). The cytoplasmic tail of E-cadherin binds β-catenin, which in turn binds α-catenin and links the cytoskeleton by itself binding to actin. Unfortunately, the nature of the E-cadherin mediated signaling events are still largely unknown. However, it has been reported that PKCε, alongside PKCα, is found to accumulate selectively at cell-cell contacts in mouse pituitary glands, the rat pituitary GH3B6 cell line and at contacts between fibroblasts and epithelial cells upon either physiological or pharmacological activation (Collazos et al., 2006, Louis et al., 2005, Quittau-Prevostel et al., 2004). This is of interest because during the cytokinetic furrowing process the presumptive daughter cell plasma membranes become juxtaposed in a manner that might trigger conventional cell-cell contact responses.

A three amino acid motif, GEE, located in the V3 region of PKCε is essential for selective targeting to cell-cell contacts (Quittau-Prevostel et al., 2004). An E374G point mutation abolishes any such selectivity and suggests that Glu374 is essential for proper

targeting (GDE and Asp294 in PKCα). However, this motif is not sufficient as replacing a Phe by Glu (GFE → GEE) at the equivalent position in PKCδ does not induce its targeting to cell-cell contacts. Currently, the role of PKCε at cell-cell contacts and the exact molecular events involved in the selective targeting remain unknown. However the pathophysiological consequences of abolishing cell-cell contact targeting are perhaps suggested in human pituitary and thyroid tumours where the naturally occurring PKCα D294G mutant is found (Alvaro et al., 1993, Prevostel et al., 1995).

1.4.5 PKCε and actin binding

Actin is one of the most highly conserved and abundant proteins in eukaryotic cells and many cellular processes (including cell motility, endocytosis and cytokinesis) are powered by its rapid polymerization (reviewed in Campellone and Welch, 2010, Firat-Karalar and Welch, 2011). Whilst cells typically contain a large pool of actin monomers (G-actin), spontaneous actin self-assembly is inefficient and to initiate assembly into a filamentous form (F-actin), cells generate free barbed ends that act as templates for polymerization by uncapping or severing existing filaments or by nucleating from monomers *de novo* using a diverse set of actin-nucleating proteins, including the actin-related protein 2/3 (Arp2/3) complex, formins and tandem-monomer-binding nucleators. During cytokinesis, the formins have been found to be of functional importance, most notably during actomyosin contractile ring assembly (Castrillon and Wasserman, 1994, Swan et al., 1998, Watanabe et al., 2008). Formins are multidomain proteins that are defined by the conserved formin homology (FH) domains, FH1 and FH2, which function to assemble unbranched actin filaments, which is in contrast to the first discovered actin nucleator, Arp2/3, forming a Y branched network (Rouiller et al., 2008). Crystal structures of both yeast (Xu et al., 2004) and mammalian formins (Lu et al., 2007) in combination with mutant analysis (Moseley et al., 2004, Copeland et al., 2004) suggest a model in which dimeric FH2 associates with the barbed end of an actin filament to promote actin filament stabilization. The proline-rich FH1 then stimulates

elongation by binding to profilin-actin (Romero et al., 2004) which serves to increase the local concentration of G-actin at the barbed end (Vavylonis et al., 2006).

Previous studies have revealed that the key formin in assembly of the mammalian contractile ring at the equatorial cortex is diaphanous-related formin, mDia (Watanabe et al., 2008), of which there are three isoforms, mDia1,mDia2 and mDia3 (Higgs and Peterson, 2005). Among these, mDia2 has been found to be essential in cytokinesis, selectively localising to the cleavage furrow and functioning downstream of the small GTPase RhoA (Watanabe et al., 2008). Interestingly on RhoA inactivation mDia2 localizes to the central spindle suggesting, like many other RhoA effectors, it responds to Rho signalling with translocation from the central spindle to the equatorial cortex (Watanabe et al., 2010). In addition, anillin, a scaffolding protein that can bind F-actin and is required for furrow stability and midbody formation (Field and Alberts, 1995, Somma et al., 2002, Echard et al., 2004) also binds mDia2 to further stabilize its localization and activation (Watanabe et al., 2010). Once assembled, the F-actin network then drives constriction of the furrow (see 1.2.4) and the depolymerization of actin at the end of cytokinesis is then associated with RhoA inactivation.

In view of the complex regulation of actin and RhoA, it is intriguing that inhibition of PKCε leads to its accumulation at the furrow/midbody with polymerized actin and RhoA (Saurin et al., 2008). This may reflect a requirement for PKCε in this pathway also. PKCε is unique among the PKC isoforms in containing an F-actin binding motif (Prekeris et al., 1996). The hexapeptide (LKKQET) is located within the inter-C1 domain (IC1D) at amino acids 223-228 and is required for the physical interaction between PKCε and F-actin. Deletion of amino acids encompassing this motif, 222-230, completely abrogates this binding activity (Prekeris et al., 1996) Despite the lack of structural evidence for a PKCε-actin interaction, the structure of actin-ciboulot complex reveals how an actin-binding motif, of similar sequence to that in PKCε, can bind in a hydrophobic cleft formed between actin subdomains (Hertzog et al., 2004). Currently, the functional roles associated with the assembled complex appear to be important for glutamate exocytosis from nerve terminals and outgrowth of cellular protrusions in fibroblasts (Hernandez et al., 2001).

1.4.6 PKCε and Cancer

Indeed substantial evidence exists implicating PKCε as a transforming oncogene (reviewed in Gorin and Pan, 2009). Its overexpression *in vitro* has been shown to increase proliferation, motility and invasion of both fibroblasts and immortalised cells (Mischak et al., 1993, Cacace et al., 1993). Furthermore, xenograft and transgenic animal models demonstrates the aggressive metastatic phenotype PKCε establishes when overexpressed (Perletti et al., 1996). Arguably, the most conclusive result supporting a role for PKCε in carcinogenesis is that PKCε has been found overexpressed in tumour derived cell-lines and histopathological tumour specimens originating from a variety organs (including: bladder, brain, breast, lung, prostate, head and neck, Varga et al., 2004, Sharif and Sharif, 1999, Pan et al,. 2005, Bae et al., 2007, Aziz et al., 2007, Martinez-Gimeno et al., 1995).

Objectives

PKCε has been recently uncovered as a key regulator acting at the end stage of cytokinesis (Saurin et al., 2008), while the evidence indicates that it functions to trigger RhoA inactivation and consequent actin depolymerization, the precise mechanism remains unclear. Defining the mechanism by which PKCε is localized to the furrow/midbody may shed light on how PKCε control is exerted during cytokinesis and more importantly whether intervention in this process might bring about benefits in the treatment of cancer. Please see Figure 1.10 for a model outlining the current understanding of PKCε regulation and localization.

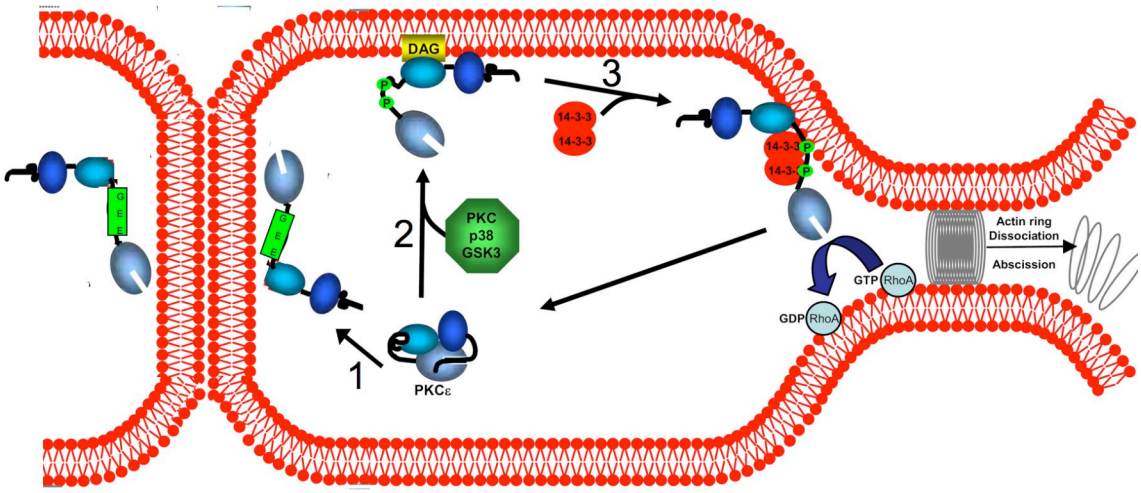

Figure 1-10 Schematic summarizing how PKCε localization is controlled
(Reprinted and adapted with permission from Macmillan Publishers Ltd: Nature Cell Biology, Saurin et al, 10, 891-901, 2008). 1) The GEE motif selectively targets PKCε to cell-cell contacts. 2) Phosphorylation by PKC, p38 and GSK3 and membrane recruitment mediates PKCε-14.3.3 complex assembly (3). This complex then accumulates at the midbody where it is thought to control RhoA-GTP loading and consequent actin depolymerization.

Chapter 2. Materials and Methods

2.1 Materials

2.1.1 General

All reagents were obtained from Sigma Aldrich unless otherwise stated. Restriction enzymes were purchased from New England biolabs and kits for the purification of DNA were from Qiagen. Dulbecco's Modified Eagle Medium (DMEM), penicillin, streptomyocin and Opti-MEM were obtained from Gibco and foetal-calf serum (FCS) was from PAA laboratories. Methanol (MeOH), ethanol (EtOH) and Trizma base were purchased from Fisher. Rabbit skeletal muscle actin and corresponding buffers were from Cytoskeleton. For a list of the pharmacological agents used and their supplier please see table 2.1. Similarly, for antibodies, see table 2.2 and 2.3 for primary and secondary respectively.

All glassware was supplied by CR-UK research services and plasticware was purchased from Eppendorf, Corning, BD Falcon, Sterilin and Scientific Specialities. Glass bottom dishes for use in live microscopy were obtained from MatTek Corporation.

2.1.2 Buffers

DNA loading buffer

0.25% (w/v) bromophenol blue, 40% (w/v) sucrose in water

LB (Agar)

Provided by CR-UK research services. 10 g L^{-1} bacto-tryptone, 5 g L^{-1}yeast extract, 10 g L^{-1} NaCl (6 g agar/400 ml LB).

$LB^{amp/kan}$ (Agar)

100 μg ml^{-1} ampicillin/25 μg ml^{-1} kanamycin in LB (Agar)

LB (Broth)

Provided by CR-UK research services, 10 g L^{-1} bacto-tryptone, 5 g L^{-1}yeast extract, 10 g L^{-1} NaCl

$LB^{amp/kan}$ (Broth)

100 μg ml^{-1} ampicillin/25 μg ml^{-1} kanamycin in LB (Broth)

2 x LDS Sample Buffer

50% (v/v) 4 x LDS Sample Buffer (Invitrogen), 0.2 M DTT

Lysis Buffer

50 mM Tris, pH 7.4, 150 nM NaCl, 0.5% NP40

Kinase Assay Mix

20 mM Tris pH 7.5, 10 mM $MgCl_2$, 1 mg ml^{-1} protamine sulphate, 100 μM ATP and 2.5 mCi [γ-^{32}P] ATP (added last to start the reaction, Amersham)

Kinase Dilution Buffer

20 mM Tris pH 7.5, 2 mM EDTA, 5 mM DTT, 0.02% Triton-X 100

PBS (Ca^{2+}/Mg^{2+} free)

Provided by CR-UK research services. 8 g L^{-1} NaCl, 0.25 g L^{-1} KCl, 1.43 g L^{-1} Na_2HPO_4, 0.25 g L^{-1} KH_2PO_4, pH 7.2

TBS

200 mM Tris pH 7.5, 0.9% (w/v) NaCl

TBS-T

0.1% (v/v) Tween-20 in TBS

TAE

0.04 M Tris, 0.1% glacial acetic acid, 1 mM EDTA

Transfer Buffer

20 mM Trizma base, 200 mM Glycine, 10% MeOH

5% Trypsin/Versene

Provided by CR-UK research services. 0.25% trypsin in versene, pH7.2, filter sterilised.

2.1.3 Pharmacological agents

Regent	Supplier	Solvent	[Stock]	[Working]
Bisindolylmalemide-1 (BIM1)	Calbiochem	DMSO	2 mM	1 μM
Latrunculin A (LatA)	Invitrogen	DMSO	1 mM	100 nM
4-amino-1-tert-butyl-3-(1'natphthyl)-pyrazolo[3,4-d] pyrimidine (NaPP1)	Calbiochem	DMSO	10 mM	4 μM
Phorbol 12-myristate 13 acetate (PMA)	Sigma	DMSO	1.6 mM	100 nM 400 nM

Table 2-1 Pharmacological agents
Pharmacological agents used throughout this thesis. The working concentrations were chosen either in accordance with current literature or identified through titration experiments.

2.1.4 Antibodies

2.1.4.1 ***Primary antibodies***

Name	Supplier	Antigen	Use	Dilution
Goat anti-Actin (I-19) sc-1616	Santa Cruz Biotechnology	Actin C-terminus	Western Blot (WB)	1:1000
Mouse anti-β-catenin	BD Transduction Laboratories	β-catenin	Immunofluorescence (IF)	1:100
Mouse anti-GFP 3E1	CR-UK	GFP	IF	1.500
Mouse anti-RhoA (26C4) sc-418	Santa Cruz Biotechnology	RhoA	IF	1:100
Mouse anti-Tubulin	Sigma	Tubulin	WB IF	1:5000 1:500
Rabbit anti-Ect2 (C-20) sc1005	Santa Cruz Biotechnology	Ect2 C-terminus	IF	1:100
Rabbit anti-Lap2 (H-130) sc-28541	Santa Cruz Biotechnology	Lab2	IF	1:100
Rabbit anti-MKLP1 (N-19) sc-867	Santa Cruz Biotechnology	MKLP1 N-terminus	IF	1:100

Rabbit anti-PKCε (C-15) sc-214	Santa Cruz Biotechnology	PKCε C-terminus	WB IF	1:1000 1:100
Rabbit anti-PKCε p729	Millipore	PKCε p729	WB	1:1000 (+ 1 μg ml^{-1} blocking de-P peptide)

Table 2-2 Primary antibodies
Primary antibodies used throughout this thesis.

2.1.4.2 ***Secondary antibodies***

Name	Provider	Use	Dilution
Alexa-Fluor-488 anti-mouse	Invitrogen	IF	1:500
Alexa-Fluor-488 anti-rabbit	Invitrogen	IF	1:500
Alexa-Fluor-543 anti-mouse	Invitrogen	IF	1:500
Alexa-Fluor-647 anti-mouse	Invitrogen	IF	1:500
Alexa-Fluor-647 anti-rabbit	Invitrogen	IF	1:500
Alex-Fluor-555 phalloidin	Invitrogen	IF	1:500
Donkey anti-rabbit HRP	GE Healthcare	WB	1:5000
Donkey anti-Goat HRP	Santa Cruz Biotechnology	IB	1.5000
IRDye 680LT anti-mouse	Li-COR Biosciences	WB	1:10000

IRDye 800CW anti-rabbit	Li-COR	WB	1:10000
Sheep anti-mouse HRP	GE Healthcare	WB	1;5000

Table 2-3 Secondary antibodies
Secondary antibodies used throughout this thesis.

2.2 Methods

2.2.1 Molecular biology

2.2.1.1 Polymerase Chain Reaction

Polymerase chain reactions (PCRs) were performed using a DNA Engine Dyad (MJ Research). The reaction mix used was as follows: 1 µl Pfu Ultra (Stratagene), 2.5 µl 10 x Pfu buffer (Stratagene), 2.5 µl 10 mM dNTPs, 2 x 100 pmol primer and 10 ng DNA template, made up to 25 µl in distilled water. The programme used was as follows, unless otherwise specified:

Step 1: 94°C, 5 mins

Step 2: 94°C, 10 secs

Step 3: (lowest primer Tm – 3)°C, 1 minute

Step 4: 72°C (length of product in bps/500) mins

Cycle back to step 2 x 30

Step 5: 72°C, 10 mins

Step 6: 6°C hold

PCR products were examined by agarose gel electrophoresis (see below) and purified using either the QIAquick Gel Extraction Kit or the QIAquick PCR Purification Kit according to the manufacturer's instruction.

2.2.1.2 Restriction digests

Restriction digests were performed in accordance with the manufacturer's instruction.

2.2.1.3 Agarose gel electrophoresis and gel purification

Samples were diluted in a 5:1 volume ratio in DNA loading buffer and separated on a 0.8% agarose gel, supplemented with 1 μM ethidium bromide, in 1x TAE buffer. Samples were run alongside a 1kb DNA ladder (Invitrogen). The DNA bands were visualised on a UV light box (254 nm wavelength) and excised as required. DNA extraction and purification were performed using the QIAquick Gel Extraction Kit.

2.2.1.4 Ligation

The ligation reaction mix used was as follows: 0.5 μl T4 DNA ligase (New England Biolabs), 2.5 μl 10 x ligase buffer (New England biolabs), 100 ng digested vector and an appropriate amount of insert DNA to achieve a typical 3:1 molar ratio (insert:vector). Ligation reactions were left overnight at room temperature.

2.2.1.5 Transformation

One Shot® chemically competent cells (Invitrogen) were transformed with purified plasmids or ligation reactions according to the manufacturer's instructions. The transformation mix was plated on LB selective agar plates (LB^{amp} or LB^{kan}) and incubated overnight at 37°C.

2.2.1.6 DNA preparation

A single transformed bacterial colony was inoculated into 5 ml LB selection media (LB^{amp} or LB^{kan} broth) and incubated overnight at 37°C with vigorous shaking. The culture was processed by the QIAprep Spin Miniprep Kit according to the manufacturer's instruction and the purified DNA was sequenced (see below). For large scale DNA production, the starting culture was diluted 1:1000 into selection media (LB^{amp} or LB^{kan} broth) and incubated for a further 16 hours at 37°C with vigorous shaking. The culture was processed by QIAprep Spin Maxiprep kit according to the manufacturer's instructions. The concentration of the purified DNA was measured by the NanoDrop 2000 (Thermo Scientific) and diluted to a stock concentration of 500 $\mu g\ \mu l^{-1}$.

2.2.1.7 DNA sequencing

DNA sequencing was performed using the BigDye® Terminator Kit (Applied Biosystems) according to the manufacturer's instructions. The reaction mix used was as follows: 150 ng DNA template, 3.2 pmol primer (PKCε sequencing primers were from Dr Angus Cameron and were chosen so as to achieve full coverage) and 8 μl 1xBigDye® Terminator Mix in sequencing buffer made up to a final volume of 20 μl in distilled water. The cycle sequencing programme used was as follows:

Step 1: Ramp to 96°C at 2.5°C sec^{-1}

Step 2: 96°C, 1 min

Step 3: 96°C, 10 sec

Step 4: Ramp to (primer Tm – 3)°C at 1°C sec^{-1}

Step 5: (primer Tm – 3)°C, 5 sec

Step 6: Ramp to 60°C at 1°C sec-1

Step 7: 60°C, 4 min

Cycle back to Step 3 x 24

Step 8: 12°C forever

To obtain clean sequencing data, the reaction products were purified using the DyeEx2.0 Spin Kit according to the manufacturer's instructions. Sequencing was performed by CR-UK services on an Applied Biosystems 3730 DNA Analyser. The sequencing results were opened with Edit View software and analysed by DNA Strider software and Clustal W2 multiple sequence alignment.

2.2.2 Cloning

The original cloning of the PKCε-WT cDNA into the pEGFP-C1 and pDsRed-Monomer-C1 vector (Clontech) was performed by Dr Adrian Saurin, as was the site directed mutagenesis for PKCε-M486A and PKCε-S346/368A, in pEGFP-C1, using the Quick change XL kit (Stratagene). The subcloning of the GFP-PKCε-WT and GFP-PKCε-M486A into the tetracycline inducible pcDNA5/FRT/TO© vector was performed by Dr Angus Cameron.

GFP-PKCε-S346/368A was subcloned into the pcDNA5/FRT/TO© vector by manipulating the pcDNA5/FRT/TO©-GFP-PKCε-M486A plasmid. The GFP and first 1204 base pair sequence were removed, leaving the M486A site, by digestion of the unique restriction sites Kpn1 and Afe1 and replaced with GFP-PKCε-S346/368A.

The E374G point mutation was introduced into the pcDNA5/FRT/TO© GFP-PKCε-M486A using the QuickChange XL kit according to the manufacturer's instructions. The primers used to obtain the mutated E374G were as follows:

Forward 5'-GACAACCGAGGA**GGG**GAGCACCGAGCG-3' (GAG → GGG)

Reverse 5'-CGCTCGGTGCTC**CCC**TCCTCGGTTGTC-3'

The deletion mutagenesis for GFP-PKCε-ΔIC1D-M486A was performed using a 2-step PCR based mutagenesis approach (Figure 2.1).

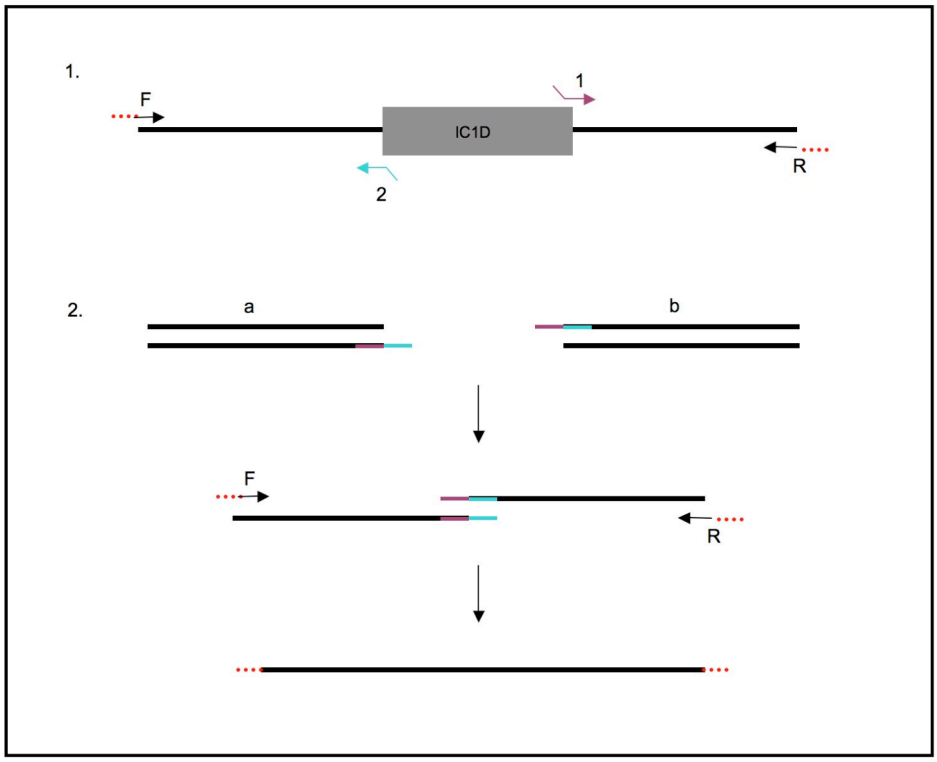

Figure 2-1 2-step PCR base approach for the IC1D deletion mutant
A schematic representation of the 2-step PCR based approach used for IC1D deletion mutagenesis. Primers are represented by arrows; red zigzags denote non-complementary sequences incorporating restriction sites for subsequent ligation reactions. Blue and purple (step 2) denote the overhangs created by the same coloured primer (from step 1).

Briefly, primer F and 2 were used to amplify product a, primer R and 1 were used to amplify product b from a pcDNA5/FRT/TO©-GFP-PKCε-M486A template. Products a and b were purified by PCR purification, analysed by gel electrophoresis and used in combination as a template in PCR using F and R primers only.

The primers used in construction of GFP-PKCε-ΔIC1D-M486A were as follows:

F 5'-TAATAATA**GGTACC**CGCCACCATGGTGAGCAAG-3', [*][**Kpn1**][5'GFP]

R 5'-ATTATTAT**GCGGCCGC**CTCAGGGCATCAGGTCTTCACCAAA-3'
[*][**Not1**] [3'Eps]

1 5’ATTATTACAAAGTGCGCTGAGGTGGGCTCCCAACGG-3’,

2 5’-CCGTTGGGAGCCCACCTCAGCGCACTTTGTAATAATGAGCT-3’

* Denotes non-complementary blank sequence.

The M486A site was subcloned into the pDsRed-Monomer-C1 vector (Clontech) by manipulating the pcDNA5/FRT/TO©-GFP-PKCε-M486A plasmid, the PKCε surrounding the M486A site were removed by digestion of the unique restriction sites Afe1 and Not1 and replaced with M486A.

mCherry-Histone 2B was kindly provided by Professor Daniel Gerlich, MARS-Lifeact-RFP was from Dr Steven Cooper and mCherry-RhoA was a gift from Dr Eric Sahai.

2.2.3 Mammalian cell culture

2.2.3.1 Cell lines

Human embryonic kidney 293 cells (HEK 293) were obtained by CR-UK research services. Flp-In™ T-Rex™-HEK 293 cells were purchased from Invitrogen.

2.2.3.2 Cell culture and transfection

Cells were cultured in DMEM containing 10% FCS, penicillin (50 units ml^{-1}) and streptomycin (50 μg ml^{-1}) at 37°C in a humidified 10% CO_2 atmosphere. Flp-In™ T-Rex™-HEK 293 cells were transfected with the pcDNA5/FRT/TO© vector encoding GFP-PKCε-WT, GFP-PKCε-M486A, GFP-PKCε-E374G-M486A, PKCε-S346/368A-M486A and GFP-PKCε-ΔIC1D-M486A using the T-Rex™ system according to the manufacturer’s instructions. Polyclonal GFP-PKCε cell lines were then selected with

hygromycin B (50 μg ml^{-1}, Invitrogen) for 4-6 weeks. To induce GFP-PKCε expression, cells were treated with tetracycline (100 ng ml^{-1}) 24 hours prior to assay.

The RFP-PKCε-M486A, cherry-H2B, MARS-lifeact-RFP and cherry-RhoA constructs were transiently transfected using Fugene 6 (Roche) according to the manufacturer's instructions. Briefly, DNA and Fugene 6 in Opti-MEM were added directly to culture media 48 hours prior to imaging.

2.2.4 Live confocal microscopy

Cells were plated on poly-L-lysine coated 35 mm glass bottom dishes in DMEM containing 10% FCS, penicillin (50 units ml^{-1}) and streptomycin (50 μg ml^{-1}). To induce GFP-PKCε expression, cells were treated with tetracycline (100 ng ml^{-1}) 24 hours prior to imaging. Cells were imaged using an inverted laser scanning confocal microscope (LSM 510, Carl Zeiss) using a Plan Apochromat oil immersion objective (x63, NA 1.4) and 488 nm/543 nm/585 nm excitation lines for GFP, RFP and mCherry respectively. The microscope was contained within a polymethylmethacrylate case and maintained at a constant temperature of 37°C with a 5% CO_2 flow. Stacks were filmed every 30 seconds for varying lengths of time and each frame (512 x 512) was comprised of 5 'Z' sections averaged over 8 μm in the z axis Movies, representing a single 1 μm 'Z' optical section of cells were exported using the LSM software (Carl Zeiss).

2.2.5 Fluorescence Recovery After Photobleaching

Live-cell fluorescence recovery after photobleaching (FRAP) experiments were performed using the above microscopic set up. GFP-PKCε-M486A cells were incubated with NaPP1 (4 μM) for 10 minutes and EGTA (4 mM) was added as indicated. Each FRAP experiment comprised a sequence of 300 frames (128 x 128, pixel dwell time of

6.40 μs, pixel size 0.37 μm) including 10 pre-bleached frames. The bleaching process consisted of 100 iterations at 90% of bleach pulse (488 nm laser excitation, 30 mW) on a circular region of 2 pixels in area, within the midbody or at cell-cell contacts. Recovery was monitored by capturing a further 290 scans after the photobleach event. Quantification was performed using the FRAP module included in the LSM software (Carl Zeiss) and plotting the graphs to a best fit two exponential model $I = I_0 - I_1 e^{-t/T1} - I_2 e^{-t/T2}$. Where I_0 is the intensity before bleach, I_1 and I_2 are the mobile fractions and T_1 and T_2 the time constants. The average of 20 measurements are presented for all conditions and the data was analysed for statistical significance using student t-test.

2.2.6 Optical trapping

Trapping experiments were performed by John Phillips, Imperial College. Briefly, cells were detached from tissue culture coated flasks by treatment with accutase (PAA laboratories) for 5 minutes, followed immediately by dilution with DMEM containing 10% FCS, penicillin (50 units ml^{-1}), streptomycin (50 μg ml^{-1}) and NaPP1/EGTA was added when indicated. Cells were then transferred to Sigmacote coated coverslips. Cells were trapped using a dual-optical trap system built onto the rear port of a Nikon TE2000-E microscope using a Plan Apochromat water immersion objective (x 60, NA 1.2). The trapping beam (IPG Photonics) was fed into the microscope light pathway via a dichroic mirror beam splitter. Cells of equivalent size were trapped with 100 mW of laser power at the sample plane and brought into contact with each other. Still images of both brightfield and fluorescence were acquired prior to cell contact, at cell contact and at 5-10 minute intervals thereafter. The images were analysed with Vision Assistant software (National Instruments). A line profile was taken across both cells and the relative fluorescence across the system was plotted.

2.2.7 Immunofluorescence

Cells were plated on acid-washed, poly-L-lysine coated coverslips in DMEM containing 10% FCS, penicillin (50 units ml^{-1}) and streptomycin (50 μg ml^{-1}). To induce GFP-PKCε expression, cells were treated with tetracycline (100 ng ml^{-1}) 24 hours prior to assay (see figure legends for conditions of individual assays). Cells were then fixed in 4% paraformaldehyde/PBS (or 10% trichloroacetic acid/water for RhoA) for 15 minutes, washed in PBS and then permeabilized and blocked using 0.2% Triton X-100/2% BSA/TBS for another 15 minutes, all at room temperature. The coverslips were incubated with the described primary antibody (Table 2.2, diluted in 2% BSA/TBS) for 1 hour at room temperature, washed 3 times in PBS and then stained using the described secondary antibody (Table 2.3, diluted in 2%BSA/TBS). The coverslips were washed twice more in PBS and once in water and mounted onto glass slides using Proglong® Gold Antifade Reagent (Invitrogen). Slides were stored at 4°C protected from light. Images were acquired using an upright laser scanning confocal microscope (LSM510, Carl Zeiss) using a Plan Apochromat oil immersion objective (x63, NA 1.4) and 405 nm/488 nm/543 nm/633 nm excitation lines for DAPI, GFP, RFP and far red respectively. Individual channels were scanned sequentially and each image (1024 x 1024) represents a single 1 μm 'Z' optical section of cells.

2.2.8 Western blotting

Cells were cultured in 6-well tissue culture coated plates in DMEM containing 10% FCS, penicillin (50 units ml^{-1}) and streptomycin (50 μg ml^{-1}). To induce GFP-PKCε expression cells were treated with tetracycline (100 ng ml^{-1}) 24 hours prior to treatment as described in figure legends. On ice, cells were washed in PBS and harvested by scraping into 500 μl LDS sample buffer. Lysed samples were heated to 100°C for 10 minutes (for actin cosedimentation preparation see below). SDS-PAGE was performed using the NuPAGE system with BisTris/4-12%-polyacryladmide gels and MOPS/SDS

running buffer according to the manufacturer's instructions (Invitrogen). Samples were run alongside Full Range Rainbow™ Molecular Weight Markers (GE Healthcare). Proteins were transferred to methanol-soaked PVDF membranes (Millipore) using a Trans-Blot Cell (Bio-Rad) and transfer buffer. Immunoblots were blocked for 1 hour in TBST and 3% BSA and then incubated for a further hour with the described primary antibodies (diluted in 3% BSA/TBST). The membranes were then washed 3 times for 10 minutes with TBST and incubated for one hour with the appropriate secondary antibodies (diluted in 5% non-fat dry milk/TBST). Following a final wash (3 times for 10 minutes with TBST) bands were visualised by enhanced chemiluminescence (ECL®, GE Healthcare) and Kodak BioMax film or using the Odyssey infrared imaging system (LI-COR Biosciences) according to the manufacturer's guidelines.

2.2.9 Kinase assay

Cells were cultured in 75 cm^2 tissue culture coated flasks in DMEM containing 10% FCS, penicillin (50 units ml^{-1}) and streptomycin (50 μg ml^{-1}). To induce GFP-PKCε expression cells were treated with tetracycline (100 ng ml^{-1}) 24 hours prior to assay. On ice. cells were washed in PBS and harvested by scraping into pre-chilled lysis buffer and complete protease inhibitor cocktail (Roche). Insoluble material was removed by centrifugation at 14,000 g for 5 minutes at 4°C and incubated with 20μl GFP trap beads (Chromotek) and rotated at 4°C for 1 hour. GFP bound complexes were washed 3 times in 1 ml lysis buffer at 4°C. To estimate PKCε concentration, samples were run alongside BSA controls in SDS-PAGE and were analysed by coomasie staining (see below).

Kinase assays were performed in a total volume of 40 μl kinase assay mix with PKCε (or the equivalent volume for the control). The reaction was started by the addition of ATP and incubated at 30°C with shaking. To stop the reaction, 15 μl of mix was spotted onto P81 phosphocellulose paper (Whatman) and washed 3 times for 5 minutes in acetic acid. The radioactivity was measured by Cerenkov counting in a Beckman LS6000IC

alongside stock ATP. All the reactions were performed in triplicate. In the assay pmol ^{32}P /min was calculated by: [(rc-b/sa) x 2.67]/10, where rc is raw counts incorporated into substrate, b is the average blank, 2.67 is a correction factor for transfer to phosphocellulose paper (15 μl spotted from a 40 μl sample) and 10 is the incubation time in min. The activity was converted from pmol ^{32}P /min to pmol ^{32}P /min/dish by multiplying by the overall dilution factor, 20.

2.2.10 Coomassie blue staining

SDS-PAGE gels were washed 3 x 5 minutes in distilled water and incubated in 20 ml GelCode Blue Stain Reagent (Thermo Scientific) at room temperature overnight with gentle shaking. Gels were destained in distilled water until bands were visible. Images were scanned using a MicroTek Scan Maker i700 and analysed using Image J quantification software.

2.2.11 Actin cosedimentation

Cells were cultured in 75 cm^2 tissue culture coated flasks in DMEM containing 10% FCS, penicillin (50 units ml^{-1}) and streptomycin (50 μg ml^{-1}). To induce GFP-PKCε expression cells were treated with tetracycline (100 ng ml^{-1}) 24 hours prior to assay. On ice, cells were washed in PBS and harvested by scraping into 1 ml pre-chilled lysis buffer with complete protease inhibitor cocktail (Roche). The lysates were pre-cleared by centrifugation at 100, 000 x g for 1 hour at 4°C. Freshly depolymerized rabbit skeletal muscle actin (50 μg) in actin buffer (200 μl, Cytoskeleton) were added to the resultant supernatant, along with 100 μl of polymerization buffer (Cytoskeleton) and samples were incubated for 1 hour at room temperature in the presence or absence of PMA as indicated. Samples were centrifuged at 100, 000 x g for 1 hour to precipitate

polymerized actin. The pellet fraction was solubilized in 20 µl LDS-Sample buffer and analysed by western blot (see above).

Chapter 3.

Distinct kinetic properties of PKCε at the cytokinetic furrow/midbody and cell-cell contacts

3.1 Summary

PKCε has been shown to localize to cell-cell contacts and to juxtaposed membranes in the cytokinetic furrow/midbody under specific conditions. To assess the relationship between these two localization responses I have compared the behaviour of PKCε-M486A during both processes. Using optical traps to manipulate cell-cell contacts, we have demonstrated that GFP-PKCε-M486A recruitment to these contacts is not modulated by the cell cycle and cannot be distinguished from that at the furrow/midbody. In contrast fluorescence recovery after photobleaching (FRAP) experiments have shown that GFP-PKCε-M486A furrow/midbody turnover is significantly slower than that at cell-cell contacts. This data indicates that despite the membrane juxtaposition of presumptive daughter cells at the furrow/midbody, the recruitment and/or retention of PKCε in this location is a distinct property and is not simply a reflection of cell-cell contacts.

3.2 Introduction

All PKCs contain an amino-terminal regulatory domain and a carboxyl-terminal catalytic domain. In contrast to their variable regulatory domains, the catalytic domains are highly conserved, with each containing an ATP binding site and a protein substrate-binding cleft (Mellor and Parker, 1998). The gatekeeper residue, which sits at the bottom of the ATP-binding pocket can be exploited to generate mutants that are specifically inhibited by kinase inhibitor analogues (Bishop et al., 2000). Point mutation of the bulky M486 residue within the ATP-binding pocket of PKCε (PKCε-M486A) renders the kinase almost uniquely sensitive to inhibition by the Src kinase-inhibitor analog, NaPP1 (Qi et al., 2007, Durgan et al., 2008). Interestingly, the selective inhibition of PKCε-M486A with NaPP1 causes localization of the enzyme at the plasma membrane and at the cytokinetic furrow/midbody. It has also been reported that activated PKCε, alongside PKCα, is found to accumulate selectively at cell-cell contacts in mouse pituitary glands, the rat pituitary GH3B6 cell line and at contacts between fibroblasts and epithelial cells upon either physiological or pharmacological activation (Collazos et al., 2006), (Quittau-Prevostel et al., 2004). While the initial plasma membrane recruitment is thought in part to be a function of DAG formation, the striking behaviour of PKCε at the furrow/midbody is possibly indicative of an interaction with a further membrane component(s) and this may relate to its accumulation at cell-cell contacts.

During the furrowing process the presumptive daughter cells plasma membranes become juxtaposed in a manner that might trigger conventional cell-cell contact responses. If evidence is generated to indicate that only contact is required for furrow/midbody accumulation it means that PKCε behavior at the furrow/midbody becomes a much more simple model to dissect given that PKCε candidates involved in cell interactions, such as cadherins can be readily tested.

Therefore, in this chapter, I address the relationship between cell-cell contact and furrow/midbody associated recruitment to determine whether the two are the same process. In collaboration with The Chemical Biology Centre, Imperial College, we use

optical traps to manipulate cell-cell contacts between interphase and mitotic cells and are able to show that recruitment of PKCε-M486A to these contacts is not cell cycle specific but cannot resolve whether the two processes are related. By contrast, analysing the dynamics of PKCε-M486A at cell-cell contacts and furrow/midbody by FRAP (Figure 3.1) I show that PKCε-M486A turnover at the furrow/midbody is slower than that at cell-cell contacts, which suggests a distinct recruitment and/or retention of PKCε at this compartment. In an attempt to probe regulatory differences, we discovered that dissociation of PKCε-M486A from cell-cell contacts in suspended cells is surprisingly dependent on Ca^{2+}.

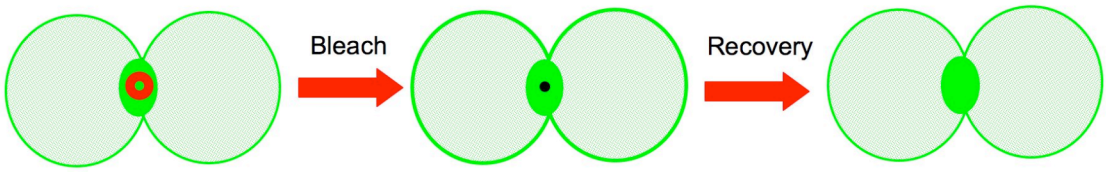

Figure 3-1 FRAP and its quantitative analysis
A simple schematic is shown to illustrate the process of FRAP as applied to the experiments here addressing the turnover at the midbody. A strong laser beam is focused to a Region Of Interest (ROI, shown here as a red circle in the furrow/midbody). The strong irradiation bleaches the fluorescence in the ROI (shown here as a black circle). Bleached molecules can then be exchanged for unbleached molecules (from either the cytoplasm or plasma membrane) and the intensity of the ROI gradually recovers. Fluorescence recovery must be monitored over time and the resultant data fit using exponential equations (see results). Kinetic parameters can then be extracted from the graph.

3.3 Results

3.3.1 Localization of PKCε-M486A at cell-cell contacts and furrow/midbody in response to NaPP1

To address the question of whether PKCε recruitment to cell-cell contacts was related to the accumulation at juxtaposed membranes in the cytokinetic furrow/midbody, flp-in T-Rex cells were used to generate tetracycline inducible expression of GFP-PKCε-WT and the NaPP1 sensitive gatekeeper mutant GFP-PKCε-M486A. NaPP1 addition to induced M486A cells, as expected, leads to a transient membrane accumulation and a more sustained furrow/midbody accumulation in mitotic cells with a concomitant delay in the final stage of cytokinesis (Figure 3.2A, Video 1). This cell-cell contact behaviour is in accordance with the pattern of response reported for PKCε in pituitary cells where agonist-dependent, transient, distributed membrane recruitment is followed by PKCε accumulation at cell-cell contacts (Quittau-Prevostel et al., 2004). In the absence of NaPP1, cells complete cytokinesis normally with no change in the distribution of GFP-PKCε-M486A (Figure 3.2B, Video 2) or GFP-PKCε-WT (Figure 3.3). Similarly, NaPP1 addition to induced WT cells caused no change in the distribution of GFP-PKCε-WT and cells complete cytokinesis normally, showing that the accumulation at the furrow/midbody seen upon NaPP1 addition is a result of specific GFP-PKCε-M486A targeting (Figure 3.3).

Optical traps were then employed on the model cell lines to compare interphase and mitotic behaviour, the latter of which were defined according to their dumbbell shape. Unfortunately, however, we haven't been able to conclusively prove the mitotic nature of these cells. Nevertheless, using optical traps to manipulate cell-cell contacts it was evident that in the presence of NaPP1 GFP-PKCε-M486A accumulated at juxtaposed cell-cell contacts (Figure 3.4). In the absence of NaPP1 or with GFP-PKCε-WT expressing cells no evidence of cell-cell contact accumulation was observed.

A

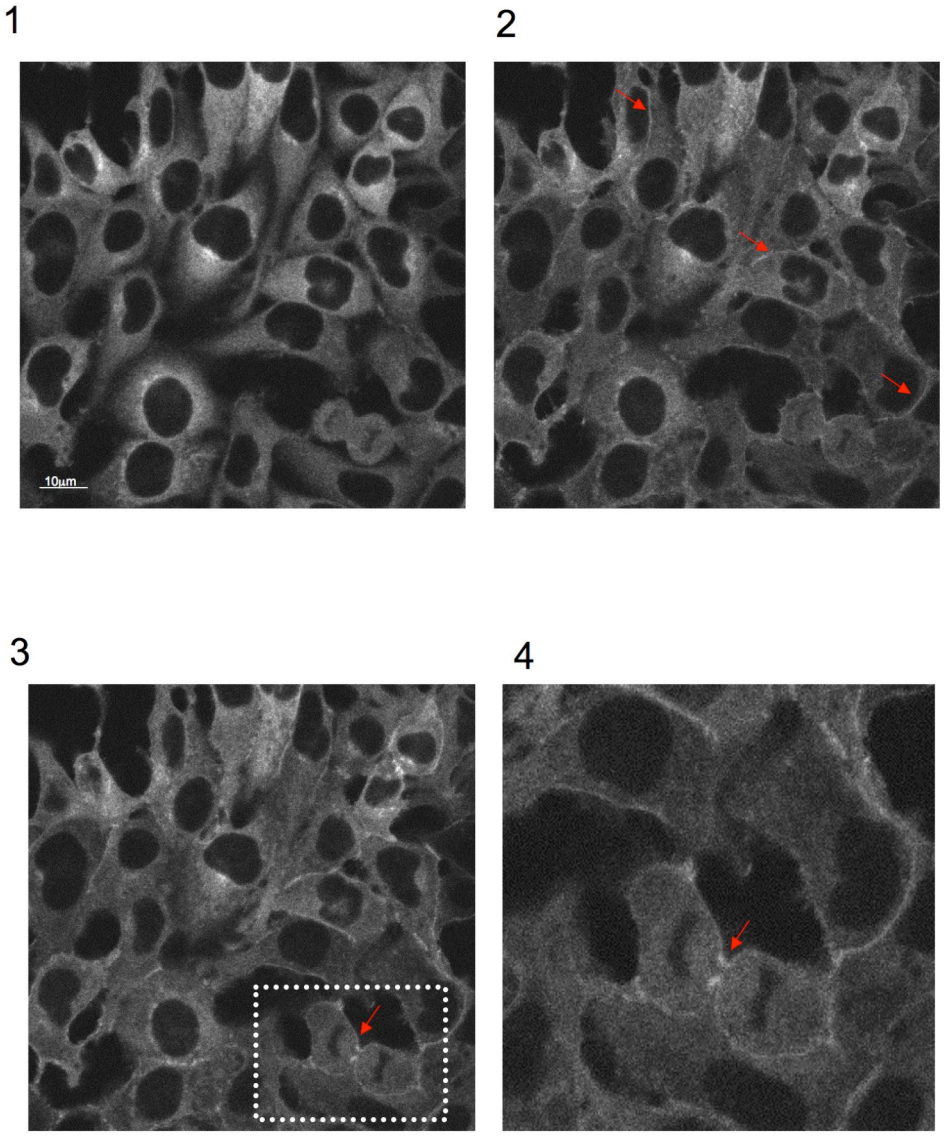

B

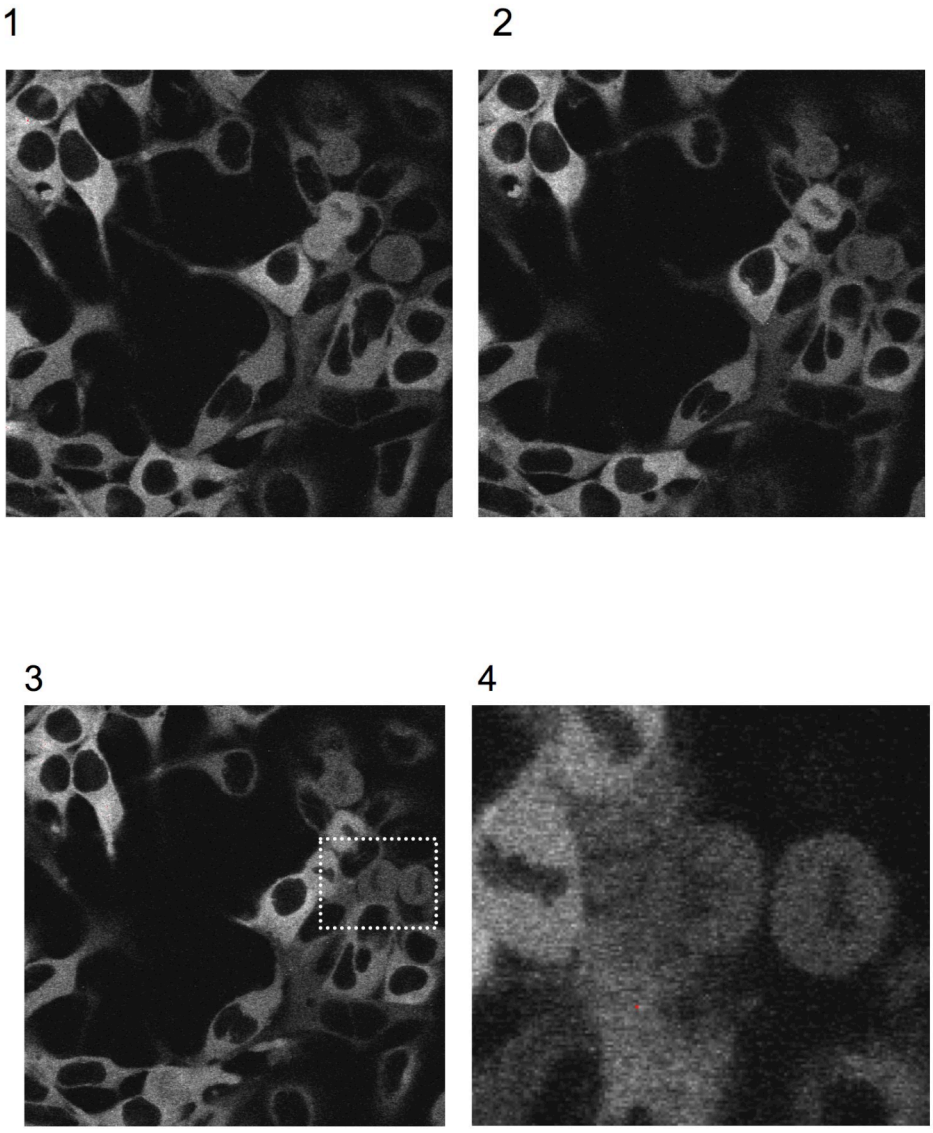

C

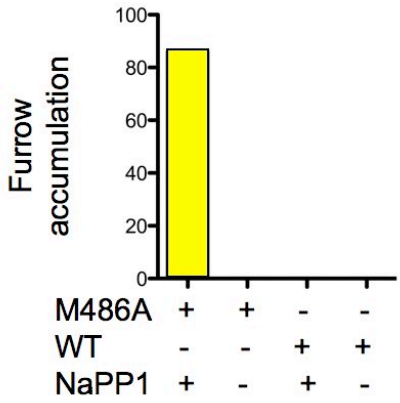

Figure 3-2 Selective inhibition of PKCε-M486A results in localization at the plasma membrane and cytokinetic furrow/midbody
Still images, taken from a time-lapse video of 30 second intervals, of the M486A cell line in the presence of NaPP1 (4 μM, A) or the absence of NaPP1 (B). A) Arrowheads in panel 2 indicate relative GFP accumulation at the plasma membrane whilst that in panel 3 is indicative of midbody accumulation in an actively dividing cell. Panel 4 is an enhanced image (magnified white box in panel 3, 2.5X) of this mitotic cell. This accumulation persists for several hours with a temporary arrest in cytokinesis. B) In the absence of NaPP1, cells complete cytokinesis normally with no change in the distribution of GFP. C) Quantification of PKCε-M486A and PKCε-WT accumulation at the furrow/midbody in the presence or absence of NaPP1, n=50.

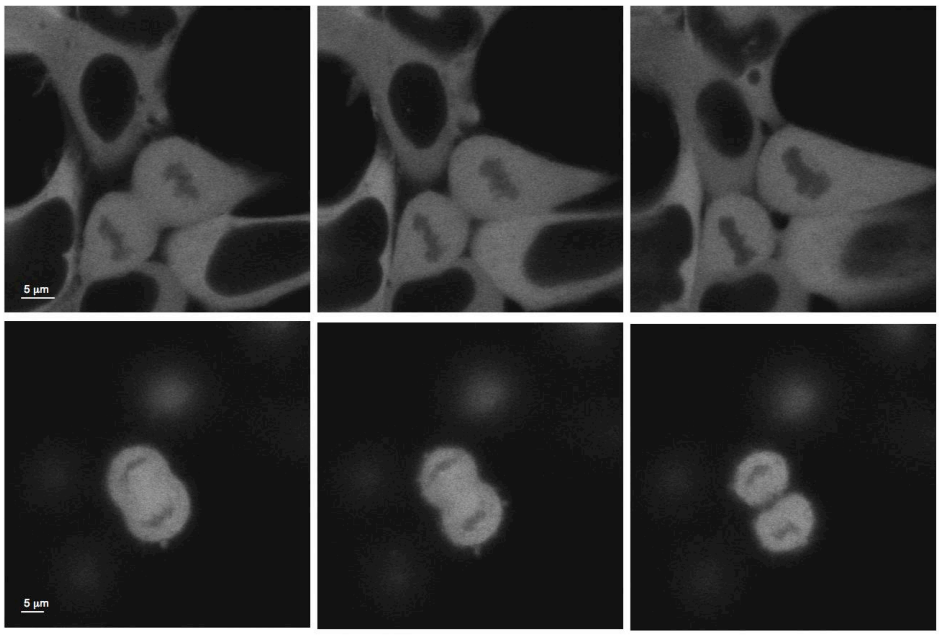

Figure 3-3 PKCε-WT does not localize to the plasma membrane or the cytokinetic furrow/midbody
Still images, taken from a time-lapse video taken at 30 second intervals, of the WT cell line in the presence of NaPP1 (4 μM, top) or the absence of NaPP1 (bottom). Regardless of treatment, cells complete cytokinesis normally with no change in the distribution of GFP.

A B

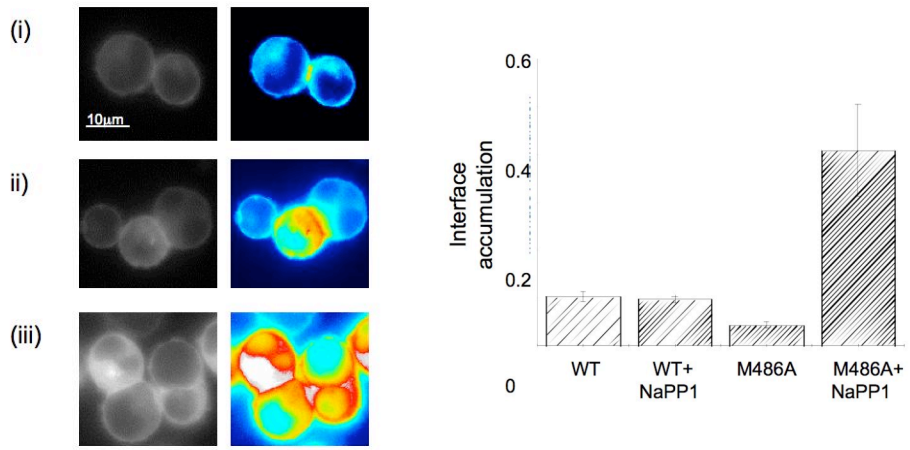

Figure 3-4 Selective inhibition of PKCε-M486A results in localization at cell-cell contacts in TRAP manipulated cells
A) Fluorescence and false colour images of M486A suspended cells in the presence of NaPP1. (i) two interphase cells; (ii) one interphase and one mitotic cell; (iii) two mitotic cells. Mitotic cells have been defined here according to their dumbbell shape. B) Changes in accumulation of PKCε at the cell-cell interface between two interphase cells. The increase in relative fluorescence shown here indicates how much more PKCε is present at the interface compared to the rest of the cell.

In these trapping experiments and those that follow, I prepared the biological samples and the trapping was carried out by John Phillips. I interpreted the resultant data.

3.3.2 Localization of PKCε-WT at the furrow/midbody in response to Bim1

To ensure that PKCε-M486A localization at the furrow/midbody is a consequence of specific PKCε inhibition and not merely an off-target effect of NaPP1 on PKCε-M486A, PKCε-WT was exposed to the structurally distinct PKC inhibitor bisindolylmaleimide 1 (Bim1). Similar to the PKCε-M486A response to NaPP1, Bim1 addition induced PKCε-WT furrow/midbody accumulation. Intriguingly, Bim1 treatment did not mediate PKCε-WT accumulation at the plasma membrane, this perhaps reflects a dependence on other Bim1 sensitive activities for its retention here when inactive or a less efficient inhibition (Figure 3.5).

3.3.3 FRAP experiments distinguish between the kinetics of PKCε-M486A at cell-cell contacts from that at the furrow/midbody

The lack of any distinction between mitotic and interphase cells, however, did not resolve whether recruitment of PKCε-M486A to cell-cell contacts and the furrow/midbody were related. In an attempt to distinguish between the two I measured the dynamics of PKCε-M486A at cell-cell contacts and the furrow/midbody using FRAP in the presence of NaPP1. Given that this approach was not routinely used in the institute, I initially titrated the area of the region of interest (ROI) and bleach intensity of the highly focused laser beam. The area of the ROI was optimised so as to avoid a significant amount of interference in data collection as seen if the area is too small but to avoid photobleaching damage as a consequence of too large an area (see material and methods for dimensions). The bleach intensity was optimised so as to avoid a saturated photobleaching effect. Furthermore, maximal recovery was found by capturing scans over a 80s period and a similar extent of recovery was observed at both compartments. Figure 3.5A illustrates a typical set of recovery images from a FRAP experiment, whilst Figure 3.6B shows typical recovery curves from data gathered in

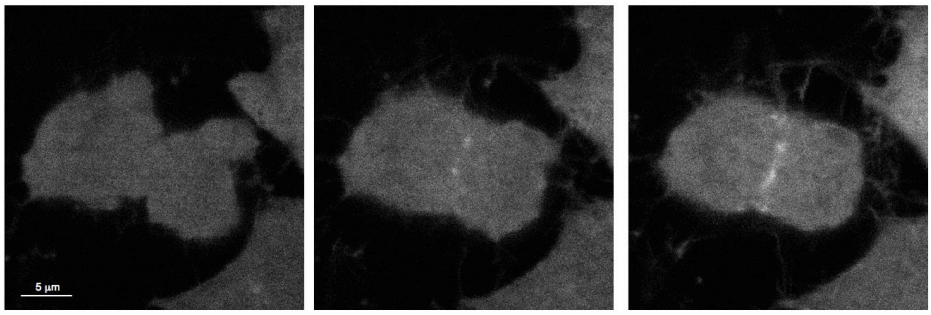

Figure 3-5 Inhibition of PKCε-WT results in localization at the cytokinetic furrow/midbody
Still images, taken from a time-lapse video with 30 second intervals from the point of addition, of the WT cell line in the presence of Bim1 (1 μM). In the absence of Bim1 see Figure 3.2.

A

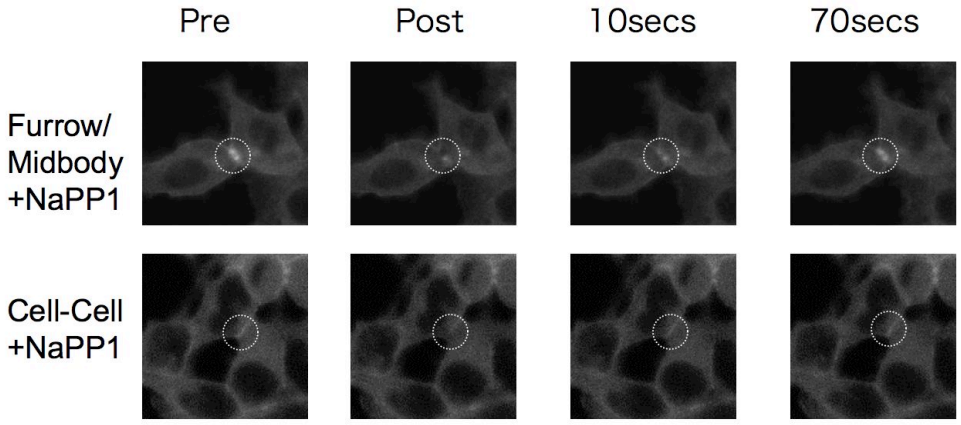
Pre
Post
10secs
70secs
Furrow/
Midbody
+NaPP1
Cell-Cell
+NaPP1

B

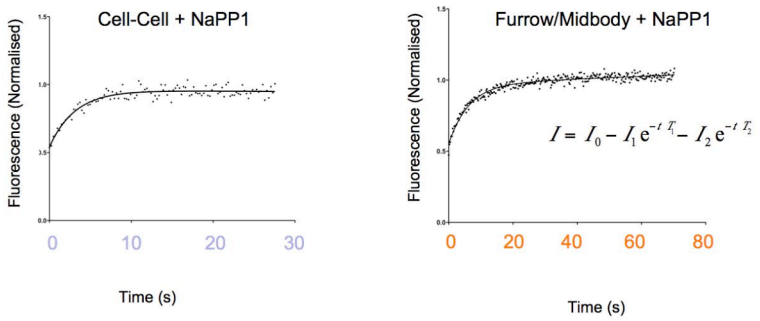
Cell-Cell + NaPP1
Fluorescence (Normalised)
0
10
20
30
Time (s)
Furrow/Midbody + NaPP1
Fluorescence (Normalised)
$I = I_0 - I_1 e^{-t/T_1} - I_2 e^{-t/T_2}$
0
20
40
60
80
Time (s)

C

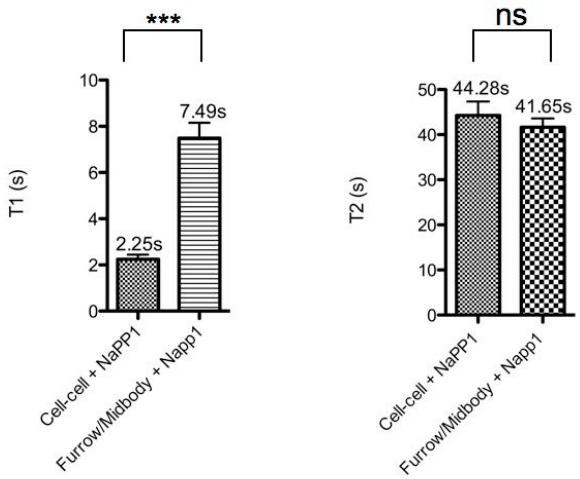
***
T1 (s)
10
8
6
4
2
0
7.49s
2.25s
Cell-cell + NaPP1
Furrow/Midbody + Napp1
ns
T2 (s)
50
40
30
20
10
0
44.28s
41.65s
Cell-cell + NaPP1
Furrow/Midbody + Napp1

Figure 3-6 PKCε-M486A turnover is significantly slower at the furrow/midbody than that at cell-cell contacts

A) Typical images obtained from a confocal time series for cells pretreated with NaPP1. Cells were bleached at either a cell-cell contact or the midbody (indicated by white circle) and fluorescence recovery was monitored at 248 ms intervals over 70 s. B) Typical normalized recovery curves from (A) fitted to a double exponential model: $I = I_0 - I_1 e^{-t/T_1} - I_2 e^{-t/T_2}$. C) Pooled data (n=20) for T_1 and T_2, determined as in (B), T_1 values averaged at 2.25 s and 7.49 s for cell-cell contacts and midbody respectively and are significantly different (determined using a student t-test and the level of significance indicated here by *). T_2 values are not significantly different (ns).

3.6A The recovery data of the mobile fraction were best fitted using the FRAP module in the LSM software (see materials and methods) and found to be of a better fit if plotted to a two exponential model as opposed to a one exponential model. Using such a model, two distinct kinetic components I_1 and I_2 with corresponding fast (T_1) and slow (T_2) recovery times, both of which are proportional to the time it takes for 50% of the fluorescence to be recovered, are determined. Indeed, use of a two exponential model is consistent with the populations of PKCε-M486A in existence. There appears to be a fast diffusing cytosolic PKCε-M486A population (with a recovery time indicated by T_1) and a much slower diffusing PKCε-M486A membrane population (with a recovery time indicated by T_2). Pooled T_1 and T_2 values are shown in Figure 3.6C for each compartment. Although there is no significant difference between the pooled T_2 values, which suggests an equal contribution from the plasma membrane PKCε population to the ROI at both cell-cell contacts and the furrow/midbody, there is a significant difference in the pooled T_1 values. PKCε-M486A turnover at the furrow/midbody is significantly slower than at cell-cell contacts. The mean value for furrow/midbody recovery is 7.49±0.67 seconds compared with 2.25±0.2 seconds at cell-cell contacts, which suggests that these compartment retentions are distinguishable and are driven by distinct mechanisms. Furthermore, the kinetic analysis has been confirmed independently of the FRAP module on the LSM software by exporting the raw recovery data into Microsoft Excel with the appropriate formula pre-programmed, which corrects for background fluorescence, normalizes the resultant data and corrects for bleaching. The recovery curves were then plotted using a biexponential model pre-programmed into the Prism software. The resultant kinetics were found to be consistent with those obtained from the LSM software (see Appendix).

3.3.4 A Ca^{2+}-dependent PKCε-M486A 'off rate' at cell-cell contacts in suspended cells only

To probe potential regulatory differences between the two recruitment processes, we assessed whether the production of DAG involved the classical Ca^{2+} dependent PI-

specific phospholipase C pathway. This was tested initially by depleting cells of Ca^{2+} using the Ca^{2+} chelator EGTA. In suspension (optical traps), Ca^{2+} depletion led to the unexpected sustained recruitment of PKCε-M486A at cell-cell contacts (Figure 3.7A). Given that the 'on rate' was found to be unchanged in the absence of calcium, we hypothesized that Ca^{2+} depletion acts to slow down the 'off rate' (Figure 3.7B).

Consistent with a slower 'off rate' Ca^{2+} depletion produced cells with patches of plasma membrane GFP-PKCε-M486A that would may to be "echoes" of transient cell-cell contacts (Figure 3.8). Interestingly, these suspension cells proved considerably harder to separate in Ca^{2+} depleted culture medium (Figure 3.9). In contrast, although I observe a general trend in the increase of T_1 values, there was no significant difference between PKCε-M486A dynamics at cell-cell contacts upon exposure to EGTA when compared to the corresponding mean T_1 value in the presence of Ca^{2+}. Nor was there any significant difference between the dynamics of PKCε-M486A at the furrow/midbody under the two conditions described (Figure 3.10). Furthermore, there was no significant difference between pooled T_2 values for the turnover of PKCε-M486A in the presence of absence of Ca^{2+} at either cell-cell contacts or the furrow/midbody. However, it is of particular note that for these FRAP experiments selective inhibition of PKCε-M486A, prior to EGTA exposure, was absolutely necessary as the depletion of Ca^{2+} in cells expressing active PKCε-M486A plated on poly-L-lysine led to cell shrinkage and disruption of cell-cell contacts (Figure 3.11, Videos 3 and 4). EGTA addition to ectopic WT PKCε expressing cells in the presence of NaPP1 (Figure 3.11, Videos 5 and 6), however, did not protect the cells from either shrinkage or cell-cell contact disruption. Similarly, a lack of protection was also observed for PKCε-M486A induced cells plated on fibronectin (Video 7 and 8), collagen (Video 9 and 10) or laminin (Video 11 and 12).

A

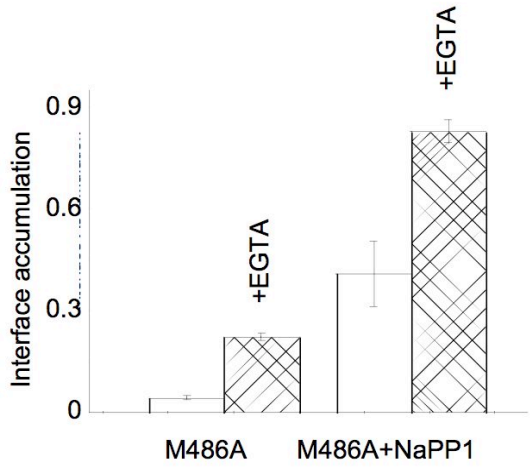

B

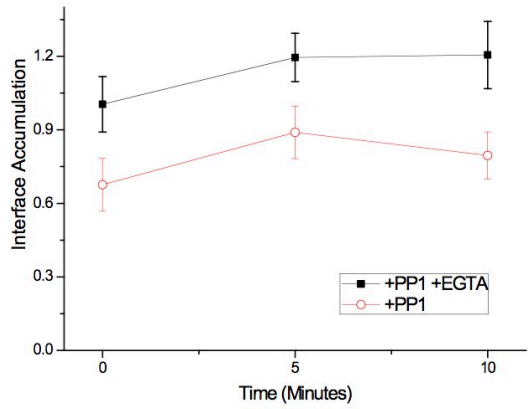

Figure 3-7 Sustained recruitment of PKCε-M486A at cell-cell contacts in TRAP manipulated cells upon exposure to EGTA

A) Changes in accumulation of PKCε-M486A in the presence of EGTA (4 mM). B) Comparison of rates of accumulation in the presence and absence of EGTA. The addition of EGTA to the cells in the presence of NaPP1 (PP1) causes no change in the rate of accumulation, increasing the overall level of PKCε-M486A fluorescence rather than its accumulation rate.

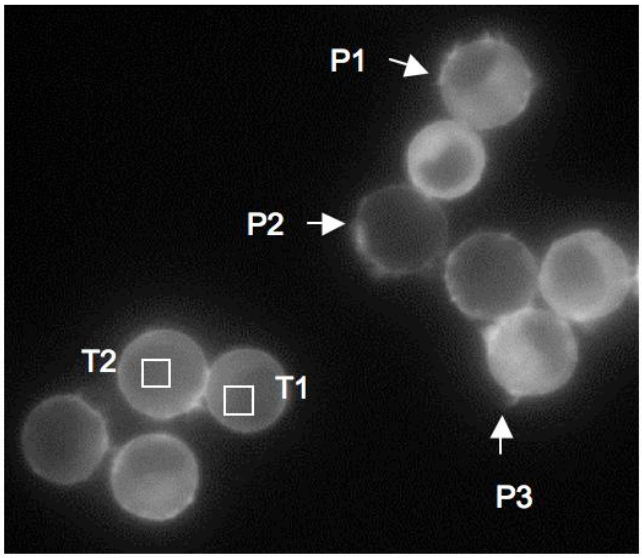

Figure 3-8 Retention of PKCε-M486A at transient cell-cell contacts in TRAP manipulated cells is consistent with a slower 'off-rate'
Fluorescence image of M486A cells in the presence of both NaPP1 and EGTA, showing 'patches' of PKCε-M486A accumulation. T1 indicates position of trap 1; T2 indicates position of trap 2 and P1, P2, P3 are examples of 'patches'.

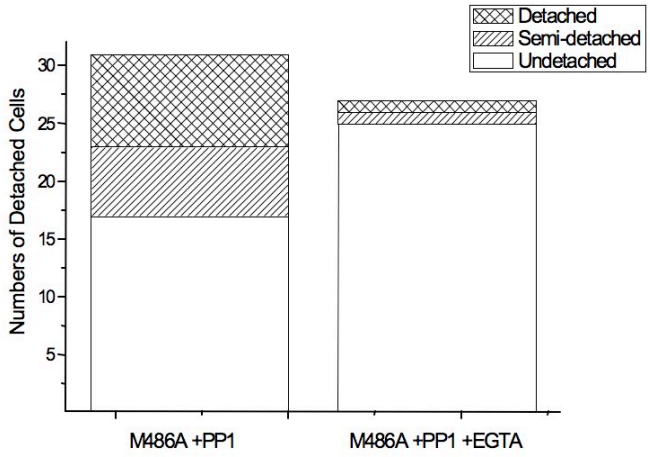

Figure 3-9 Calcium depletion increases the strength of cell-cell contacts
Cells were treated as indicated and optical forces applied to tease pairs of cells apart. The numbers of cell pairs able to be detached using optical traps is shown in the histogram. The definition of undetached pairs are those that could not be separated at the maximum trapping force of approximately 55pN. Detached cell pairs could be completely separated and manipulated independently. Semi-detached cell pairs could be separated to the extent that the cellular interface was no longer visible by eye but could not be independently manipulated.

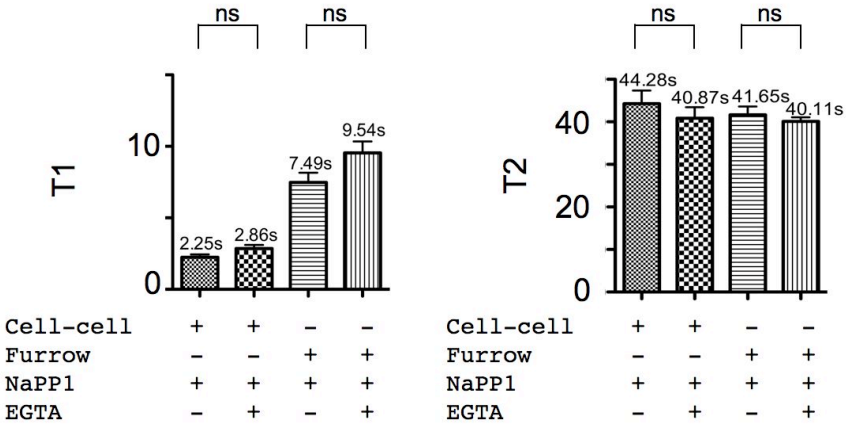

Figure 3-10 PKCε-M486A turnover is not significantly different at either furrow/midbody or cell-cell contacts upon exposure to EGTA
A similar approach was taken as in Figure 3.5. Pooled data (n=20) for T_1 and T_2 for all conditions described.

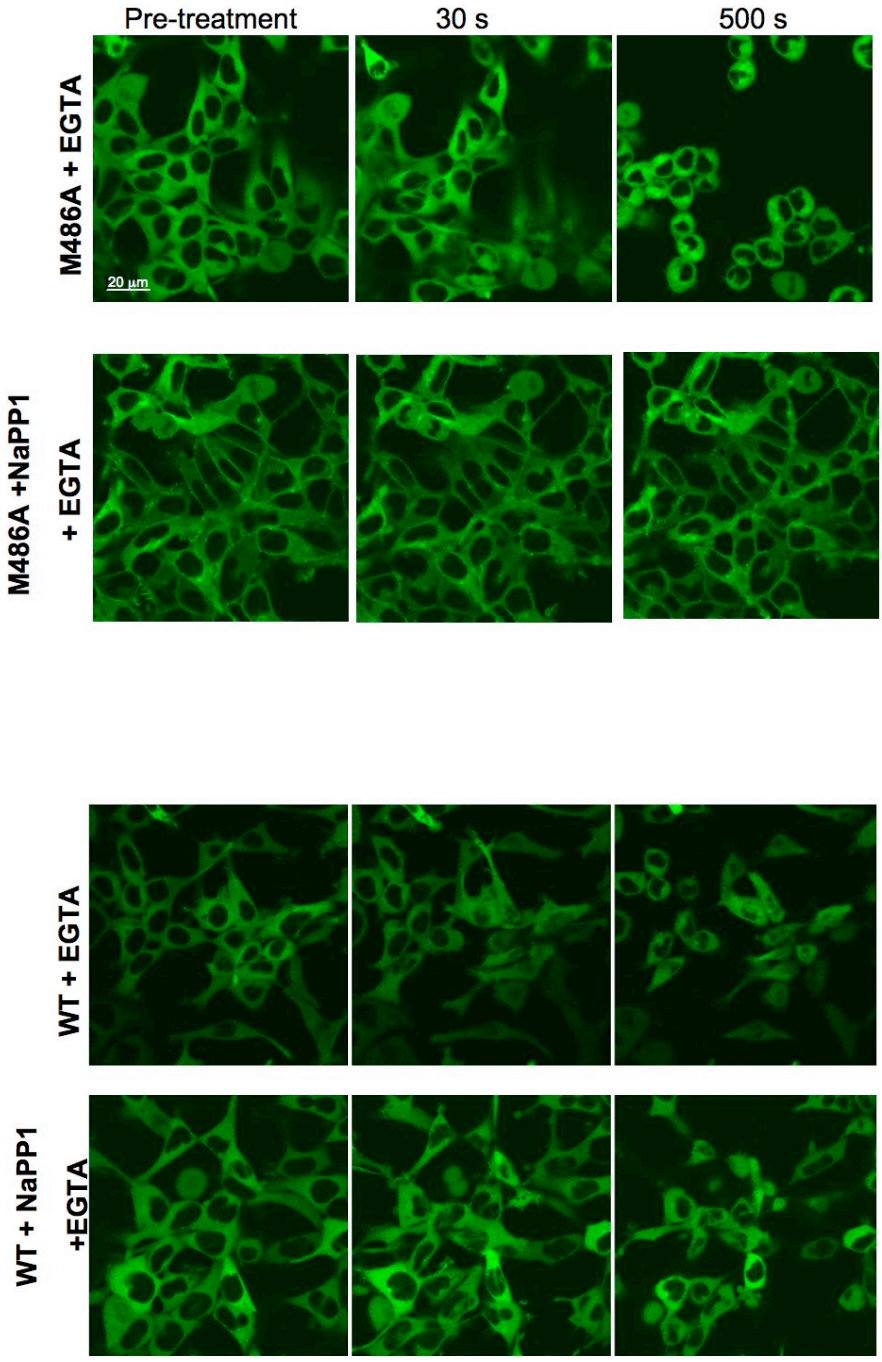

Figure 3-11 Calcium depletion leads to cell-shrinkage and cell-cell contact disruption unless pre-treated with NaPP1
Still images taken from a time lapse video. Top panel indicative of M486A cells exposed to EGTA (4 mM) over a time course described. 2nd row represents M486A cells pre-treated with NaPP1 (4 μm, 10 minutes) and then EGTA (4 mM) over a time course described. WT cells exposed to EGTA (4 mM, 3rd row) have a similar phenotype as seen in M486A but there is no rescue of the EGTA phenotype in the presence of NaPP1 (bottom).

3.4 Discussion

PKCε has been shown to localize to cell-cell contacts and to the cytokinetic furrow/midbody under conditions of PKCε-M486A inhibition (Figure 3.2), suggesting that in its active state PKCε retention at membrane compartments is poor and that catalytic activity is critical for its release. This was confirmed using Bim1 to target WT PKCε (Figure 3.5). We also show that in the presence of NaPP1, PKCε-M486A accumulates at juxtaposed cell-cell contacts (Figure 3.4). However, the lack of any distinction between mitotic and interphase cells did not resolve whether cell-cell contacts and furrow/midbody localization were related, to distinguish between the two I have used FRAP. Here, using a double exponential model which best fits the data, we consider there are two distinct populations, a fast diffusing cytosolic component (with a corresponding T_1 recovery time) and a second much slower diffusing membrane population (with a T_2 recovery time), I show that PKCε-M486A turnover is significantly slower at the furrow/midbody as compared with the turnover at cell-cell contacts, with mean T_1s of 7.49 s and 2.25 s respectively (Figure 3.6). Thus I can conclude that the inactivity dependent furrow/midbody accumulation of PKCε-M486A in mitotic cells is not the same process as that at interphase cell-cell contacts. Rather, this instead represents a relatively infrequent event where the distinctive and more avid behaviour of PKCε-M486A is indicative of other factors contributing to its retention (see Chapter 4). It is notable however, that cell-cell contact related recruitment might still serve as a possible prelude to furrow/midbody accumulation and this too will be tested in the next chapter.

In view of the role of DAG in PKCε plasma membrane recruitment it is plausible that membrane recruitment in cell-cell contacts and at the furrow/midbody is in part a function of DAG. To probe potential regulatory differences we assessed whether DAG was involved, via a Ca^{2+} dependent PLC pathway, by depleting Ca^{2+}. Although a negative affect on the retention and/or dynamics was anticipated, it was surprising to find that Ca^{2+} depletion in cell suspension led to the sustained recruitment of inactive PKCε-M486A at cell-cell contacts (Figure 3.7) and produced cells with patches of

plasma membrane PKCε-M486A that would appear to be echoes of transient cell-cell contacts (Figure 3.8). If this is true, these domains maybe enriched with cell-cell contact specific proteins such as cadherins or β-catenin (see below). Alternatively, given the raft-like nature of these patches, this may represent an increase in lipid raft affinity of PKCε in the presence of EGTA. Currently, these explanations remain merely speculative. I have been unable to conclusively show the underlying mechanism. However, with no change in the 'on rate' of membrane contact accumulation (Figure 3.7) it is hypothesized that Ca^{2+} depletion acts to slow down the 'off rate'. Unfortunately, the FRAP analysis performed here provides conflicting evidence for Ca^{2+}-dependent turnover of PKCε-M486A at cell-cell contacts. There was no evidence of any significant change to the mean T_1 values for cell-cell contacts in the presence or absence of Ca^{2+} in FRAP experiments (Figure 3.10). This result may reflect the suspension behaviour of these cells and/or the nature of the cell-cell contacts in the two environments. For example, the transient nature of the cell-cell contacts in suspension may be fundamentally different from the sustained cell-cell contacts observed in culture especially with regard to the engagement of cadherins (see below).

Given PKCε's classification as a Ca^{2+}-independent PKC with respect to membrane recruitment it is intriguing to find that dissociation of PKCε-M486A at cell-cell contacts is Ca^{2+} dependent in suspended cells. As there are almost no precedents for Ca^{2+} dependent behaviour of PKCε, I propose a scenario in which Ca^{2+} regulates PKCε interactors specifically at cell-cell contacts where integrins are not (fully) engaged and this is then stabilized upon PKCε-M486A inhibition and Ca^{2+} depletion. Candidate PKCε partners include members of the cadherin family and their various cytoplasmic binding partners, given that collectively they are responsible for adhesive interactions via a Ca^{2+}-dependent mechanism (Takeichi, 1991) and have been implicated in signal transduction via PKC (Lewis et al., 1994). Consistent with this proposed increase in stability, upon treatment with NaPP1 and EGTA, suspension cells proved considerably harder to separate and in cell culture, the cells were resistant to disruption of cell-cell contacts (Figure 3.9). Furthermore, in support of an integrin independent mechanism , Ca2+ depletion induced cell shrinkage is only PKCε-M486A controlled on poly-L-lysine. If cells are plated on collagen, fibronectin or laminin which are adhesive

solutions that do engage integrins, this control is lost. To test the involvement of cadherins and their cytoplasmic binding partners, antibodies or siRNA directed at potential candidates could be tried and PKCε-M486A localization monitored under all the conditions described.

Nonetheless, in this chapter I have shown that physical contact is sufficient to induce recruitment of PKCε-M486A to cell-cell contacts and retention here is, surprisingly, increased upon depletion of Ca2+ with EGTA. Furthermore, selective inhibition of PKCε-M486A protects 293 cells from EGTA cell-cell contact loss. Collectively, this indicates a role for PKCε in cell-cell contact maintenance. In addition, PKCε-M486A has a significantly slower turnover at the furrow/midbody that at cell-cell contacts which is indicative of a distinct regulatory mechanism. Attempts to further characterize this mechanism are now described in Chapter 4.

Chapter 4.

Recruitment of PKCε to the cytokinetic furrow/midbody

4.1 Summary

To assess the relationship between previously identified binding motifs within PKCε and PKCε-M486A furrow/midbody recruitment I have used a combination of mutagenesis and confocal microscopy. Using this approach I have shown that cell-cell contact targeting disruption does not alter GFP-PKCε-M486A furrow/midbody recruitment nor does furrow/midbody recruitment require 14.3.3 binding. Rather, localization is in part a function of a motif previously identified as a requirement for actin-binding, the IC1D. This implies an intriguing relationship between PKCε and the cytokinetic actomyosin ring.

4.2 Introduction

In Chapter 3 I show that recruitment to the furrow/midbody and cell-cell contacts may not be through a common mechanism and consequently I have been unable to take advantage of the possibly easier route of analysing the abundant interphase cell-cell contacts. Instead, to determine how this relatively infrequent event is controlled a mutation study in PKCε-M486A using extensive live microscopy, has been employed. Given that small sequence motifs or signal patches found in the N-terminal and variable regions of PKCε have been proposed to contribute to its specific localization I have manipulated a variety of these and started to unravel the requirements and possible binding partners involved in PKCε-M486A furrow/midbody recruitment.

In view of the evidence generated in chapter 3, it is notable, that cell-cell contacts may still serve as a possible prelude to furrow/midbody accumulation whereby the more distinct behaviour of PKCε reflect an interaction with further furrow/midbody components. The selective targeting of PKCε at cell-cell contacts can be attributed to a three amino acid motif located in the V3 hinge region, GEE, at residues 373-375 and a GEE to GGE mutation abolishes the selectivity of such targeting (Quittau-Prevostel et al., 2004). Interestingly, PKCε uniquely associates with 14.3.3 through its V3 hinge region also and PKCε-14.3.3 complex formation is required for the successful completion of cytokinesis (Saurin et al., 2008). Currently, the exact role of 14.3.3 in this complex remains unresolved and therefore it is plausible that 14.3.3 functions to influence recruitment of PKCε to the furrow/midbody. 14.3.3 binds to PKCε through the action of p38 and GSK3 which provide a phosphopeptide binding motif, termed mode 1, RSXpSXP at residues 343-348 whilst an autophosphorylation site produces a divergent mode 2 motif, RXXXpSXP, at residues 364-370. 14.3.3 binding to these motifs occurs in a cooperative, dimeric fashion as confirmed through crystallography and mutation. Indeed, mutations that prevent this association (PKCε-S346/368A, PKCε-R343A) cause defects in the completion of cytokinesis (Saurin et al., 2008, Kostelecky et al., 2009).

PKCε is also unique among the PKC isoforms in containing an F-actin binding motif (Prekeris et al., 1996). This motif, LKKQET, is located inbetween the C1A and C1B at amino acids 223-228 and is predicted to become exposed upon PKCε activation. Deletion of amino acids encompassing this motif, 222-230/IC1D, completely abrogates this binding activity (Prekeris et al., 1998). Despite biochemical evidence confirming an actin-PKCε interaction, direct structural evidence remains elusive. Rather, the structure of an actin-WASP-homolgy domain 2 (WH2) complexes reveals how an actin-binding motif, of similar sequence to that in PKCε, can bind in a hydrophobic cleft formed between actin subdomains (reviewed in Dominguez, 2004). As the pocket remains accessible in F-actin (the predominant form of actin during furrow/midbody formation) it may represent the primary target for the LKKQET of PKCε during cytokinesis. Consistent with an actin-PKCε interaction during cytokinesis and a possible role in PKCε recruitment, here I show that recent evidence indicates that the selective inhibition of PKCε-M486A causes colocalization of the enzyme with actin at the furrow/midbody (Saurin et al., 2008).

In this chapter I have addressed the relationship between these three binding motifs and PKCε-M486A furrow/midbody recruitment by generating these previously published mutations (E374G, S346/368A and Δ222-230/IC1D). In doing so, I demonstrate that PKCε-M486A recruitment is not cell-cell contact or 14.3.3 binding dependent. Rather, I show that localization is in part a function of the IC1D, a motif previously identified as actin-binding.

4.3 Results

4.3.1 Cell-cell contact selective targeting is not required for PKCε-M486A furrow/midbody localization

To address the question of whether cell-cell contacts serve as a prelude to PKCε-M486A recruitment to the furrow/midbody, flp-in T-Rex cells were used to generate tetracycline inducible expression of the NaPP1 sensitive, cell-cell contact targeting mutant GFP-PKCε-E374G-M486A. It is anticipated that manipulation of any of the critical motifs involved in PKCε-M486A recruitment will alter its retention at the furrow/midbody. As shown in Figure 4.1, the E374G mutation was sufficient to abolish the selectivity of targeting to cell-cell contacts upon PMA stimulation with the GFP signal evenly distributed at the contacted and uncontacted plasma membrane. However, this mutation was not sufficient to alter the accumulation of PKCε-M486A at the furrow/midbody. In a representative dividing GFP-PKCε-E374G-M486A expressing cell, NaPP1 addition leads to a transient membrane accumulation followed by a more sustained furrow/midbody accumulation and a concomitant delay in the final stage of cytokinesis (Figure 4.2). This behaviour is entirely consistent with the pattern of response reported for PKCε-M486A in the previous chapter (Figure 3.2), suggesting that cell-cell contact associated functions doe not serve as a prelude to PKCε-M486A furrow/midbody localization. In the absence of NaPP1, cells complete cytokinesis normally with no change in the distribution of GFP-PKCε-E374G-M486A.

A B

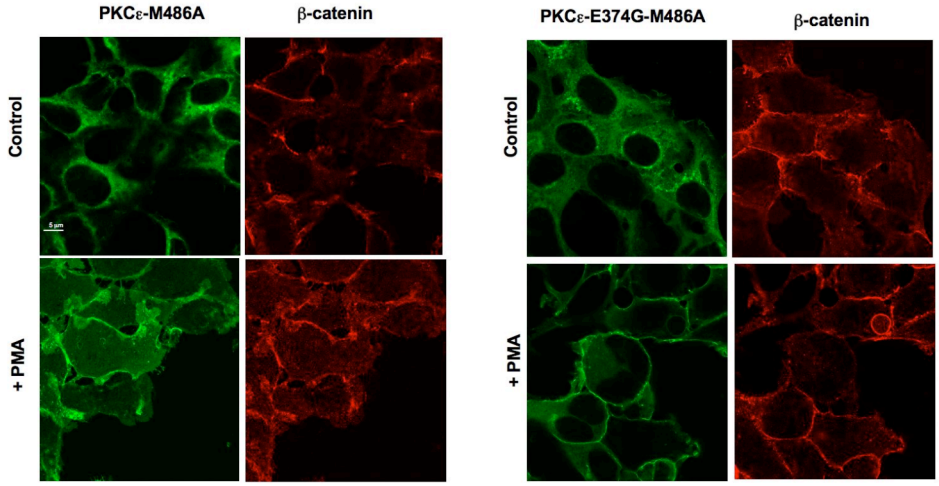

C

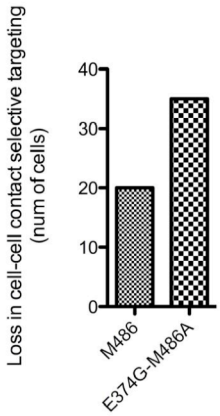

Figure 4-1 Immunofluorescent analysis of PKCε-M486A and PKCε-E374G-M486A.
M486A (A) and E374G –M486A (B) cells, after 10 minutes in the presence or absence of 100 nM PMA, were co-stained with anti-GFP and β-catenin. A selective translocation to cell-cell contacts was observed for PKCε-M486A. This selective targeting was lost in PKCε-E374G-M486A cells. C) Quantification of such targeting, where n=50.

A

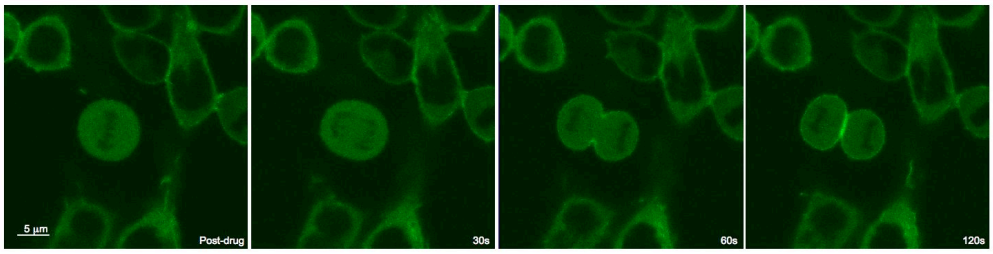
5 µm
Post-drug
30s
60s
120s

B

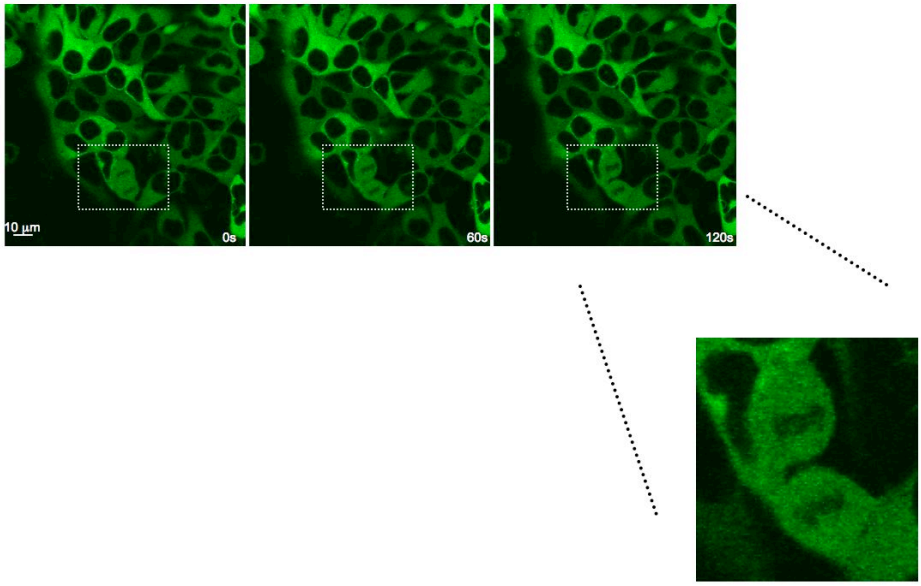
10 µm
0s
60s
120s

C

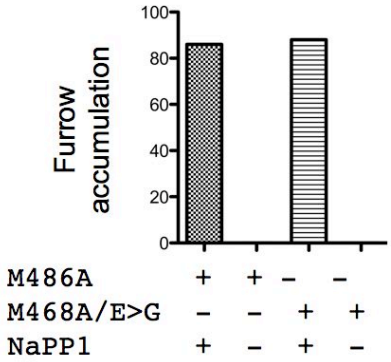
Furrow accumulation
100
80
60
40
20
0
M486A + + − −
M468A/E>G − − + +
NaPP1 + − + −

Figure 4-2 Selective inhibition of PKCε-E374G-M486A results in localization at the plasma membrane and cytokinetic furrow/midbody.
A)Still images, taken from a time-lapse video, of the E374G-M486A cell line in the presence of NaPP1 (4 μM). Progression through the time lapse (left to right) shows GFP accumulation at the plasma membrane and at the cytokinetic furrow/midbody, with an accompanying arrest in cytokinesis. B) In the absence of NaPP1, cells complete cytokinesis normally and there is no change in the distribution of GFP-PKCε-E374G-M486A. Although a widefield image is shown, the dividing cell is highlighted within the white box and the panel furthest to the right has been enhanced to demonstrate this unchanged GFP distribution. C) Quantification of PKCε-E374G-M486A accumulation at the furrow/midbody in the presence or absence of NaPP1 and compared with PKCε-M486A, n=20.

4.3.2 14.3.3 binding is not an absolute requirement for PKCε-M486A localization at the furrow/midbody

To address the question of whether PKCε recruitment to the furrow/midbody was related to the binding of 14.3.3, flp-in T-Rex cells were used to generate tetracycline inducible expression of the NaPP1 sensitive, 14.3.3 binding mutant GFP-PKCε-S346,368A-M486A (Saurin et al., 2008). It is of note, that the construct itself had been previously subjected to pull-down assays with GST-14.3.3.β beads by Dr. Adrian Saurin and was found to be devoid of 14.3.3 binding capabilities. In dividing GFP-PKCε-S346,368A-M486A expressing cells, NaPP1 addition leads to a similar furrow/midbody accumulation of GFP-PKCε as seen previously using GFP-PKCε-M486A and GFP-PKCε-E374G-M486A expressing cells. Cells halt at the final stage of cytokinesis whilst a transient membrane accumulation of GFP-PKCε-S346,368A-M486A is promptly followed by a more sustained furrow/midbody accumulation (Figure 4.3). In the absence of NaPP1, cells complete cytokinesis normally with no change in the distribution of GFP-PKCε-S346,368A-M486A. The lack of any distinction between GFP-PKCε-M486A and GFP-PKCε-S346,368A-M486A suggests that 14.3.3 binding to PKCε is not responsible for furrow/midbody recruitment/retention.

A

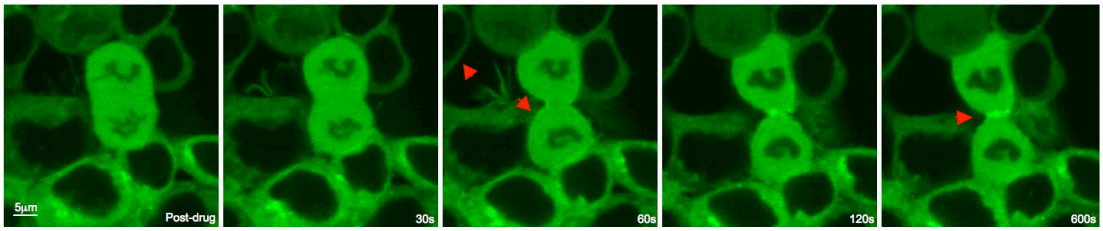

B

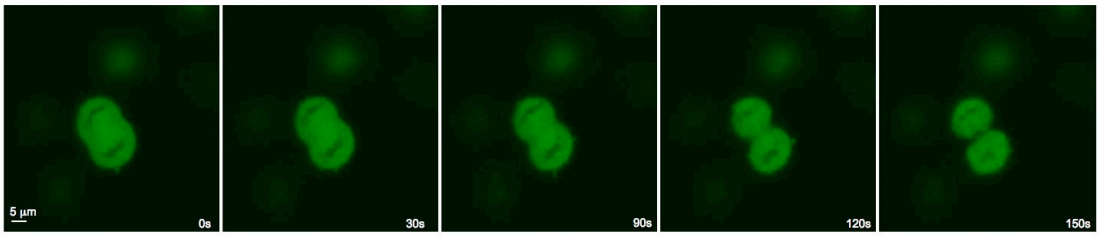

C

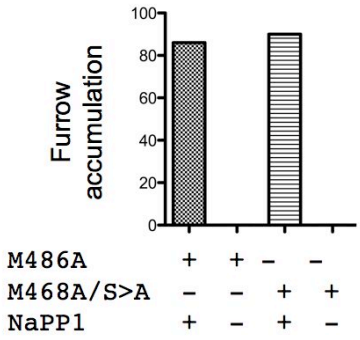

Figure 4-3 Selective inhibition of PKCε-S346/368A-M486A results in localization at the plasma membrane and cytokinetic midbody/furrow.
A) Still images, taken from a time-lapse video, of the S346/368A-M486A cell line in the presence of NaPP1 (4µM) Arrowheads in panel 3 (top row, from left to right) indicate relative GFP accumulation at the plasma membrane whilst that in panel 5 is indicative of furrow/midbody accumulation in an actively dividing cell. B) In the absence of NaPP1, cells complete cytokinesis normally with no change in the distribution of GFP-PKCε-S346/368A-M468A. C) Quantification of PKCε-S346/368A-

M486A accumulation at the furrow/midbody in the presence or absence of NaPP1 and compared with PKCε-M486A, n=20.

4.3.3 PKCε -M486A plasma membrane and furrow/midbody localization is in part a function of the IC1D

To assess the involvement of the actin binding motif, IC1D in PKCε recruitment to the furrow/midbody, flp-in T-Rex cells were used to generate tetracycline inducible expression of the NaPP1 sensitive, IC1D deletion mutant GFP-PKCε-ΔIC1D-M486A. In a representative dividing GFP-PKCε-ΔIC1D-M486A cell, the addition of NaPP1 triggered no change in the distribution of GFP-PKCε-ΔIC1D-M486A and cytokinesis completes normally (Figure 4.4A, Video 13), in contrast to GFP-PKCε-M486A expressing cells. Furthermore, deletion of the domain prevents the kinase from accumulating at either the plasma membrane or furrow/midbody. Coexpressed RFP-PKCε-M486A transiently expressed in the same cells (Figure 4.4B) is successfully recruited.

4.3.4 A PMA and NaPP1 responsive PKCε -ΔIC1D-M486A is phosphorylated at S729 and is catalytically activity

Although the nonapeptide sequence deleted from PKCε -ΔIC1D-M486A is critically located between the C1A and C1B, this mutation did not significantly alter its local topology or response to phorbol esters. Immunofluorescence microscopy was used to examine the GFP-PKCε-ΔIC1D-M486A response to PMA. In both the intact and mutated kinase staining for GFP in unstimulated cells was found diffuse throughout the cytoplasm whereas upon activation with PMA it selectively redistributed to cell membranes, indicative of an intact and functioning C1 domain (Figure 4.5).

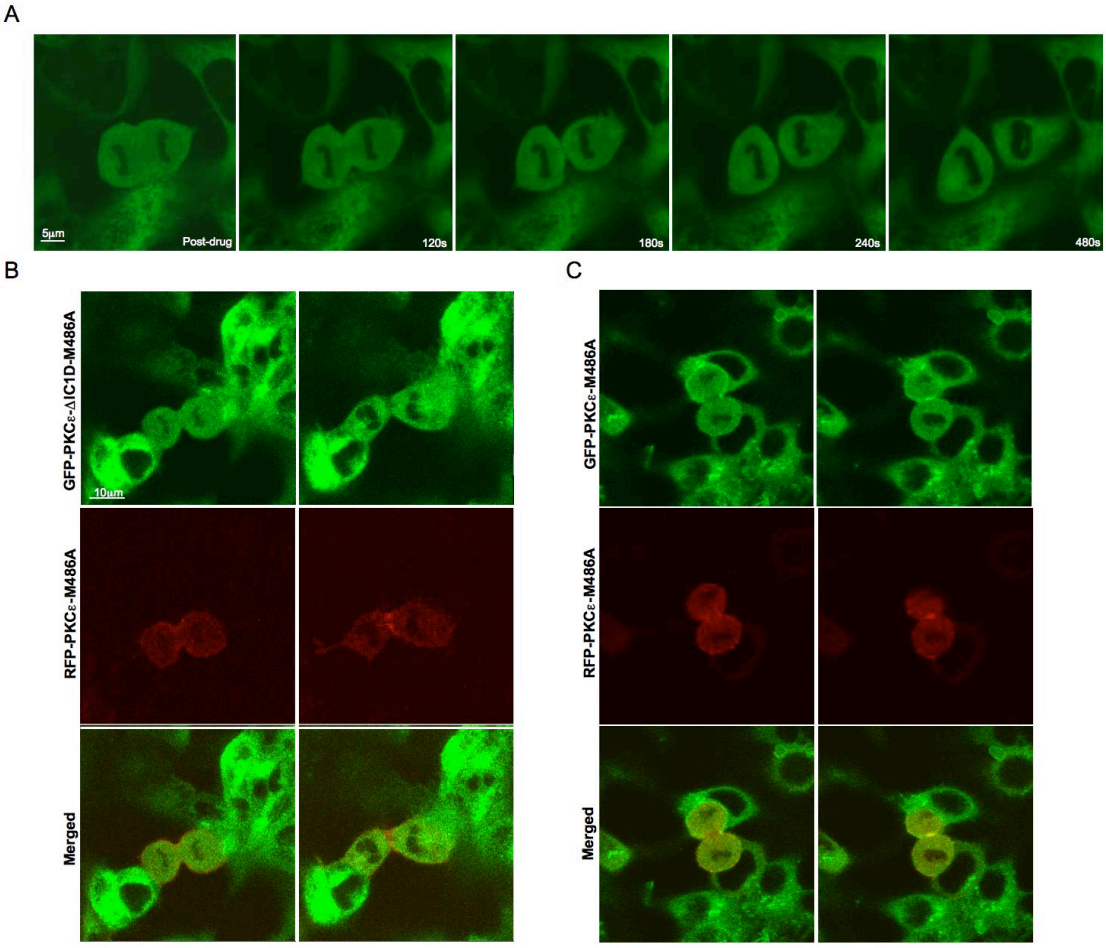
A
5μm
Post-drug
120s
180s
240s
480s
B
C
GFP-PKCε-ΔIC1D-M486A
10μm
RFP-PKCε-M486A
Merged
GFP-PKCε-M486A
RFP-PKCε-M486A
Merged

C

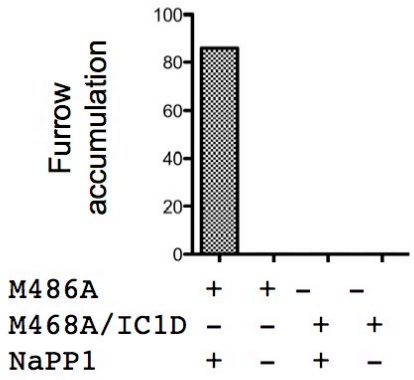
Furrow accumulation
100
80
60
40
20
0
M486A + + – –
M468A/IC1D – – + +
NaPP1 + – + –

Figure 4-4 Selective inhibition of PKCε-ΔIC1D-M486A does not result in localization at the plasma membrane or furrow/midbody
A) Still images, taken from a time-lapse video, of the ΔIC1D-M486A cell line in the presence of NaPP1 (4 μM). B) Coexpression of RFP-PKCε-M486A with GFP-PKCε-ΔIC1D-M486A cells 'rescues' the localization response to NaPP1. RFP-PKCε-M486A localizes to both the plasma membrane and to the furrow/midbody on exposure to NaPP1 (left column, 5 minutes post NaPP1, right column, 2 minutes later). C) RFP-PKCε-M486A has no effect on GFP-PKCε-M486A localization. Coexpression of RFP-PKCε-M486A with GFP-PKCε-M486A cells results in a colocalization of both RFP and GFP at the plasma membrane and furrow/midbody (left column, 5 minutes post NaPP1, right column 2 minutes later). C) Quantification of PKCε-ΔIC1D-M486A accumulation at the furrow/midbody in the presence or absence of NaPP1 and compared with PKCε-M486A, n=20.

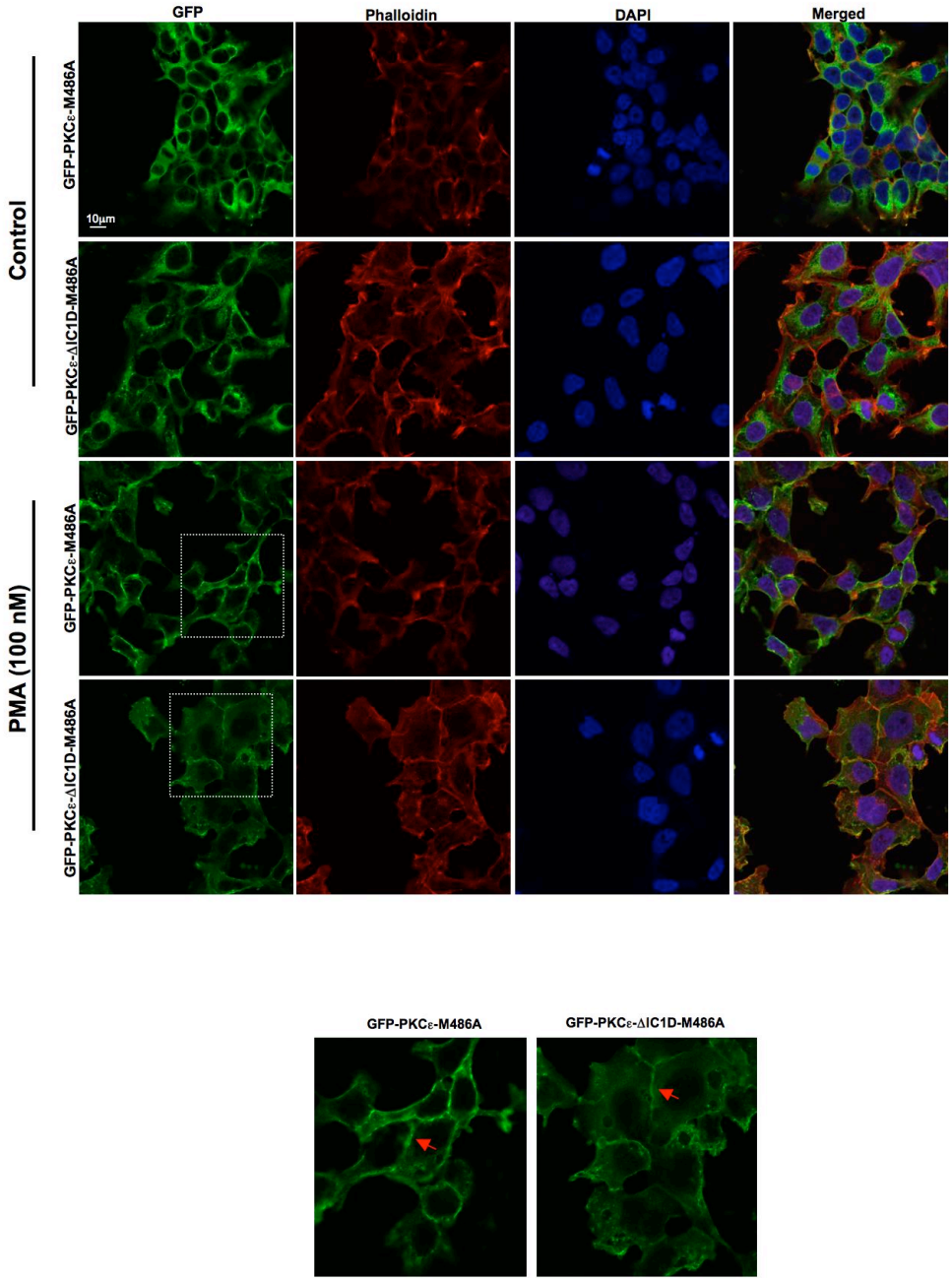

Figure 4-5 Immunofluorescent analysis of PKCε-M486A and PKCε-ΔIC1D-M486A

M486A and ΔIC1D –M486A cells were simultaneously costained with anti-GFP, phalloidin and DAPI after 10 minutes in the presence (bottom half) or absence (top half) of 100 nM PMA. In unstimulated cells, GFP is found diffuse in the cytoplasm. Exposure to PMA induces translocation of GFP to the plasma membrane in both cell lines, as highlighted in the enhanced images (bottom two panels).

Work in the laboratory has previously demonstrated a reduced affinity for ATP in PKCε-M486A which is reflected in the instability of priming phosphorylations and exposure to PMA induces a substantial dephosphorylation at all three priming sites within 30 minutes. Treatment with NaPP1, however, promotes phosphorylation whilst a combinatorial approach protects the kinase from net dephosphorylation (Cameron et al., 2009). To determine whether other indicators of normal functioning are in place for the IC1D, I analysed the priming phosphorylation in the S729 site. PKCε-ΔIC1D-M486A and PKCε-M486A expressing cells were treated with PMA, NaPP1 and a combination of both before being processed by Western blotting using the pS729 antibody (Figure 4.6). Consistent with Cameron and colleagues, PKCε-M486A and PKCε-ΔIC1D-M486A are similarly primed at S729 under basal conditions and the addition of NaPP1 induces a small increase in phosphorylation. As expected, PMA induced a substantial dephosphorylation of this priming site in both proteins within 30 minutes whilst simultaneous treatment of NaPP1 and PMA entirely protects the kinases from net dephosphorylation. Despite a deletion of the IC1D, the data indicate that PKCε-ΔIC1D-M486A retains priming site phosphorylations and is responsive to NaPP1. However, whilst it is clear that PMA causes loss of phosphorylation at the priming site in both cell lines, there is a differential effect on these two sties. The less striking dephosphorylation of the ΔIC1D cell line may reflect a reduction in the efficiency in which the construct is recruited to the membrane. To assess catalytic funcion directly proteins were tested *in vitro*. Following immunopurification of GFP-PKCε-M486A and GFP-PKCε-ΔIC1D-M486A *in vitro* kinase assays were employed and these demonstrated that the mutant retained comparable kinase activity. 920 pmol min^{-1} $dish^{-1}$ and 860 pmol min^{-1} $dish^{-1}$ for PKCε-M486A and PKCε-ΔIC1D-M486A respectively (Figure 4.7).

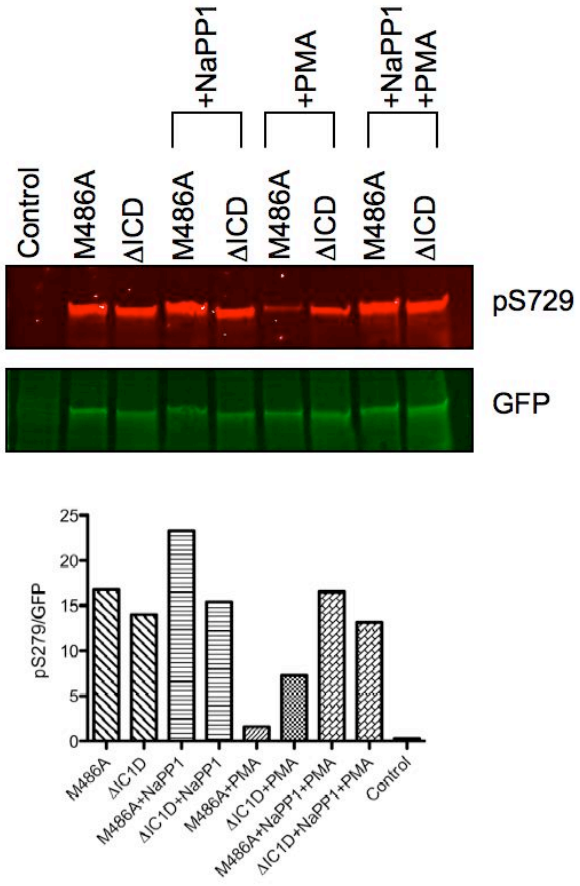

Figure 4-6 PKCε-ΔIC1D-M486A is primed at S729 and NaPP1 responsive
Cells were treated with DMSO control, NaPP1(4 μM), PMA (400 nM) or a combination of both for 30 minutes before western blot analysis with anti-pS279 and GFP antibodies. Data normalized to GFP loading control showing that S279 is phosphorylated under basal conditions, phosphorylation is induced upon exposure to NaPP1 and PMA induces dephosphorylation in the both cell lines. Treatment with a combination of drug protects the kinase from net dephosphoryation.

A

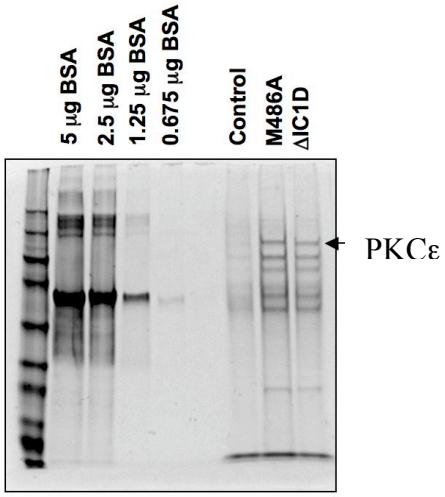

B

Cells	μg PKC	Raw Counts	pmol ^{32}P /min	Average Activity pmol/min/dish
Control	0.8 eq	1904	0.1440785	≤1
	0.8 eq	1637	0.0941836	≤1
	0.8 eq	1702	0.1063303	≤1
	0.2 eq	781	-0.065779	
	0.2 eq	1546	0.0771782	0
	0.2 eq	1000	-0.024854	
M486A	0.8	475050	88.561925	NL
	0.8	281219	52.340294	NL
	0.8	329517	61.36585	NL
	0.2	210566	39.137211	
	0.2	300891	56.016445	922
	0.2	232696	43.27269	
ΔIC1D	0.8	487620	90.910909	NL
	0.8	453489	84.532773	NL
	0.8	443441	82.655081	NL
	0.2	256853	47.786966	
	0.2	137328	25.451063	863
	0.2	302389	56.296379	

Figure 4-7 The kinase activity of PKCε-ΔIC1D-M486A is comparable to that of PKCε-M486A

Figure 4.7 continued. An immunoprecipitation of the different forms of PKCε from cells followed by a kinase assay. A) Coomassie stain to roughly quantify protein concentration used in assay, PKCε calculated at approximately 1 μg for both M486A and ΔIC1D using Image J quantification software and BSA standard curve. B) 1 μg of PKCε, per triplicate, diluted as indicated, used in a kinase assay with protamine sulphate as the substrate. [γ-^{32}P] incorporation over 10 minutes was analysed by Cerenkov counting. 0.8 eq and 0.2 eq represents an equivalent volume of pull down used in kinase assay for the control. NL denotes non-linear, as does the highlighted yellow cell based on substrate use of over 25%. Specific radioactivity (sa) of ATP (cpm/pmol) = 1427. In the assay pmol ^{32}P /min was calculated by: [(rc-b/sa) x 2.67]/10, where rc is raw counts incorporated into substrate, b is the average blank, 2.67 is a volume correction factor for transfer to phosphocellulose paper and 10 is the incubation time in min. The activity was converted from average pmol ^{32}P /min to pmol ^{32}P /min/dish by multiplying by the dilution factor 20.

4.3.5 PKCε-ΔIC1D-M486A displays a weaker association with F-actin when compared to PKCε-M486A

The ability of PKCε-ΔIC1D-M486A to bind F-actin was measured using cosedimentation assays and compared with that of 'full length' PKCε-M486A (Figure 4.8). Briefly, PKCε lysates were incubated with polymerized actin for a period of one hour after which the samples were subjected to high-speed ultracentrifugation (see Materials and Methods). PKCε-ΔIC1D-M486A displays a weaker association with precipitated F-actin, when directly compared with PKCε-M486A, that is significantly enhanced by increasing the concentration of PMA. Of particular note, however, is the ability of recombinant PKCε to sediment even in the absence of actin, which reflects the difficulty in interpreting this assay.

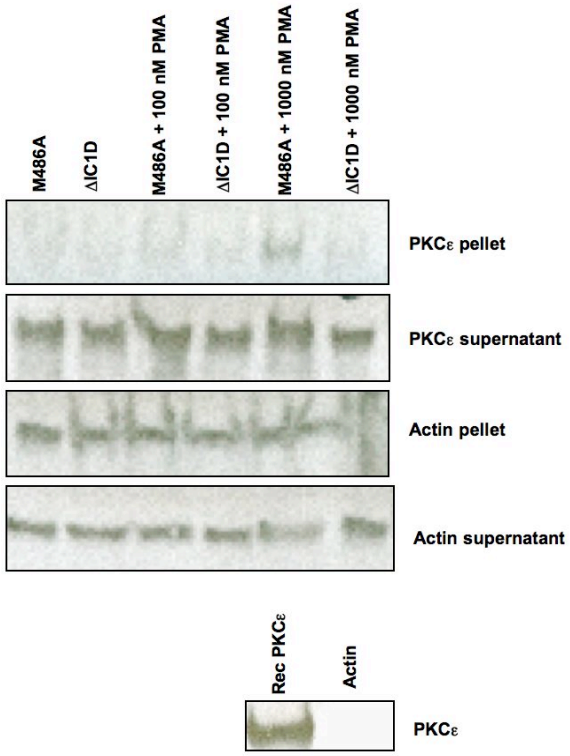

Figure 4-8 Cosedimentation of purified F-actin with PKCε-M486A and PKCε-ΔIC1D-M486A

Cosedimentation of F-actin (50 μg) with PKCε-M486A and PKCε-ΔIC1D-M486A in the presence of varying concentrations of PMA. Supernatant and pellets were analysed by western blot and probed for PKCε and actin. PKCε can sediment even in the absence of polymerized actin (bottom panel).

4.4 Discussion

In the previous chapter, I show that PKCε-M486A accumulation at the furrow/midbody is not the same process as that at cell-cell contacts, however the possibility that cell-cell contacts serve as a prelude to PKCε-M486A accumulation was not excluded. In this chapter, I have demonstrated that GEE motif required for selective targeting to cell-cell contacts does not mediate PKCε-M486A furrow/midbody accumulation (Figure 4.2). Rather the behaviour of PKCε-M486A at the furrow/midbody appears to be indicative of an entirely different mechanism. Furthermore, despite the requirement for PKCε-14.3.3 complex formation in the completion of cytokinesis (Saurin et al., 2008), 14.3.3 binding to the phosphorylated S346 and S368 residues (or indeed their phosphorylation *per se*) does not mediate PKCε-M486A recruitment to the furrow/midbody either (Figure 4.3). In contrast, I have shown that the IC1D, encompassing a previously identified actin-binding motif (Prekeris et al., 1996), is required for the accumulation of PKCε-M486A at the furrow/midbody upon NaPP1 stimulation (Figure 4.4). Given that the only difference between this and full length construct is the presence or absence of the IC1D this data demonstrates that the IC1D in PKCε-M486A is needed for recruitment whilst also confirming the specificity of the NaPP1. Crucially, PKCε-ΔIC1D-M486A appeared to remain correctly folded, primed and catalytically active, as demonstrated by Figures 4.5, 4.6 and 4.7. It therefore, seems unlikely that the lack of accumulation at this compartment is a consequence of the non-functional folding of PKCε-ΔIC1D-M486A, rather it reflects a specific involvement of the IC1D in the furrow/midbody recruitment process. Interestingly, whilst not influencing the C1 domain recruitment through phorbol esters, this domain is also required for the initial membrane association when selectively inhibited with NaPP1 (Figure 4.4). Based on the data from Chapter 3, this suggests that yet other specific contacts are made and/or distinct regulatory inputs operate at the midbody. Although 14.3.3 was shown not to mediate the absolute PKCε-M486A furrow/midbody recruitment, perhaps it more subtly affects the dynamics once localized there. The dynamics of PKCε-S346,368A-M486A association at the midbody could be assessed by FRAP analysis.

It has not been possible to determine whether the IC1D is unequivocally required for the physical association of PKCε-M486A and actin. Cosedimentation assays were performed to compare the ability of PKCε-ΔIC1D-M486A to bind F-actin with that of PKCε-M486A (Figure 4.8). While the evidence indicates that on activation with PMA, PKCε-ΔM486A interacts better with F-actin than that of PKCε-ΔIC1D-M486A, the ability of recombinant PKCε to sediment in the absence of polymerized actin, indicates that some portion of epsilon is insoluble or aggregates during the assay despite attempts to preclear this lysate. Consequently it is very difficult to interpret this assay unequivocally. Indeed, these assays were tested under a variety of conditions with fresh or precleared PKCε, however, the consistency of behaviour was lacking not enabling a clear conclusion to be drawn at all. An alternate strategy would be to assess whether a linear binding epitope of IC1D can bind actin using a peptide array. It is of note, however, that the linearization of both the IC1D and actin in this approach may prove problematic.

Nonetheless, in this chapter I have demonstrated that the IC1D functions in part to recruit PKCε -M486A to the plasma membrane and furrow/midbody. Although previously identified as an actin-binding motif formal confirmation of this direct interaction has not been accomplished. An attempt to assess the relationship between actin and PKCε-M486A furrow/midbody recruitment is described in Chapter 5.

Chapter 5.

F-actin regulation of a PKCε-RhoA compartment during cytokinesis

5.1 Summary

To assess the relationship between actin and PKCε-M486A recruitment I have manipulated actin polymerization. Using latrunculin A (latA), an inhibitor of F-actin assembly, I have shown that PKCε-M486A and RhoA colocalize and are stabilized in the same compartment in conditions where F-actin is destabilized independently of PKCε-M486A inhibition (in contrast to PKCε-M486A and NaPP1, see chapter 3). This condition may be analogous to a stage in midbody biogenesis and may be evidence of the requirement of F-actin for normal PKCε and RhoA kinetics. The equatorial accumulation of PKCε-M486A-RhoA in this assay is short lived and its disappearance correlates with the appearance of residual actin-rich structures, possibly reflecting a complex relationship between RhoA and actin during cytokinesis. Interestingly, treatment with NaPP1 prolongs the association of PKCε-M486A with this undefined structure, which may reflect PKCε's actin binding/turnover capability and subsequent retention at the structure if in an inhibited state.

5.2 Introduction

Actin is one of the most highly conserved and abundant proteins in eukaryotic cells and many cellular processes (including cell motility, endocytosis and cytokinesis) are powered by its rapid polymerization (recently reviewed in Campellone, 2010, Firat-Karalar and Welch, 2011). In cytokinesis, F-actin is a major constituent of the actomyosin ring and assembles downstream of RhoA activation (Glotzer, 2005). Specifically, RhoA is activated in anaphase by Ect2 (Kimura et al., 2000) and then functions at the cleavage furrow to directly activate the actin-nucleating protein mDia2 and promote the phosphorylation of the regulatory light chain of myosin II (Amano et al., 1996, Madaule et al., 1998, Yuce et al., 2005). Once the filaments are assembled, the progressive sliding of myosin minifilaments along actin filaments is then believed to provide the contractile force necessary to drive furrow ingression. The RhoA activated furrow continues to ingress until the dividing cells remain connected by an intracellular bridge containing a midbody. Completion finally occurs when the bridge is resolved to create two daughter cells.

It has been proposed that the removal of actin is a necessary prerequisite for this final stage of abscission and could be controlled by the inactivation of RhoA. Given that PKCε-M486A accumulates at the furrow/midbody on exposure to NaPP1 and is associated with an enrichment of RhoA-GTP and polymerized actin (Saurin et al., 2008), it is anticipated that PKCε triggers RhoA inactivation during cytokinesis. Interestingly, evidence from chapter 4 indicates that the IC1D, which has been shown previously to bind actin, is required for PKCε-M486A plasma membrane and furrow/midbody recruitment.

To address the relationship between PKCε-M486A and actin, I have used the actin depolymerizer latrunculin A, latA. LatA functions by sequestering monomeric actin and as a consequence filamentous actin structures fall apart (Gerisch et al., 2004). Through the use of live imaging techniques, to capture different stages of the cytokinetic process with a high temporal and spatial resolution, I have uncovered an actin-PKCε-M486A-RhoA linked compartment. Consistent with a requirement for PKCε in RhoA

regulation, a PKCε-M486A-RhoA positive structure stabilizes temporarily in response to latA and importantly is observed without PKCε's inhibition. The local reappearance of actin is then associated with the breakdown of PKCε-M486A-RhoA which might suggest a PKCε-M486A-actin requirement for RhoA inactivation.

5.3 Results

5.3.1 Equatorial accumulation of PKCε-M486A, post anaphase onset, in response to depolymerized actin

To assess the relationship between actin and PKCε-M486A recruitment I have manipulated actin polymerization with latA. Initially I titrated latA to determine the optimum concentration of the drug to use. Treatment of the M486A cell line with 100 nM latA caused the immediate collapse of any ingressing furrows without significant blebbing, as observed with higher concentrations of the drug i.e. > 200 nM. Following a 5-10 minute incubation with latA at 100 nM PKCε-M486A appeared, equatorially positioned, in all cells which had undergone anaphase onset, defined here by the separation of chromosomes (Figure 5.1, Video 14). By contrast interphase cells did not show a PKC accumulation in any such structures. As demonstrated in the cell denoted by a white star (Figure 5.1, panel 1), accumulation of PKCε-M486A does not require visible furrow formation, latA was added whilst the cell was in metaphase and no visible furrow forms but a distinctive PKCε-M486A is clearly visible (2nd arrow). Initially PKCε-M486A appears to be endomembrane in nature (panel 3, red arrow) and becomes progressively compact over time. What resembles filamentous protrusions and retractions from within the structure towards the chromatin are also observed during the time course (panel 5, red arrow) albeit irregular and short lived. The accumulated GFP-PKCε-M486A persists for up to 20 minutes after which it disappears and becomes indistinguishable from cytoplasmic GFP-PKCε-M486A. Interestingly, treatment with jasplakinolide, another actin modifying agent, did not show PKC accumulation in any such structures in either interphase or mitotic cells (Figure 5.2) for anyconcentration tested (25-1000 nM). In contrast to latA, jasplakinolide is an actin polymerising and filament stabilising drug (Bubb et al., 1994).

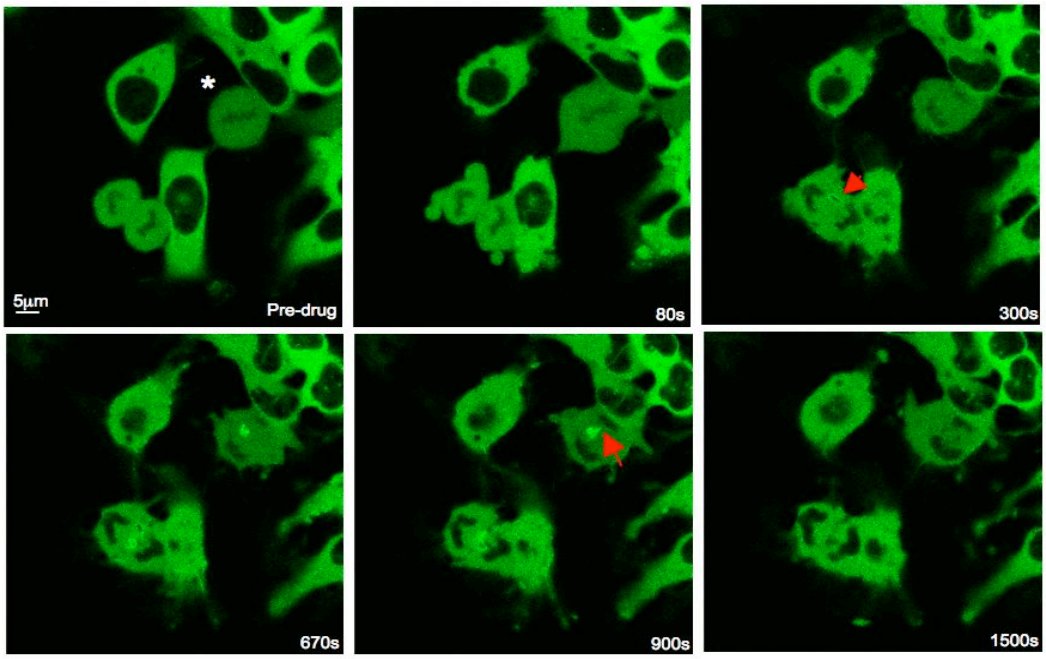

Figure 5-1 Depolymerization of actin with latA causes an equatorial accumulation of PKCε-M486A during anaphase/telophase
Still images, taken from a time-lapse video, of the M486A cell line in the presence of latA (100 nM). The white star in panel 1 (top left) is indicative of the cell in metaphase. The arrowhead in panel 3 (top right) indicates the vesicular nature of the initial equatorial GFP-PKCε-M486A positive structure whereas the arrowhead in panel 5 (middle bottom) indicates the protrusion of the structure towards DNA. The absence of the GFP-PKCε-M486A positive structure in panel 6 (10 minutes later) highlights its dynamic nature.

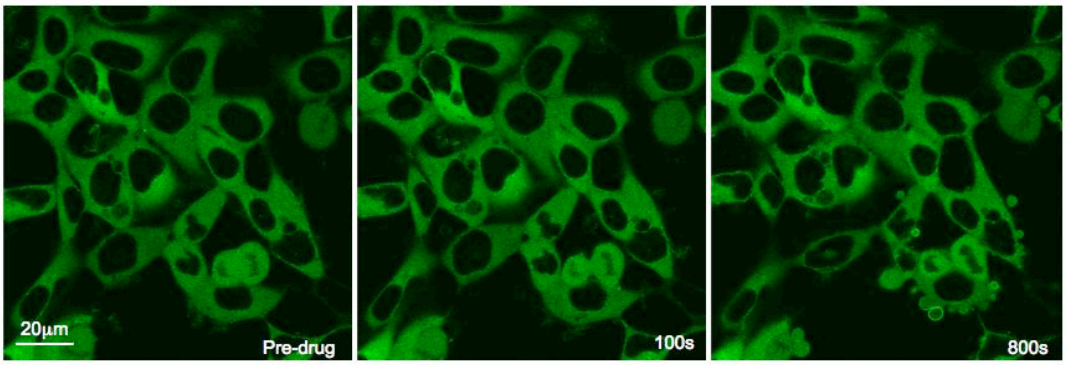

Figure 5-2 Deplolymerization of actin with jasplakinolide does not result in an equatorial accumulation of PKCε-M486A during anaphase/telophase
Still images, taken from a time-lapse video, of the M486A cell line in the presence of jasplakinolide (500 nM).

5.3.2 Equatorial accumulation of PKCε-M486A does not colocalize with lagging chromosomes

To assess whether the latA induced PKCε-M486A positive structure is positioned adjacent to or has any close association with DNA I have used the M486A cell line stably expressing mCherry-Histone 2B (H2B). In a representative dividing PKCε-M486A-H2B expressing cell (Figure 5.3), latA addition as expected leads to a reasonably equatorial, transient GFP-PKCε–M486A positive structure. This behaviour is similar to that observed in the PKCε-M486A only expressing cells. PKCε-M486A does not colocalize with the bulk of DNA nor is it localized adjacent to it. It is of particular note, however, that this doesn't exclude the possibility of an interaction with fine chromatin bridges. Indeed there is an indication of possible interactions between this structure and DNA, as evidenced by a transient protrusion towards condensed chromosomes on one side of the dividing cell (panel 4). In the absence of latA, PKCε-M486A-H2B expressing cells complete cytokinesis normally with no change in the distribution of PKCε-M486A.

5.3.3 The dynamic nature of PKCε-M486A is linked to the state of actin polymerization

In order to determine when actin depolymerization influences PKCε-M486A accumulation I monitored the appearance and localization of MARS-lifeact-RFP (Riedl et al., 2008) coexpressed in the PKCε-M486A cell line (Figure 5.4). Prior to the addition of drug, in a dividing cell, actin is distinctly cortical and as expected accumulates at the ingressing furrow (Figure 5.4, panel 1, Video 16). Following treatment with latA, the furrow regresses accompanied by a simultaneous loss of polymerized actin (Figure 5.4 panel 2). The behaviour of PKCε-M486A is then similar to that observed in the PKCε-M486A only expressing cells and its accumulation is not associated with any detectable

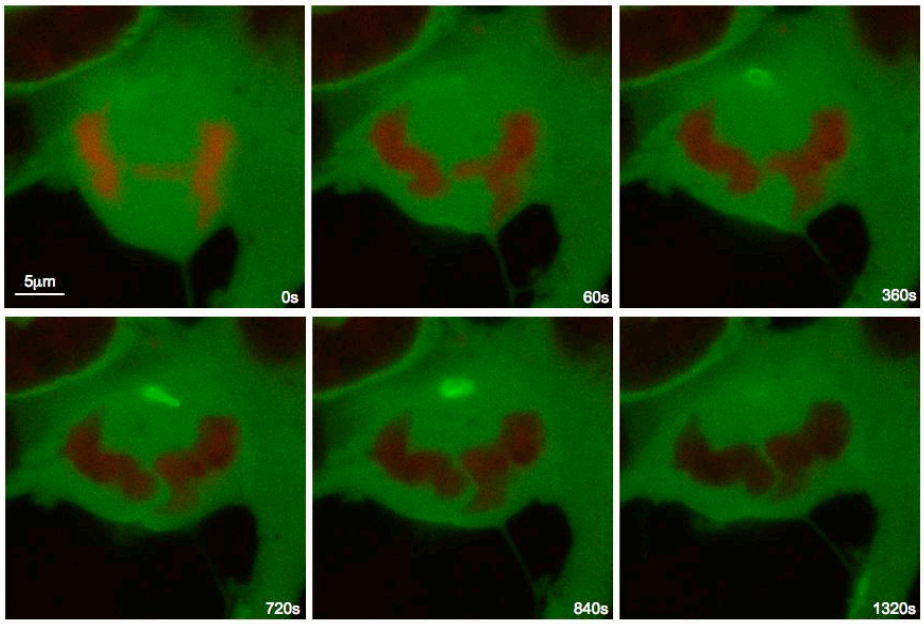

Figure 5-3 The latA induced PKCε-M486A positive structure does not colocalize with lagging chromosomes
Still images, taken from a time-lapse video, of the M486A cell line stably expressing H2B. The accumulation of GFP-PKCε-M486A is spatially distinct from that of DNA.

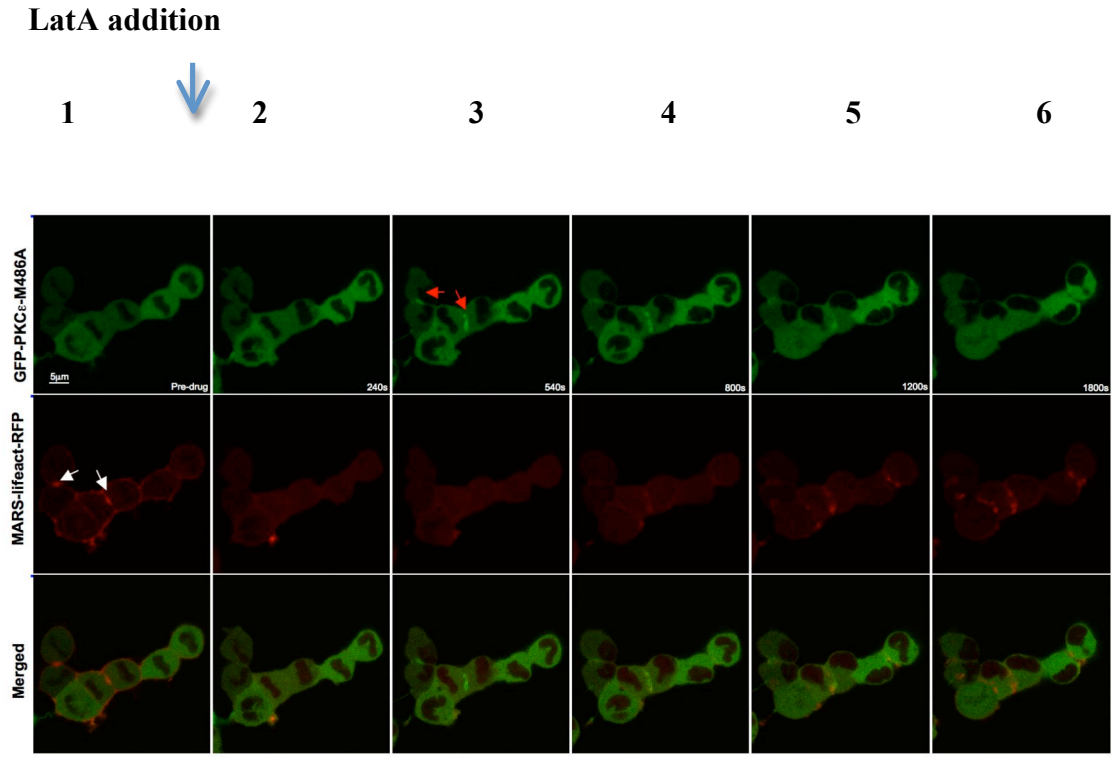

B

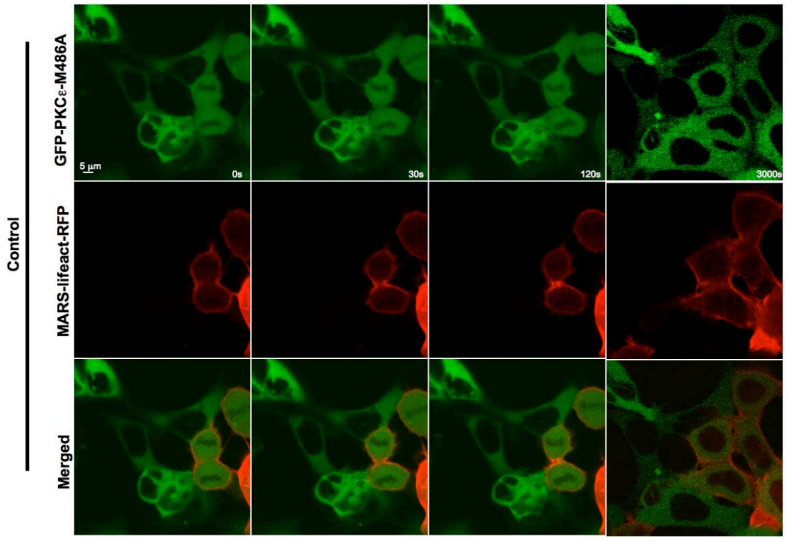

Figure 5-4 The dynamic behaviour of the latA induced PKCε-M486A positive structure is linked to actin depolymerization and the reappearance of residual actin rich structures

Still images, taken from a time-lapse video, of the M486A cell line transiently expressing MARS-lifeact-RFP. A) Arrowheads in panel 1 (far left, second row) indicate

Figure 5.4 continued relative cortical actin accumulation and preferential furrow accumulation in actively dividing cells prior to treatment with latA. Panel 2 shows the loss of MARS-lifeact upon latA exposure whilst arrowheads in panel 3 (top row) are indicative of the equatorial GFP-PKCε-M486A accumulation. The GFP-PKCε-M486A positive structure persists for approximately 15 minutes and disappearance correlates with the robust reappearance of MARS-lifeact, as shown in panels 5 and 6. B) In the absence of latA, cells complete furrowing normally with no change in the distribution of GFP-PKCε-M486A. Actin accumulates as expected at the furrow and midbody, where it persists for approximately 40 minutes until its disassembly coincides with abscission. In panel 4, the contrast has been modified to take into account unpreventable bleaching.

levels of MARS-lifeact-RFP (panel 3). Surprisingly, the local reappearance of MARS-lifeact-RFP briefly overlaps with the PKCε-M486A positive structure (panel 4) until the GFP-PKCε-M486A breaks down (panels 5 and 6). This suggests that actin polymerization is linked directly to the control of a PKCε-M486A positive structure and/or PKCε retention to a structure.

5.3.4 The PKCε-M486A positive structure is more pronounced and long-lived upon the addition of NaPP1

As previously mentioned, the latA induced PKCε-M486A positive structure persists for up to 20 minutes, all attempts to biochemically fix the structure failed, which suggest that either the structure itself is impenetrable to antibody or it's simply a reflection of its fragility. Surprisingly, upon the addition of NaPP1 and consequent PKCε-M486A inhibition, the latA-induced PKCε-M486A positive structure is much more pronounced and long-lived, with life-times ranging from 40-60 minutes (Figure 5.5, Video 15). This may reflect its retention on the re-localized actin whilst in an inactive state. The inactive PKCε-M486A positive structure is now amenable to fixing (Figure 5.6, 5.7).

5.3.5 RhoA colocalizes with the PKCε-M486A positive structure whilst key RhoA regulators do not

Although the polymerization state of actin appears intricately linked to the dynamics of PKCε-M486A, it does not resolve the molecular composition of its associated structure. To probe for potential candidates, M486A cells in the presence of latA and NaPP1 have been fixed. This has provided evidence for the co-localization of RhoA with PKCε-M486A (Figure 5.6) but not other cell cycle proteins associated with cytokinesis (Figure 5.7) and potentially influencing RhoA function, including Ect2 and MKLP1.

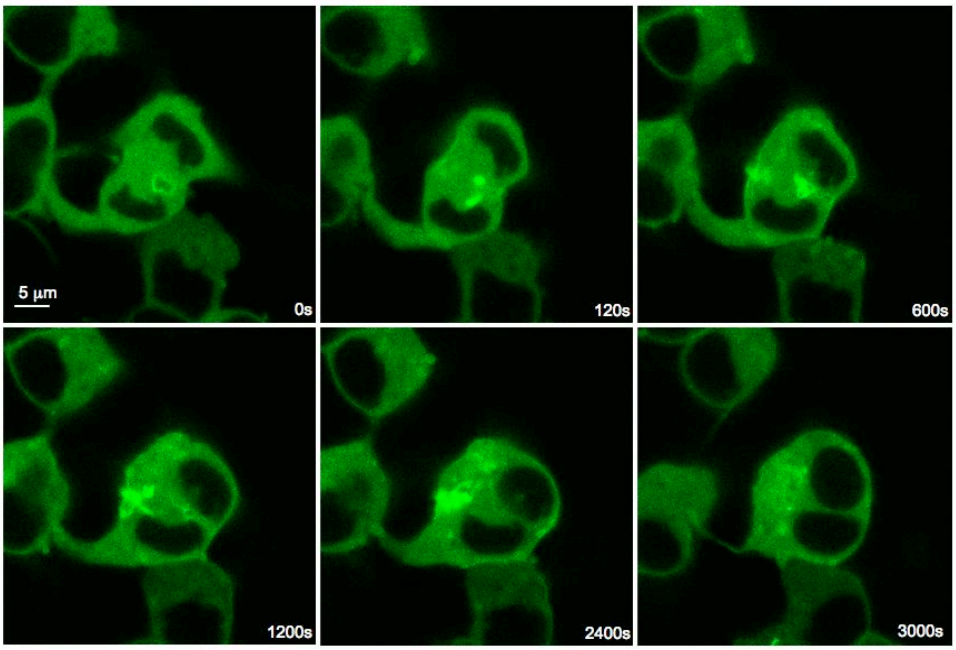

Figure 5-5 The latA induced PKCε-M486A positive structure is much more pronounced and long-lived when treated with NaPP1
Still images, taken from a time-lapse video, of the M486A cell line pre-treated with latA (100 nM for 5-10 minutes- or until first visual of GFP-PKCε positive structure) and then NaPP1 (4 μM). The panels are indicative of the progression of a PKCε-M486A positive structure under both these conditions.

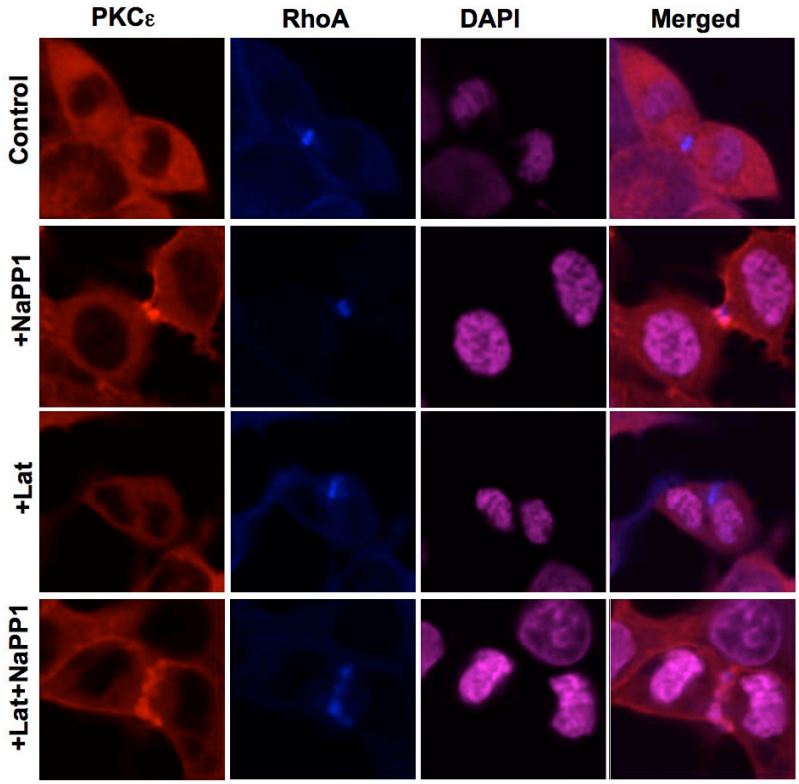

Figure 5-6 A latA and NaPP1 induced PKCε-M486A positive structure colocalizes with RhoA

For the fixed images in the first three rows, GFP-PKCε-M486A cells were treated with either a DMSO control, NaPP1 (4 μM) or latA (100 nM) for 10 minutes. In the final row of images, cells were pre-treated with latA for 10 minutes followed by a further 10 minute treatment with NaPP1. Cells were fixed and stained for PKCε (red), RhoA (blue) and DAPI (pink). PKCε and RhoA colocalize following either NaPP1 treatment or a combination of latA and NaPP1 treatment. For the fixed images in panel row 3, no PKCε positive structure is observed with latA treatment only.

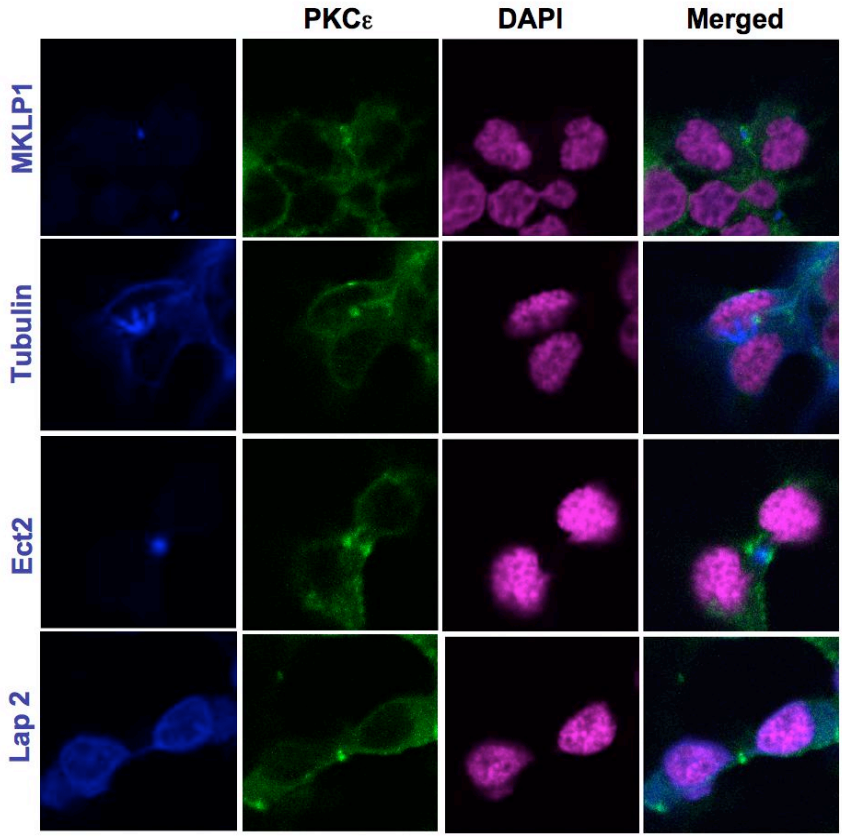

Figure 5-7 A latA and NaPP1 induced PKCε-M486A positive structure does not colocalize with other proteins associated with cytokinesis
GFP-PKCε-M486A cells were pre-treated with latA (100 nM) for 10 minutes followed by treatment with NaPP1 (4 μM) for a further 10 minutes. Cells were fixed and stained for a variety of cytokinetic associated proteins as indicated in the Figure (blue), PKCε (green) and DAPI (pink).

It is of note that two different methods of fixing were employed (see materials and methods).

5.3.6 A dynamic PKCε-M486A-RhoA structure in response to latA

In order to confirm the latA induced colocalization of RhoA with PKCε-M486A, I monitored the appearance and localization of cherry-RhoA coexpressed in the M486A cell line (Figure 5.8A, Video 17). Following treatment with latA the transient behaviour of PKCε-M486A is similar to that observed in the PKCε-M486A only expressing cells but importantly, its accumulation precisely overlaps with cherry-RhoA. In the absence of latA no such PKCε-M486A-RhoA positive structure accumulates and the distribution of the two are expected. To test for spectral bleed-through in these double-labelled cells, I monitored the appearance of a latA induced GFP-PKCε-M486A positive structure in a cell not expressing cherry-RhoA (Figure 5.8C). GFP-PKCε-M486A accumulation did not bleed-through to the cherry-RhoA channel.

A

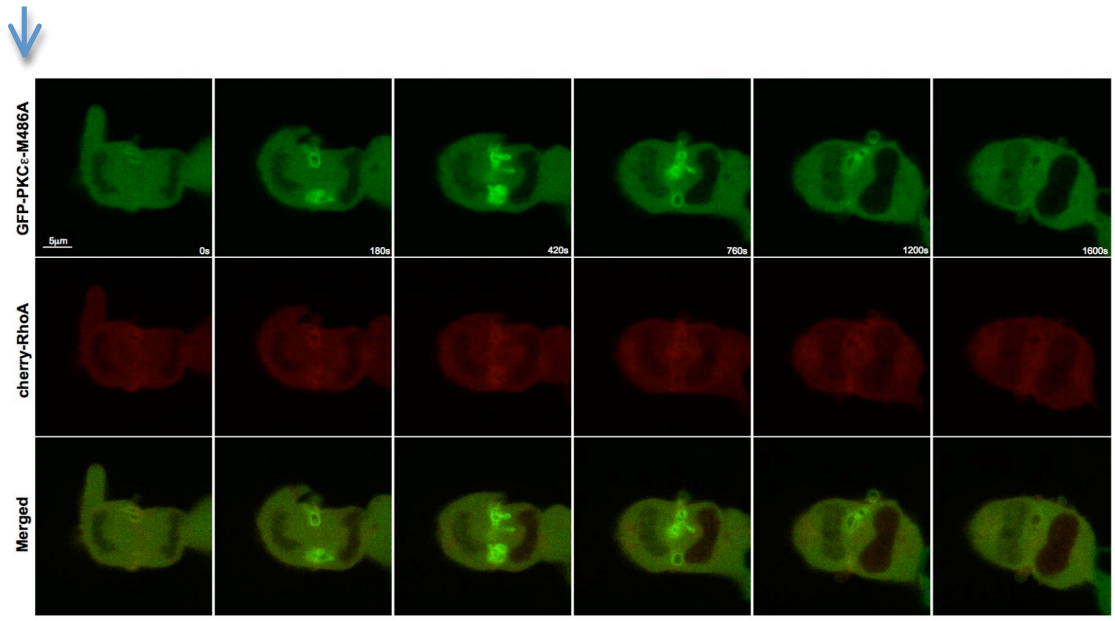

B

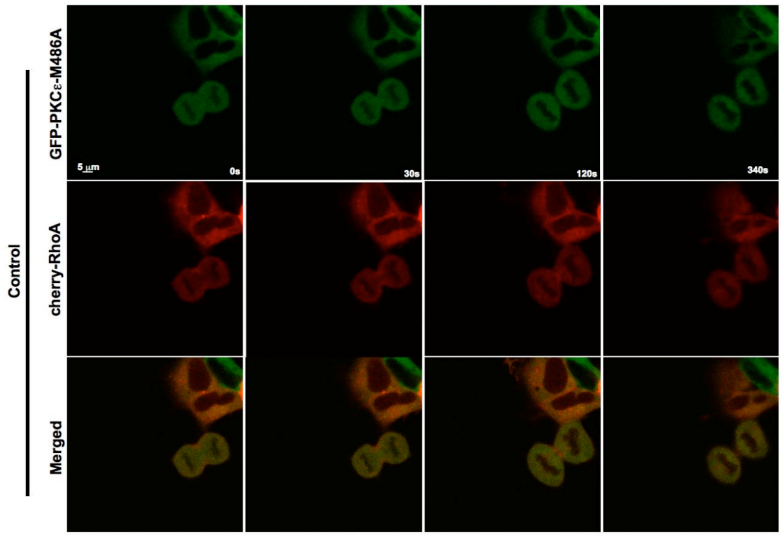

Figure 5-8 The latA induced PKCε-M486A positive structure colocalizes with RhoA

Still images, taken from a time-lapse video, of the M486A cell line transiently expressing cherry-RhoA. A) The accumulation and disappearance of GFP-PKCε-M486A precisely overlaps with that of cherry-RhoA. B) In the absence of latA cells

Figure 5.8 continued complete furrowing normally with no PKCε-M486A-RhoA positive structure forming. Cherry-RhoA accumulates as expected at the furrow/midbody .C) The colocalization of PKCε and RhoA is not a consequence of GFP spectral bleed-through.

C

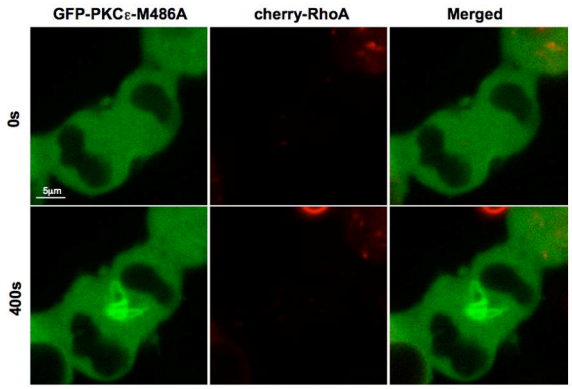

5.4 Discussion

Selective inhibition of PKCε-M486A causes localization of the enzyme at the furrow/midbody with RhoA-GTP and polymerized actin (Saurin et al., 2008). How its particular control is exerted here remains to be defined but it has been proposed that PKCε functions to reduce RhoA-GTP and permit actin depolymerization. Consistent with the role of PKCε in regulating this final stage of cytokinesis, I have uncovered an actin-PKCε-M486A-RhoA linked compartment, which importantly is observed without PKCε-M486A's inhibition and may help define its behaviour here.

Work in the previous chapter identified the IC1D as being involved in the recruitment of PKCε-M486A to the furrow/midbody. Although, previously identified as an actin-binding motif (Prekeris et al., 1996), I have been unable to provide direct evidence to support this interaction. Rather, to assess the relationship between actin and PKCε-M486A recruitment I have manipulated actin polymerization using latA. At the normal time of furrowing, the addition of latA leads to the depolymerization of actin and the stabilisation of an equatorial PKCε-M486A-RhoA positive structure (Figure 5.1 and 5.8). The accumulation of PKCε-M486A and RhoA is relatively short lived, persisting for up to a maximum of 20 minutes and then disappearing, surprisingly, correlating with the re-appearance of residual actin-rich structures. Whilst it has been demonstrated that the reorganisation of F-actin following depolymerization with latA is possible upon the removal of the drug (Gerisch et al., 2004), it is intriguing that residual actin rich structures can form here whilst still in the presence of latA (albeit low concentrations). Interestingly, these actin structures specifically relocalize to the furrow, accumulating either adjacent to or slightly overlapping with the GFP-PKCε-M486A positive structure (Figure 5.4). Nevertheless, this data suggests that F-actin maybe required for PKCε turnover. Consistent, with this hypothesis, treatment with the actin stabilising drug jasplakinolide, does not induce the appearance of any such PKC positive structures (Figure 5.2) suggesting that the mere retention of F-actin, albeit in a non-physiological form, is not sufficient to suppress PKCε turnover. Furthermore, the addition of NaPP1

prolongs the existence of the GFP-PKCε-M486A positive structure, perhaps reflecting a stronger retention of inactive PKCε-M486A on actin (Figure 5.5).

In view of the proposed role of actin in recruiting PKCε-M486A to the furrow/midbody, it is intriguing that PKCε-M486A is located here apparently in the absence of actin. It has been suggested previously that Rab11/FIP3 endosomes, in addition to membrane expansion, deliver proteins that are necessary for the completion of cytokinesis. Specifically, the sequential binding of MgcRacGAP to Ect2 and FIP3 is thought to regulate actomyosin ring dissociation (Simon et al., 2008). Given the probable endomembrane nature of the latA-induced GFP-PKCε-M486A positive structure, it is plausible that accumulation of PKCε-M486A is in part a function of membrane trafficking, whether this reflects an alternative actin-independent pathway or whether it is merely indicative of an interaction with further components at the midbody in an actin-dependent pathway remains to be defined. Nonetheless, to test the involvement of Rab11 and other potential candidates involved in membrane trafficking it would be informative to monitor PKCε-M486A recruitment in response to latA after employing siRNA knock-down of Rab11 and functionally related proteins. In addition, the delivery of these vesicles has been reported to be mediated by microtubules. This is of interest because of the protrusions observed from the GFP-PKCε-M486A positive structure toward DNA. To test whether these reflect a dependence on the microtubule network, more specifically the central spindle, the microtubule destabilizer nocodazole could be tested.

It seems unlikely that the latA induced GFP-PKCε-M486A positive structure described is a non-specific aggregate of proteins given its transient nature and the fact it can be stabilized by PKCε-M486A inhibition. Rather, I propose that the disruption of F-actin causes an active PKCε-M486A-RhoA positive structure to stabilize in a manner possibly analogous to a snapshot of midbody biogenesis and could therefore be useful in understanding how PKCε exerts its function there. PKCε may reduce RhoA-GTP loading by either driving a decrease in RhoGEF activity or an increase in RhoGAP activity. However, whilst anticipating an increase in RhoA-GTP loading in the presence of latA due to its phenocopy with PKCε-M486A and NaPP1, the activation status of

RhoA in the presence of latA remains uncharacterized. Confirmation of the activity of RhoA during this process is still required. If evidence is generated to indicate that latA maintains RhoA in an active state, there are many candidate proteins PKCε might then influence to inactivate RhoA, most notably Ect2 and MgcRacGAP. Recent work in our laboratory has uncovered 3 very high scoring candidate nPKC sites on Ect2 and Minoshima et al have reported a phosphorylation at S387 on MgcRacGAP which induces GAP activity at the late stages of cytokinesis (Minoshima et al., 2003). These could be tested for PKCε control and their phosphorylation monitored during latA treatment. Furthermore, the effect of siRNA on GEF/GAP candidates and RhoA itself could be investigated in conjunction with overexpression studies of GEF/GAP and their mutant forms. In an attempt to summarize the findings of this chapter please see Figure 5.9.

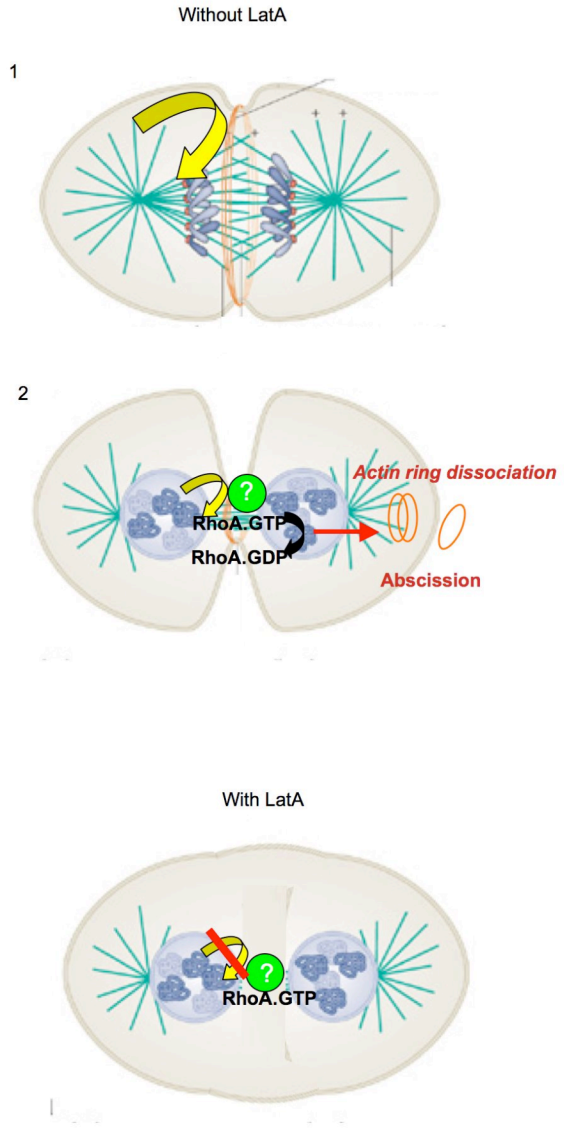

Figure 5-9 A model outlining the understanding of PKCε regulation in the absence and presence of latA
(Reprinted by permission from Macmillan Publishers Ltd, Nat Rev Mol Cell Biol, Glotzer, The 3Ms of central spindle assembly: microtubules, motors and MAPs, 10, 9-20, 2009). With latA. 1)Actin (orange ring) is required for PKCε (yellow arrow) delivery and turnover at the furrow/midbody. 2) RhoA inactivation is required for actin ring dissociation which may be driven by an interaction with PKCε and as yet an unidentified component (green). With latA. Loss of pre-formed actin ring causes the collapse of any ingressing furrow and prevents the turnover of PKCε such that it becomes 'trapped' on the unknown with RhoA.

Chapter 6. Discussion

Prior to this thesis work had demonstrated that recruitment of PKCε to the furrow/midbody and assembly into a complex with 14.3.3 is required for the successful completion of cytokinesis (Saurin et al., 2008). Although the molecular mechanism of this control is undefined, PKCε is thought to be required for the inactivation of RhoA and consequent actin depolymerization associated with abscission (Saurin et al., 2008). Importantly, failure to complete cytokinesis can lead to genetically unstable tetraploid cells, a prelude to aneuploidy and tumour formation (Fujiwara et al., 2005). Precise mapping of cytokinesis at a molecular level is, therefore, a necessary prerequisite for the assessment of whether intervention in this process might bring about benefits in the treatment of cancer. In an attempt to derive a more specific understanding of how PKCε exerts its function during cytokinesis, I have addressed the mechanism by which PKCε is localized at the furrow/midbody. Unfortunately, the furrow/midbody has proved difficult to assess biochemically due to its relatively infrequent nature and the intrinsic difficulty in synchronizing cells in cytokinesis. To overcome this problem I have attempted to molecularly define aspects associated with the furrow/midbody with the use of extensive live confocal microscopy and mutagenesis. Indeed this has proved relatively successful, however, monitoring the process in single cells does prove challenging for vast data collections.

As demonstration of the localization of an uninhibited PKCε at the furrow/midbody has remained elusive, perhaps reflecting the transient nature of the association, I have employed the use of a chemical genetic approach using the NaPP1 sensitive PKCε-M486A (Bishop et al., 1998, Bishop et al., 2000, Durgan et al., 2008, Saurin et al., 2008). Although this system relies on ectopic expression of mutant forms of PKCε and non-physiological stimuli, it has provided key mechanistic insight concerning the involvement of PKCε in cytokinesis. Furthermore, the validity of this approach is evidenced by the finding that NaPP1 addition to induced WT cells has no effect (Figure 3.3) and treatment with a c/nPKC inhibitor, Bim1, shows a similar PKCε midbody localization (Figure 3.5). Although the PKCε-M486A, when compared with PKCε-WT,

demonstrates a reduced affinity for ATP, which is reflected in the instability of priming phosphorylations (Cameron et al., 2009), this loss is acceptable and indeed proved useful when characterising the PKCε-ΔIC1D-M486A deletion mutant (Figure 4.6).

Demonstration of an interaction of endogenous kinase at the furrow/midbody would be preferable but as already mentioned, the transient nature of this association is currently not amenable to probing with the approaches available. However, the PKCε-M486A-RhoA positive structure that appears independently of PKCε-M486A inhibition during cytokinesis (Chapter 5, Figure 5.1) may shed light on PKCε behaviour here.

6.1 PKCε-M486A furrow/midbody recruitment and retention

PKCε-M486A localizes to the plasma membrane before becoming concentrated at the furrow/midbody when selectively inhibited with NaPP1 (Chapter 3, Figure 3.2). Using mutation and deletion analysis I have shown that localization at both compartments is in part a function of the IC1D (Figure 4.4), a motif previously identified as actin binding (Chapter 4, Prekeris et al., 1996, Prekeris et al., 1998). If evidence is generated to confirm that the IC1D is an actin-binding motif, then the working hypothesis becomes such that whilst in its active state PKCε-M486A retention on actin (cortical and contractile ring) is poor in response to normal physiological stimuli; it is implicit that catalytic activity is required for its release from actin, regardless of the stage of the cell cycle.

Given that at the early stages of furrow formation PKCε-M486A is associated with non-juxtaposed plasma membranes, I propose that the IC1D functions in a similar manner to recruit PKCε-M486A to both the plasma membrane and early furrow. It seems likely that the initial plasma membrane recruitment of PKCε serves as a prelude to that at the furrow by bringing about a conformational change, however it is also plausible that PKCε is involved in monitoring the site of cell division, in a concentration dependent manner. Perhaps the inhibition of PKCε at this early stage in then only evident at the

point of RhoA inactivation. Or perhaps, PKCε could have dual functionality and once reaching a threshold at the midbody change function and acts on abscission. To test the involvement of PKCε in furrow formation it might informative to monitor PKCε knockdown cells and measure the distance between the centralspindlin complex and the actomyosin ring to see if there are any changes.

Nevertheless, the distinct and concentrated localization of the enzyme at the invaginating furrow/midbody may reflect further interactions of the open conformer with other specific contacts These additional contacts at the furrow/midbody, however, do not appear to be related to those at cell-cell contacts. In Chapter 3 (Figure 3.6), I demonstrated, using FRAP, that PKCε-M486A has a significantly slower turnover at the furrow/midbody compared with the dynamics at cell-cell contacts, which is indicative of a distinct, more complex retention mechanism at the furrow/midbody. When probing other potential candidates involved in PKCε-M486A retention at the furrow/midbody FRAP analysis may prove invaluable. For example, despite the finding that 14.3.3 is not required for PKCε-M486A recruitment to the furrow/midbody (Figure 4.3) it is plausible that 14.3.3 may act to subtly alter PKCε dynamics once localized there. Given that Saurin and colleagues proposed that 14.3.3 binding serves to act as a 'conformational clamp' locking PKCε into an active open conformation, a consequence of such stabilization could increase its retention at the furrow/midbody; it might be useful to compare the dynamics of PKCε-M486A and PKCε-S346,368A-M486A.

An alternative explanation for the source of additional contacts at the midbody may come from the latA experiments (Chapter 5). It is intriguing that PKCε-M486A is localized to a structure reminiscent of the midbody, without prior accumulation at the furrow, when cells are treated with latA (Figure 5.1, 5.5, 5.7). As suggested in the chapter, the endomembrane nature of the latA-induced structure may reflect a dependence on the membrane trafficking network. Two distinct populations of vesicles have been associated with the completion of cytokinesis, Rab6 golgi-derived vesicles and Rab11 vesicles derived from recycling endosomes (Simon et al., 2008, Hill et al., 2000). It is of particular interest that Rab11 localization to the midbody depends on binding FIP3. The latter has itself been implicated in regulating Ect2 dissociation at the centralspindlin by binding to MgcRacGAP and consequently reducing RhoA-GTP

(Simon et al., 2008). It is plausible, therefore, that PKCε-M486A may exert its function on RhoA via this pathway. It might be informative to monitor the effect of PKCε-M486A in response to latA and NaPP1 after siRNA knockdown of Rab11, Rab6 and other potential trafficking candidates. Regardless of whether evidence is generated to support the requirement of membrane trafficking for PKCε-M486A localization at the midbody, the microtubule network should also be investigated. In addition to it facilitating membrane trafficking, it is also plausible that microtubules function at this stage as a platform for key cytokinetic regulators that could include PKCε. To assess the involvement of the microtubule network it would be possible to treat the cells with the microtubule destabilizer, nocodazole and monitor the PKCε-M486A response. However, given that nocodazole treatment might act to disrupt the midbody and its associated proteins, perhaps a less destructive approach would be to target the motor proteins that power transport along microtubules instead, such as a small screen using a library of kinesin inhibitors or siRNA.

In addition to the IC1D, it was hypothesized that DAG formation, via Ca^{2+} dependent-PLC hydrolysis of PIP_2, functions to regulate PKCε-M486A recruitment to the plasma membrane and furrow/midbody. Interestingly, the local production of PIP_2 at the furrow is required for the successful completion of cytokinesis (Saul et al., 2004, Wong et al., 2005) and may reflect the downstream, albeit short-lived, DAG production at this compartment. An attempt in Chapter 3 was made to assess the contribution of DAG in PKCε-M486A localization. Surprisingly, rather than having a negative effect, Ca^{2+} depletion led to the retention of PKCε-M486A at the plasma membrane in suspended cells (Figure 3.7, 3.8) however, in contrast FRAP analysis failed to demonstrate any significant change in the kinetics of PKCε-M486A at either cell-cell contacts or the furrow/midbody (Figure 3.10), the discrepancy between these two results may reflect the unique suspension behaviour of these cells and/or the nature of the cell-cell contacts in the two environments. These results are preliminary and the destruction of DAG may be incomplete in this experiment and off-target effects may occur due to the non-specific nature of this experiment. Perhaps a more conclusive approach would be the employment of siRNA directed specifically at PLCs and/or mutations within the C1 domain of PKCε-M486A preventing DAG binding. Given that DAG binds to the

tandem C1A and C1B domains I would propose to convert critical prolines to glycines at sites 180 in C1A and 253 in C1B (Hurley et al., 1997, Bogi et al., 1998).

Collectively, the results of these studies show a requirement for the IC1D in both plasma membrane and furrow/midbody localization. The reason for the altered association of PKCε-M486A at the furrow/midbody is not yet clearly resolved. However, I have shown through FRAP experiments that the process may be different to PKCε-M486A accumulation at cell-cell contacts. I have identified other potential candidates that could be involved and have proposed the necessary follow-up experiments. It is hoped that these will define the distinct behaviour of PKCε-M486A at the furrow/midbody. For a revised model of PKCε regulation and localization see Figure 6.1.

6.2 PKCε-M486A and actin, consequences for RhoA control

Work throughout this thesis has attempted to characterize PKCε-M486A recruitment to the furrow/midbody. Although refinement of this pathway is required, actin has been implicated as a key regulator. Actin not only functions during cytokinesis to drive the constriction of the invaginating furrow but may also serve as a platform to recruit and maintain the constant turnover of PKCε-M486A, as described in my working hypothesis. Furthermore, as identified in Chapter 5, it also appears to be intimately linked to PKCε-M486A control of RhoA (Figure 5.5, 5.7). Manipulation of actin polymerization (latA) at the normal time of furrowing leads to an equatorial PKCε-M486A-RhoA compartment temporarily forming, independently of PKCε-M486A inhibition (Figure 5.1). Consistent with my working hypothesis, the local reappearance of actin, then triggers the release of active PKCε-M486A along with RhoA from this undefined structure (5.3, 5.7).

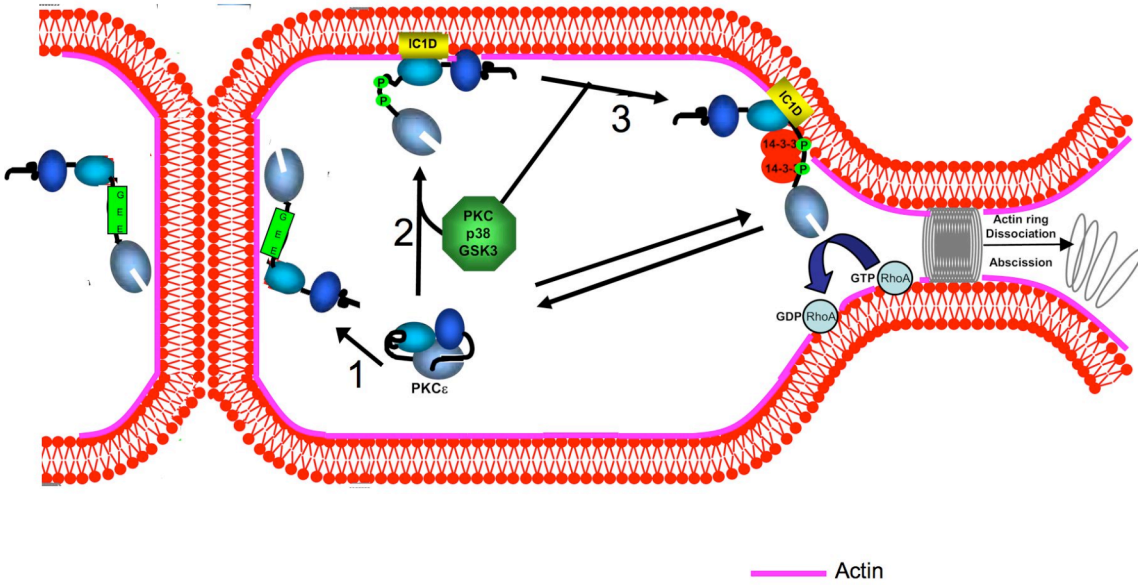

Figure 6-1 Updated schematic summarizing how PKCε localization is controlled (Reprinted and adapted with permission from Macmillan Publishers Ltd: Nature Cell Biology, Saurin et al, 10, 891-901, 2008). 1) The GEE motif selectively targets PKCε to cell-cell contacts (as in previous model) but is not required for furrow/midbody recruitment. 2) Membrane and furrow/midbody recruitment is mediated through the IC1D which is thought to be actin (pink) binding. As to whether membrane binding is a prerequisite for furrow/midbody binding remains unknown. As does the precise timing of phosphorylation by PKC, p38 and GSK3 but importantly PKCε-14.3.3 complex assembly is not required for PKCε localization at the furrow/midbody (3). Once at the furrow/midbody, 14.3.3 is then believed to maintain PKCε in an active, open conformation where it is thought to control RhoA-GTP loading.

In principle, treatment with latA could effectively 'stabilize/trap' PKCε-M486A at components with which it additionally associates once at the midbody. Interestingly active PKCε-M486A colocalizes at this structure with RhoA (Figure 5.5, 5.7), similar to the midbody localization of PKCε-M486A and RhoA in response to NaPP1 (Saurin et al., 2008). Given that treatment with NaPP1 is also associated with an increase in RhoA-GTP (Saurin et al 2008) due to this phenocopy it is expected that RhoA may be in its GTP bound form during latA treatment. However, this is purely speculative, it is possible that the depolymerization of actin, may function to mimic the terminal stage of cytokinesis, by-passing the need for active RhoA and instead trigger its inactivation. Therefore, monitoring the activity of RhoA during latA treatment is now required to clarify the nature of this compartment.

With regards to PKCε's function in this undefined structure, like that at the midbody in response to NaPP1, it is expected to control RhoA via either decreasing the activity of a GEF or increasing activity of a GAP. There are many candidate proteins that PKCε might influence including Ect2 and MgcRacGAP. A generic approach to identify PKCε targets should be tractable through a combination of NaPP1 and latA treatment using immuno-fluorescence. Although preliminary evidence indicates that MKLP1, a marker of the centralspindlin and Ect2 do not colocalize with this structure (Figure 5.6) their phosphorylation status remains unknown and MgcRacGAP has not been tested. Given the transient nature of this structure and the difficulty in fixing, a complementary and arguably more conclusive approach would be to also employ a single-cell readout approach using RFP constructs of potential candidates coexpressed with GFP-PKCε-M486A in live imaging.

Nevertheless, the observation that PKCε-M486A can accumulate with RhoA in its active state is important and may shed light on PKCε behaviour in cytokinesis. Indeed this condition may be analogous to a stage in midbody biogenesis and may be evidence of the requirement for F-actin for normal PKCε-M484A and RhoA turnover. I therefore propose that work should continue to address the additional components of this undefined structure. This would also include probing the aforementioned vesicle

trafficking system and deducing the activity/phosphorylation states of those components successfully identified.

6.3 PKCε-M486A and Ca^{2+}

In view of the classification of PKCε as a Ca^{2+} independent PKC, it is surprising to observe that PKCε-M486A displays Ca^{2+} sensitivity in terms of its cell-cell contact recruitment (Figure 3.7, 3.8). In suspension, I have shown that Ca^{2+} depletion leads to an increase in retention of inactive PKCε-M486A at cell-cell contacts and cells prove considerably harder to separate (Figure 3.9), both indicative of a change in the affinity or avidity of the interactions found here. Consistent with this response, in culture, disruption to cell-cell contacts and extensive shrinkage induced by EGTA was completely blocked by pre-treatment with NaPP1 (Figure 3.11). Interestingly, this PKCε protection is only apparent if the cells are plated on poly-L-lysine coated cover slips and their integrins are not engaged. As such, this may reflect a unique pathway in operation when for example cancer cells are undergoing metastatic spread and consequently this phenomenon deserves further investigation.

Given the increasing amount of evidence which shows that Ca^{2+} can directly regulate protein-protein interactions, I propose that Ca^{2+} directly regulates a PKCε-M486A-protein interacting protein specifically at cell-cell contacts. A candidate interacting protein would be the scaffold protein ENH. Ca^{2+} regulates the association of PKCε-ENH and consequently the formation of a PKCε-ENH-N_type Ca^{2+} channel complex in neuronal cells (Chen et al., 2006). Whether this scaffolding protein plays a role in conferring Ca^{2+} sensitivity of PKCε-M486A in HEK293 cells remains to be determined but could be assessed by employing siRNA against ENH.

One other notable family of potential PKCε interacting proteins are the cadherins. Interestingly, they are linked to actin through catenins and a variety of studies have shown that they are internalized by Ca^{2+} depletion (Alexander et al., 1993, Alexander et

al., 1998, Le et al., 1999, Kamei et al., 1999). In view of the proposed role of the IC1D in binding actin it is plausible that inhibited PKCε-M486A accumulates at actin and consequently prevents the internalization of cadherins when exposed to EGTA. Consistent with this hypothesis, pre-treatment with staurosporine, an ATP-competitive kinase inhibitor, has been shown to block low Ca^{2+} mediated cell rounding and cadherin endocytosis (Alexander et al., 1998). To determine whether cadherins play a role in conferring PKCε-M486A Ca^{2+} sensitivity in HEK 293 cells it would be useful to employ siRNA and monitor PKCε-M486A response in both suspended and cultured cells. Furthermore, to assess the internalization of cadherins one could employ a trypsin protection assay whereby surface vs. internalized cadherins can be measured and their reappearance monitored after calcium restoration.

Final comments

To derive a more specific understanding of PKCε function in cytokinesis I have addressed the mechanism by which PKCε-M486A is localized to the furrow/midbody. The data presented throughout this thesis suggests that actin is a key regulator required for PKCε-M486A accumulation at the furrow/midbody and once at the midbody maybe required for PKCε-RhoA turnover.

Appendix

Supplementary Videos

Chapter 3

Video 1: PKCε-M486A expressing cells undergoing normal mitosis
Video 2: Selective inhibition of PKCε-M486A, showing accumulation at the furrow/midbody
Video 3: EGTA addition to PKCε-M486A expressing cells (plated on poly-L-lysine) causes significant cell shrinkage and disruption to cell-cell contacts
Video 4: NaPP1 addition to PKCε-M486A expressing cells (plated on poly-L-lysine) protects cells from the effects of EGTA
Video 5: EGTA addition to PKCε-WT expressing cells (plated on poly-L-lysine) causes cell shrinkage and disruption to cell-cell contacts
Video 6: NaPP1 addition to PKCε-WT expressing cells (plated on poly-L-lysine) does not protect cells from the effects of EGTA
Video 7: EGTA addition to PKCε-M486A expressing cells (plated on fibronectin) causes significant cell shrinkage and disruption to cell-cell contacts
Video 8: NaPP1 addition to PKCε-M486A expressing cells (plated on fibronectin) does not protect cells from the effects of EGTA

Video 9: EGTA addition to PKCε-M486A expressing cells (plated on collagen) causes significant cell shrinkage and disruption to cell-cell contacts

Video 10: NaPP1 addition to PKCε-M486A expressing cells (plated on collagen) does not protect cells from the effects of EGTA

Video 11: EGTA addition to PKCε-M486A expressing cells (plated on laminin) causes significant cell shrinkage and disruption to cell-cell contacts

Video 12: NaPP1 addition to PKCε-M486A expressing cells (plated on laminin) does not protect cells from the effects of EGTA

Chapter 4

Video 13: Selective inhibition of PKCε-ΔIC1D-M486A does not result in GFP-PKCε-ΔIC1D-M486A accumulation at the furrow/midbody despite accumulation of the coexpressed RFP-PKCε-M486A

Chapter 5

Video 14: LatA addition to PKCε-M486A expressing cells results in the appearance of a transient GFP-PKCε-M486A positive structure in mitotic cells only (duration of positive structure = 20minutes)

Video 15: Selective inhibition of PKCε-M486A prolongs the appearance and intensity of the latA induced GFP-PKCε-M486A positive structure (duration of positive structure = 1 hour)

Video 16: The transient nature of the latA induced GFP-PKCε-M486A positive structure is linked to the polymerization state of actin

Video 17: LatA induced GFP-PKCε-M486A colocalizes with RhoA at the undefined equatorial structure

Independent confirmation of FRAP analysis using Microsoft Excel

1) Export raw data into Microsoft Excel (cells A2-D291)
2) Background subtraction (cells G2-I291)
3) Normalisation and corrections for fluorescence loss during photobleaching (cells L2-O291)
4) Plot final fluorescence (cells R2-R291) against time, using a biexponential model, in Prism.

Reference List

ABERLE, H., SCHWARTZ, H. & KEMLER, R. (1996) Cadherin-catenin complex: protein interactions and their implications for cadherin function. *J Cell Biochem,* 61**,** 514-23.

ALAIMO, P. J., SHOGREN-KNAAK, M. A. & SHOKAT, K. M. (2001) Chemical genetic approaches for the elucidation of signaling pathways. *Curr Opin Chem Biol,* 5**,** 360-7.

ALESSI, D. R., JAMES, S. R., DOWNES, C. P., HOLMES, A. B., GAFFNEY, P. R., REESE, C. B. & COHEN, P. (1997) Characterization of a 3-phosphoinositide-dependent protein kinase which phosphorylates and activates protein kinase Balpha. *Curr Biol,* 7**,** 261-9.

ALEXANDER, J. S., BLASCHUK, O. W. & HASELTON, F. R. (1993) An N-cadherin-like protein contributes to solute barrier maintenance in cultured endothelium. *J Cell Physiol,* 156**,** 610-8.

ALEXANDER, J. S., JACKSON, S. A., CHANEY, E., KEVIL, C. G. & HASELTON, F. R. (1998) The role of cadherin endocytosis in endothelial barrier regulation: involvement of protein kinase C and actin-cadherin interactions. *Inflammation,* 22**,** 419-33.

ALVARO, V., LEVY, L., DUBRAY, C., ROCHE, A., PEILLON, F., QUERAT, B. & JOUBERT, D. (1993) Invasive human pituitary tumors express a point-mutated alpha-protein kinase-C. *J Clin Endocrinol Metab,* 77**,** 1125-9.

AMANO, M., ITO, M., KIMURA, K., FUKATA, Y., CHIHARA, K., NAKANO, T., MATSUURA, Y. & KAIBUCHI, K. (1996) Phosphorylation and activation of myosin by Rho-associated kinase (Rho-kinase). *J Biol Chem,* 271**,** 20246-9.

APARICIO, O. M., WEINSTEIN, D. M. & BELL, S. P. (1997) Components and dynamics of DNA replication complexes in S. cerevisiae: redistribution of MCM proteins and Cdc45p during S phase. *Cell,* 91**,** 59-69.

AZIZ, MH., MANOHARAN, HT., VERMA, AK. (2007) Protein kinase C epsilon which sensitizes skin to sun's UV radiation-induced cutaneous damage and development of squamouse cell carcinomas, associates with Stat3. *Cancer Res,* 67**,** 1385-94.

BAE, KM., WANG, H, JIANG, G., CHEN, MG., LU, L., XIAO, L. (2007) Protein kinase C epsilon is overexpressed in primary human non-small cell lung cancers and functionally required for proliferation of non-small cell lung cancer cells in a p21/Cip1-dependent manner. *Cancer Res,* 67**,** 6053-63.

BALENDRAN, A., HARE, G. R., KIELOCH, A., WILLIAMS, M. R. & ALESSI, D. R. (2000) Further evidence that 3-phosphoinositide-dependent protein kinase-1 (PDK1) is required for the stability and phosphorylation of protein kinase C (PKC) isoforms. *FEBS Lett,* 484**,** 217-23.

BAN, R., IRINO, Y., FUKAMI, K. & TANAKA, H. (2004) Human mitotic spindle-associated protein PRC1 inhibits MgcRacGAP activity toward Cdc42 during the metaphase. *J Biol Chem,* 279**,** 16394-402.

BARR, F. A. & GRUNEBERG, U. (2007) Cytokinesis: placing and making the final cut. *Cell,* 131**,** 847-60.

BASHIR, T., HORLEIN, R., ROMMELAERE, J. & WILLWAND, K. (2000) Cyclin A activates the DNA polymerase delta -dependent elongation machinery in vitro: A parvovirus DNA replication model. *Proc Natl Acad Sci U S A,* 97**,** 5522-7.

BEHN-KRAPPA, A. & NEWTON, A. C. (1999) The hydrophobic phosphorylation motif of conventional protein kinase C is regulated by autophosphorylation. *Curr Biol,* 9**,** 728-37.

BENTON, R., PALACIOS, I. M. & ST JOHNSTON, D. (2002) Drosophila 14-3-3/PAR-5 is an essential mediator of PAR-1 function in axis formation. *Dev Cell,* 3**,** 659-71.

BETSON, M. & SETTLEMAN, J. (2007) A rho-binding protein kinase C-like activity is required for the function of protein kinase N in Drosophila development. *Genetics,* 176**,** 2201-12.

BISHOP, A. C., SHAH, K., LIU, Y., WITUCKI, L., KUNG, C. & SHOKAT, K. M. (1998) Design of allele-specific inhibitors to probe protein kinase signaling. *Curr Biol,* 8**,** 257-66.

BISHOP, A. C., UBERSAX, J. A., PETSCH, D. T., MATHEOS, D. P., GRAY, N. S., BLETHROW, J., SHIMIZU, E., TSIEN, J. Z., SCHULTZ, P. G., ROSE, M. D., WOOD, J. L., MORGAN, D. O. & SHOKAT, K. M. (2000) A chemical switch for inhibitor-sensitive alleles of any protein kinase. *Nature,* 407**,** 395-401.

BOGI, K., LORENZO, P. S., SZALLASI, Z., ACS, P., WAGNER, G. S. & BLUMBERG, P. M. (1998) Differential selectivity of ligands for the C1a and C1b phorbol ester binding domains of protein kinase Cdelta: possible correlation with tumor-promoting activity. *Cancer Res,* 58**,** 1423-8.

BORNANCIN, F. & PARKER, P. J. (1996) Phosphorylation of threonine 638 critically controls the dephosphorylation and inactivation of protein kinase Calpha. *Curr Biol,* 6**,** 1114-23.

CASCACE, AM., GUADAGNO, SN., KRAUSS, RS., FABBRO, D., WEINSTEIN, IB. (1993) The epsilon isoform of protein kinase C is an oncogene when overexpressed in rat fibroblasts. *Oncogene,* 8**,** 2095-2104.

CAMERON, A. J., ESCRIBANO, C., SAURIN, A. T., KOSTELECKY, B. & PARKER, P. J. (2009) PKC maturation is promoted by nucleotide pocket occupation independently of intrinsic kinase activity. *Nat Struct Mol Biol,* 16**,** 624-30.

CAMERON, A. J., LINCH, M. D., SAURIN, A. T., ESCRIBANO, C. & PARKER, P. J. (2011) Dissecting the role of Sin1 in AGC kinase regulation by TORC2. *Biochem J*.

CAMPELLONE, K. G. (2010) Cytoskeleton-modulating effectors of enteropathogenic and enterohaemorrhagic Escherichia coli: Tir, EspFU and actin pedestal assembly. *FEBS J,* 277**,** 2390-402.

CAMPELLONE, K. G. & WELCH, M. D. (2010) A nucleator arms race: cellular control of actin assembly. *Nat Rev Mol Cell Biol,* 11**,** 237-51.

CASTAGNA, M., TAKAI, Y., KAIBUCHI, K., SANO, K., KIKKAWA, U. & NISHIZUKA, Y. (1982) Direct activation of calcium-activated, phospholipid-dependent protein kinase by tumor-promoting phorbol esters. *J Biol Chem,* 257**,** 7847-51.

CASTRILLON, D. H. & WASSERMAN, S. A. (1994) Diaphanous is required for cytokinesis in Drosophila and shares domains of similarity with the products of the limb deformity gene. *Development,* 120**,** 3367-77.

CAZAUBON, S., BORNANCIN, F. & PARKER, P. J. (1994) Threonine-497 is a critical site for permissive activation of protein kinase C alpha. *Biochem J,* 301 (Pt 2)**,** 443-8.
CHALAMALASETTY, R. B., HUMMER, S., NIGG, E. A. & SILLJE, H. H. (2006) Influence of human Ect2 depletion and overexpression on cleavage furrow formation and abscission. *J Cell Sci,* 119**,** 3008-19.
CHEN, R. H., WATERS, J. C., SALMON, E. D. & MURRAY, A. W. (1996) Association of spindle assembly checkpoint component XMAD2 with unattached kinetochores. *Science,* 274**,** 242-6.
CHEN, Y., LAI, M., MAENO-HIKICHI, Y. & ZHANG, J. F. (2006) Essential role of the LIM domain in the formation of the PKCepsilon-ENH-N-type Ca2+ channel complex. *Cell Signal,* 18**,** 215-24.
COLLAZOS, A., DIOUF, B., GUERINEAU, N. C., QUITTAU-PREVOSTEL, C., PETER, M., COUDANE, F., HOLLANDE, F. & JOUBERT, D. (2006) A spatiotemporally coordinated cascade of protein kinase C activation controls isoform-selective translocation. *Mol Cell Biol,* 26**,** 2247-61.
COPELAND, J. W., COPELAND, S. J. & TREISMAN, R. (2004) Homo-oligomerization is essential for F-actin assembly by the formin family FH2 domain. *J Biol Chem,* 279**,** 50250-6.
CORBALAN-GARCIA, S., GARCIA-GARCIA, J., RODRIGUEZ-ALFARO, J. A. & GOMEZ-FERNANDEZ, J. C. (2003) A new phosphatidylinositol 4,5-bisphosphate-binding site located in the C2 domain of protein kinase Calpha. *J Biol Chem,* 278**,** 4972-80.
DALBY, K. N., MORRICE, N., CAUDWELL, F. B., AVRUCH, J. & COHEN, P. (1998) Identification of regulatory phosphorylation sites in mitogen-activated protein kinase (MAPK)-activated protein kinase-1a/p90rsk that are inducible by MAPK. *J Biol Chem,* 273**,** 1496-505.
DEAK, M., CLIFTON, A. D., LUCOCQ, L. M. & ALESSI, D. R. (1998) Mitogen- and stress-activated protein kinase-1 (MSK1) is directly activated by MAPK and SAPK2/p38, and may mediate activation of CREB. *EMBO J,* 17**,** 4426-41.
DOMINGUEZ, R. (2004) Actin-binding proteins--a unifying hypothesis. *Trends Biochem Sci,* 29**,** 572-8.
DOUGLAS, M. E., DAVIES, T., JOSEPH, N. & MISHIMA, M. (2010) Aurora B and 14-3-3 coordinately regulate clustering of centralspindlin during cytokinesis. *Curr Biol,* 20**,** 927-33.
DOUGLAS, M. E. & MISHIMA, M. (2010) Still entangled: assembly of the central spindle by multiple microtubule modulators. *Semin Cell Dev Biol,* 21**,** 899-908.
DRIES, D. R., GALLEGOS, L. L. & NEWTON, A. C. (2007) A single residue in the C1 domain sensitizes novel protein kinase C isoforms to cellular diacylglycerol production. *J Biol Chem,* 282**,** 826-30.
DURGAN, J., CAMERON, A. J., SAURIN, A. T., HANRAHAN, S., TOTTY, N., MESSING, R. O. & PARKER, P. J. (2008) The identification and characterization of novel PKCepsilon phosphorylation sites provide evidence for functional cross-talk within the PKC superfamily. *Biochem J,* 411**,** 319-31.
ECHARD, A., HICKSON, G. R., FOLEY, E. & O'FARRELL, P. H. (2004) Terminal cytokinesis events uncovered after an RNAi screen. *Curr Biol,* 14**,** 1685-93.

EDWARDS, A. S., FAUX, M. C., SCOTT, J. D. & NEWTON, A. C. (1999) Carboxyl-terminal phosphorylation regulates the function and subcellular localization of protein kinase C betaII. *J Biol Chem,* 274**,** 6461-8.
EGGERT, U. S., MITCHISON, T. J. & FIELD, C. M. (2006) Animal cytokinesis: from parts list to mechanisms. *Annu Rev Biochem,* 75**,** 543-66.
FIELD, C. M. & ALBERTS, B. M. (1995) Anillin, a contractile ring protein that cycles from the nucleus to the cell cortex. *J Cell Biol,* 131**,** 165-78.
FIRAT-KARALAR, E. N. & WELCH, M. D. (2011) New mechanisms and functions of actin nucleation. *Curr Opin Cell Biol,* 23**,** 4-13.
FRANKE, T. F., YANG, S. I., CHAN, T. O., DATTA, K., KAZLAUSKAS, A., MORRISON, D. K., KAPLAN, D. R. & TSICHLIS, P. N. (1995) The protein kinase encoded by the Akt proto-oncogene is a target of the PDGF-activated phosphatidylinositol 3-kinase. *Cell,* 81**,** 727-36.
FREELEY, M., KELLEHER, D. & LONG, A. (2011) Regulation of Protein Kinase C function by phosphorylation on conserved and non-conserved sites. *Cell Signal,* 23**,** 753-62.
FUJIWARA, T., BANDI, M., NITTA, M., IVANOVA, E. V., BRONSON, R. T. & PELLMAN, D. (2005) Cytokinesis failure generating tetraploids promotes tumorigenesis in p53-null cells. *Nature,* 437**,** 1043-7.
GAO, T., BROGNARD, J. & NEWTON, A. C. (2008) The phosphatase PHLPP controls the cellular levels of protein kinase C. *J Biol Chem,* 283**,** 6300-11.
GARRETT, M. D. & COLLINS, I. (2011) Anticancer therapy with checkpoint inhibitors: what, where and when? *Trends Pharmacol Sci,* 32**,** 308-16.
GERISCH, G., BRETSCHNEIDER, T., MULLER-TAUBENBERGER, A., SIMMETH, E., ECKE, M., DIEZ, S. & ANDERSON, K. (2004) Mobile actin clusters and traveling waves in cells recovering from actin depolymerization. *Biophys J,* 87**,** 3493-503.
GIANSANTI, M. G., BONACCORSI, S., WILLIAMS, B., WILLIAMS, E. V., SANTOLAMAZZA, C., GOLDBERG, M. L. & GATTI, M. (1998) Cooperative interactions between the central spindle and the contractile ring during Drosophila cytokinesis. *Genes Dev,* 12**,** 396-410.
GIORGIONE, J. R., LIN, J. H., MCCAMMON, J. A. & NEWTON, A. C. (2006) Increased membrane affinity of the C1 domain of protein kinase Cdelta compensates for the lack of involvement of its C2 domain in membrane recruitment. *J Biol Chem,* 281**,** 1660-9.
GLOTZER, M. (2004) Cleavage furrow positioning. *J Cell Biol,* 164**,** 347-51.
GLOTZER, M. (2005) The molecular requirements for cytokinesis. *Science,* 307**,** 1735-9.
GORIN, MA. & PAN, Q. (2009) Protein kinase Cε: an oncogene and emerging tumor biomarker. *Mol Cancer,* 8**,** 9-16.
GOULD, C. M., ANTAL, C. E., REYES, G., KUNKEL, M. T., ADAMS, R. A., ZIYAR, A., RIVEROS, T. & NEWTON, A. C. (2011) Active site inhibitors protect protein kinase C from dephosphorylation and stabilize its mature form. *J Biol Chem,* 286**,** 28922-30.
GRODSKY, N., LI, Y., BOUZIDA, D., LOVE, R., JENSEN, J., NODES, B., NONOMIYA, J. & GRANT, S. (2006) Structure of the catalytic domain of human protein kinase C beta II complexed with a bisindolylmaleimide inhibitor. *Biochemistry,* 45**,** 13970-81.

GUIZETTI, J. & GERLICH, D. W. (2010) Cytokinetic abscission in animal cells. *Semin Cell Dev Biol,* 21**,** 909-16.
HAN, D. C., RODRIGUEZ, L. G. & GUAN, J. L. (2001) Identification of a novel interaction between integrin beta1 and 14-3-3beta. *Oncogene,* 20**,** 346-57.
HANAHAN, D. & WEINBERG, R. A. (2000) The hallmarks of cancer. *Cell,* 100**,** 57-70.
HANAHAN, D. & WEINBERG, R. A. (2011) Hallmarks of cancer: the next generation. *Cell,* 144**,** 646-74.
HANKS, S. K. & HUNTER, T. (1995) Protein kinases 6. The eukaryotic protein kinase superfamily: kinase (catalytic) domain structure and classification. *FASEB J,* 9**,** 576-96.
HARBOUR, J. W. & DEAN, D. C. (2000) The Rb/E2F pathway: expanding roles and emerging paradigms. *Genes Dev,* 14**,** 2393-409.
HARBOUR, J. W., LUO, R. X., DEI SANTI, A., POSTIGO, A. A. & DEAN, D. C. (1999) Cdk phosphorylation triggers sequential intramolecular interactions that progressively block Rb functions as cells move through G1. *Cell,* 98**,** 859-69.
HARTWELL, L. H. & WEINERT, T. A. (1989) Checkpoints: controls that ensure the order of cell cycle events. *Science,* 246**,** 629-34.
HAUGE, C., ANTAL, T. L., HIRSCHBERG, D., DOEHN, U., THORUP, K., IDRISSOVA, L., HANSEN, K., JENSEN, O. N., JORGENSEN, T. J., BIONDI, R. M. & FRODIN, M. (2007) Mechanism for activation of the growth factor-activated AGC kinases by turn motif phosphorylation. *EMBO J,* 26**,** 2251-61.
HAZAN, R. B., KANG, L., ROE, S., BORGEN, P. I. & RIMM, D. L. (1997) Vinculin is associated with the E-cadherin adhesion complex. *J Biol Chem,* 272**,** 32448-53.
HEASMAN, S. J. & RIDLEY, A. J. (2008) Mammalian Rho GTPases: new insights into their functions from in vivo studies. *Nat Rev Mol Cell Biol,* 9**,** 690-701.
HERNANDEZ, R. M., WESCOTT, G. G., MAYHEW, M. W., MCJILTON, M. A. & TERRIAN, D. M. (2001) Biochemical and morphogenic effects of the interaction between protein kinase C-epsilon and actin in vitro and in cultured NIH3T3 cells. *J Cell Biochem,* 83**,** 532-46.
HERTZOG, M., VAN HEIJENOORT, C., DIDRY, D., GAUDIER, M., COUTANT, J., GIGANT, B., DIDELOT, G., PREAT, T., KNOSSOW, M., GUITTET, E. & CARLIER, M. F. (2004) The beta-thymosin/WH2 domain; structural basis for the switch from inhibition to promotion of actin assembly. *Cell,* 117**,** 611-23.
HIGGS, H. N. & PETERSON, K. J. (2005) Phylogenetic analysis of the formin homology 2 domain. *Mol Biol Cell,* 16**,** 1-13.
HILL, E., CLARKE, M. & BARR, F. A. (2000) The Rab6-binding kinesin, Rab6-KIFL, is required for cytokinesis. *EMBO J,* 19**,** 5711-9.
HINDS, P. W., MITTNACHT, S., DULIC, V., ARNOLD, A., REED, S. I. & WEINBERG, R. A. (1992) Regulation of retinoblastoma protein functions by ectopic expression of human cyclins. *Cell,* 70**,** 993-1006.
HOLLOWAY, S. L., GLOTZER, M., KING, R. W. & MURRAY, A. W. (1993) Anaphase is initiated by proteolysis rather than by the inactivation of maturation-promoting factor. *Cell,* 73**,** 1393-402.
HOUSE, C. & KEMP, B. E. (1987) Protein kinase C contains a pseudosubstrate prototope in its regulatory domain. *Science,* 238**,** 1726-8.

HURLEY, J. H., NEWTON, A. C., PARKER, P. J., BLUMBERG, P. M. & NISHIZUKA, Y. (1997) Taxonomy and function of C1 protein kinase C homology domains. *Protein Sci,* 6**,** 477-80.

IKENOUE, T., INOKI, K., YANG, Q., ZHOU, X. & GUAN, K. L. (2008) Essential function of TORC2 in PKC and Akt turn motif phosphorylation, maturation and signalling. *EMBO J,* 27**,** 1919-31.

JACINTO, E. & LORBERG, A. (2008) TOR regulation of AGC kinases in yeast and mammals. *Biochem J,* 410**,** 19-37.

KAITNA, S., MENDOZA, M., JANTSCH-PLUNGER, V. & GLOTZER, M. (2000) Incenp and an aurora-like kinase form a complex essential for chromosome segregation and efficient completion of cytokinesis. *Curr Biol,* 10**,** 1172-81.

KIKKAWA U, TAKAI Y, TANAKA Y, MIYAKE R , NISHIZUKA Y (1983) Protein kinase C as a possible receptor protein of tumor-promoting phorbol esters. *J Biol Chem,* 258**,** 11442-45.

KAMEI, T., MATOZAKI, T., SAKISAKA, T., KODAMA, A., YOKOYAMA, S., PENG, Y. F., NAKANO, K., TAKAISHI, K. & TAKAI, Y. (1999) Coendocytosis of cadherin and c-Met coupled to disruption of cell-cell adhesion in MDCK cells--regulation by Rho, Rac and Rab small G proteins. *Oncogene,* 18**,** 6776-84.

KIM, D. H., SARBASSOV, D. D., ALI, S. M., KING, J. E., LATEK, R. R., ERDJUMENT-BROMAGE, H., TEMPST, P. & SABATINI, D. M. (2002) mTOR interacts with raptor to form a nutrient-sensitive complex that signals to the cell growth machinery. *Cell,* 110**,** 163-75.

KIM, J. E., BILLADEAU, D. D. & CHEN, J. (2005) The tandem BRCT domains of Ect2 are required for both negative and positive regulation of Ect2 in cytokinesis. *J Biol Chem,* 280**,** 5733-9.

KIMURA, K., TSUJI, T., TAKADA, Y., MIKI, T. & NARUMIYA, S. (2000) Accumulation of GTP-bound RhoA during cytokinesis and a critical role of ECT2 in this accumulation. *J Biol Chem,* 275**,** 17233-6.

KING, R. W., JACKSON, P. K. & KIRSCHNER, M. W. (1994) Mitosis in transition. *Cell,* 79**,** 563-71.

KITAGAWA, M., MUKAI, H., SHIBATA, H. & ONO, Y. (1995) Purification and characterization of a fatty acid-activated protein kinase (PKN) from rat testis. *Biochem J,* 310 (Pt 2)**,** 657-64.

KNIGHTON, D. R., ZHENG, J. H., TEN EYCK, L. F., ASHFORD, V. A., XUONG, N. H., TAYLOR, S. S. & SOWADSKI, J. M. (1991) Crystal structure of the catalytic subunit of cyclic adenosine monophosphate-dependent protein kinase. *Science,* 253**,** 407-14.

KNUDSEN, K. A., SOLER, A. P., JOHNSON, K. R. & WHEELOCK, M. J. (1995) Interaction of alpha-actinin with the cadherin/catenin cell-cell adhesion complex via alpha-catenin. *J Cell Biol,* 130**,** 67-77.

KOBAYASHI, T. & COHEN, P. (1999) Activation of serum- and glucocorticoid-regulated protein kinase by agonists that activate phosphatidylinositide 3-kinase is mediated by 3-phosphoinositide-dependent protein kinase-1 (PDK1) and PDK2. *Biochem J,* 339 (Pt 2)**,** 319-28.

KOPS, G. J., WEAVER, B. A. & CLEVELAND, D. W. (2005) On the road to cancer: aneuploidy and the mitotic checkpoint. *Nat Rev Cancer,* 5**,** 773-85.

KOSAKO, H., YOSHIDA, T., MATSUMURA, F., ISHIZAKI, T., NARUMIYA, S. & INAGAKI, M. (2000) Rho-kinase/ROCK is involved in cytokinesis through the phosphorylation of myosin light chain and not ezrin/radixin/moesin proteins at the cleavage furrow. *Oncogene,* 19**,** 6059-64.

KOSTELECKY, B., SAURIN, A. T., PURKISS, A., PARKER, P. J. & MCDONALD, N. Q. (2009) Recognition of an intra-chain tandem 14-3-3 binding site within PKCepsilon. *EMBO Rep,* 10**,** 983-9.

LE, T. L., YAP, A. S. & STOW, J. L. (1999) Recycling of E-cadherin: a potential mechanism for regulating cadherin dynamics. *J Cell Biol,* 146**,** 219-32.

LEACH KL,JAMES ML, BLUMBERG PM. (1983) InCharacterization of a specific phorbol ester aporeceptor in mouse brain cytosol. *Proc Natl Acad Sci USA,* 80**,** 4208-12.

LEBRON, C., CHEN, L., GILKES, D. M. & CHEN, J. (2006) Regulation of MDMX nuclear import and degradation by Chk2 and 14-3-3. *EMBO J,* 25**,** 1196-206.

LEE, H. W., SMITH, L., PETTIT, G. R., VINITSKY, A. & SMITH, J. B. (1996) Ubiquitination of protein kinase C-alpha and degradation by the proteasome. *J Biol Chem,* 271**,** 20973-6.

LEWIS, J. E., JENSEN, P. J., JOHNSON, K. R. & WHEELOCK, M. J. (1994) E-cadherin mediates adherens junction organization through protein kinase C. *J Cell Sci,* 107 (Pt 12)**,** 3615-21.

LI, X. & NICKLAS, R. B. (1995) Mitotic forces control a cell-cycle checkpoint. *Nature,* 373**,** 630-2.

LI, Y. & BENEZRA, R. (1996) Identification of a human mitotic checkpoint gene: hsMAD2. *Science,* 274**,** 246-8.

LIU, Y., GRAHAM, C., LI, A., FISHER, R. J. & SHAW, S. (2002) Phosphorylation of the protein kinase C-theta activation loop and hydrophobic motif regulates its kinase activity, but only activation loop phosphorylation is critical to in vivo nuclear-factor-kappaB induction. *Biochem J,* 361**,** 255-65.

LO, M. C., GAY, F., ODOM, R., SHI, Y. & LIN, R. (2004) Phosphorylation by the beta-catenin/MAPK complex promotes 14-3-3-mediated nuclear export of TCF/POP-1 in signal-responsive cells in C. elegans. *Cell,* 117**,** 95-106.

LOUIS, K., GUERINEAU, N., FROMIGUE, O., DEFAMIE, V., COLLAZOS, A., ANGLARD, P., SHIPP, M. A., AUBERGER, P., JOUBERT, D. & MARI, B. (2005) Tumor cell-mediated induction of the stromal factor stromelysin-3 requires heterotypic cell contact-dependent activation of specific protein kinase C isoforms. *J Biol Chem,* 280**,** 1272-83.

LU, J., MENG, W., POY, F., MAITI, S., GOODE, B. L. & ECK, M. J. (2007) Structure of the FH2 domain of Daam1: implications for formin regulation of actin assembly. *J Mol Biol,* 369**,** 1258-69.

MACKAY, H. J. & TWELVES, C. J. (2007) Targeting the protein kinase C family: are we there yet? *Nat Rev Cancer,* 7**,** 554-62.

MADAULE, P., EDA, M., WATANABE, N., FUJISAWA, K., MATSUOKA, T., BITO, H., ISHIZAKI, T. & NARUMIYA, S. (1998) Role of citron kinase as a target of the small GTPase Rho in cytokinesis. *Nature,* 394**,** 491-4.

MANNING, G., PLOWMAN, G. D., HUNTER, T. & SUDARSANAM, S. (2002) Evolution of protein kinase signaling from yeast to man. *Trends Biochem Sci,* 27**,** 514-20.

MARTINEZ-GIMENO, C., DIAZ-MECO, MT., DOMINGUEZ, I., MOSCAT, J. (1995) Alterations in levels of different protein kinase C isotypes and their influence on behavior of squamous cell carcinoma of the oral cavity: epsilon PKC, a novel prognositc factor for relapse and survival. *Head Neck,* 17**,** 516-25.

MATSUSHIME, H., EWEN, M. E., STROM, D. K., KATO, J. Y., HANKS, S. K., ROUSSEL, M. F. & SHERR, C. J. (1992) Identification and properties of an atypical catalytic subunit (p34PSK-J3/cdk4) for mammalian D type G1 cyclins. *Cell,* 71**,** 323-34.

MELLOR, H. & PARKER, P. J. (1998) The extended protein kinase C superfamily. *Biochem J,* 332 (Pt 2)**,** 281-92.

MING, X. F., BURGERING, B. M., WENNSTROM, S., CLAESSON-WELSH, L., HELDIN, C. H., BOS, J. L., KOZMA, S. C. & THOMAS, G. (1994) Activation of p70/p85 S6 kinase by a pathway independent of p21ras. *Nature,* 371**,** 426-9.

MINOSHIMA, Y., KAWASHIMA, T., HIROSE, K., TONOZUKA, Y., KAWAJIRI, A., BAO, Y. C., DENG, X., TATSUKA, M., NARUMIYA, S., MAY, W. S., JR., NOSAKA, T., SEMBA, K., INOUE, T., SATOH, T., INAGAKI, M. & KITAMURA, T. (2003) Phosphorylation by aurora B converts MgcRacGAP to a RhoGAP during cytokinesis. *Dev Cell,* 4**,** 549-60.

MISCHAK, H., GOODNIGHT, JA., KOLCH, W., MARTINY-BARON, G., SHAECHTLE, C., KAZANIETZ, MG., BLUMBERG, PM., PIERCE, JH., MUSHINSKI, JF. (1993) Overexpression of protein kinase c-delta and -epsilon in NIH 3T3 cells induces opposite effects on growth, morphology and anchorage dependence and tumorigenicity. *J Bio Chem,* 268**,** 6090-96.

MISHIMA, M., KAITNA, S. & GLOTZER, M. (2002) Central spindle assembly and cytokinesis require a kinesin-like protein/RhoGAP complex with microtubule bundling activity. *Dev Cell,* 2**,** 41-54.

MISHIMA, M., PAVICIC, V., GRUNEBERG, U., NIGG, E. A. & GLOTZER, M. (2004) Cell cycle regulation of central spindle assembly. *Nature,* 430**,** 908-13.

MOLLINARI, C., KLEMAN, J. P., JIANG, W., SCHOEHN, G., HUNTER, T. & MARGOLIS, R. L. (2002) PRC1 is a microtubule binding and bundling protein essential to maintain the mitotic spindle midzone. *J Cell Biol,* 157**,** 1175-86.

MORRISON, D. K. (2009) The 14-3-3 proteins: integrators of diverse signaling cues that impact cell fate and cancer development. *Trends Cell Biol,* 19**,** 16-23.

MOSELEY, J. B., SAGOT, I., MANNING, A. L., XU, Y., ECK, M. J., PELLMAN, D. & GOODE, B. L. (2004) A conserved mechanism for Bni1- and mDia1-induced actin assembly and dual regulation of Bni1 by Bud6 and profilin. *Mol Biol Cell,* 15**,** 896-907.

NEWTON, A. C. (2009) Lipid activation of protein kinases. *J Lipid Res,* 50 Suppl**,** S266-71.

NIGG, E. A. (1995) Cyclin-dependent protein kinases: key regulators of the eukaryotic cell cycle. *Bioessays,* 17**,** 471-80.

NISHIMURA, Y. & YONEMURA, S. (2006) Centralspindlin regulates ECT2 and RhoA accumulation at the equatorial cortex during cytokinesis. *J Cell Sci,* 119**,** 104-14.

NISHITANI, H., LYGEROU, Z., NISHIMOTO, T. & NURSE, P. (2000) The Cdt1 protein is required to license DNA for replication in fission yeast. *Nature,* 404**,** 625-8.

OBSIL, T., GHIRLANDO, R., KLEIN, D. C., GANGULY, S. & DYDA, F. (2001) Crystal structure of the 14-3-3zeta:serotonin N-acetyltransferase complex. a role for scaffolding in enzyme regulation. *Cell,* 105**,** 257-67.

OCHOA, W. F., CORBALAN-GARCIA, S., ERITJA, R., RODRIGUEZ-ALFARO, J. A., GOMEZ-FERNANDEZ, J. C., FITA, I. & VERDAGUER, N. (2002) Additional binding sites for anionic phospholipids and calcium ions in the crystal structures of complexes of the C2 domain of protein kinase calpha. *J Mol Biol,* 320**,** 277-91.

OHTSUBO, M., THEODORAS, A. M., SCHUMACHER, J., ROBERTS, J. M. & PAGANO, M. (1995) Human cyclin E, a nuclear protein essential for the G1-to-S phase transition. *Mol Cell Biol,* 15**,** 2612-24.

ORR, J. W. & NEWTON, A. C. (1994) Requirement for negative charge on "activation loop" of protein kinase C. *J Biol Chem,* 269**,** 27715-8.

OZAWA, M., BARIBAULT, H. & KEMLER, R. (1989) The cytoplasmic domain of the cell adhesion molecule uvomorulin associates with three independent proteins structurally related in different species. *EMBO J,* 8**,** 1711-7.

PAGANO, M., PEPPERKOK, R., VERDE, F., ANSORGE, W. & DRAETTA, G. (1992) Cyclin A is required at two points in the human cell cycle. *EMBO J,* 11**,** 961-71.

PALMER, R. H., RIDDEN, J. & PARKER, P. J. (1994) Identification of multiple, novel, protein kinase C-related gene products. *FEBS Lett,* 356**,** 5-8.

PAN, Q., BAO, LW., KLEER, CG., SABEL, MS., GRIFFITH, KA., TEKNOS, TN., MERAJVER, S. (2005) Protein kinase C epsilon is a predictive biomarker of aggressive breast cancer and a validated target for RNA interference anticancer therapy. *Cancer Res,* 65**,** 8366-71.

PEARCE, L. R., HUANG, X., BOUDEAU, J., PAWLOWSKI, R., WULLSCHLEGER, S., DEAK, M., IBRAHIM, A. F., GOURLAY, R., MAGNUSON, M. A. & ALESSI, D. R. (2007) Identification of Protor as a novel Rictor-binding component of mTOR complex-2. *Biochem J,* 405**,** 513-22.

PEARCE, L. R., KOMANDER, D. & ALESSI, D. R. (2010) The nuts and bolts of AGC protein kinases. *Nat Rev Mol Cell Biol,* 11**,** 9-22.

PERLETTI, GP., FOLINI, M., LIN, HC., MISCHAK, H., PICCININI, F., TASHJIAN, AH. (1996) Overexpression of protein kinase C epsilon is oncogenic in rat colonic epithelial cells. *Oncogene,* 12**,** 847-54.

PETERSEN, B. O., LUKAS, J., SORENSEN, C. S., BARTEK, J. & HELIN, K. (1999) Phosphorylation of mammalian CDC6 by cyclin A/CDK2 regulates its subcellular localization. *EMBO J,* 18**,** 396-410.

PETRONCZKI, M., GLOTZER, M., KRAUT, N. & PETERS, J. M. (2007) Polo-like kinase 1 triggers the initiation of cytokinesis in human cells by promoting recruitment of the RhoGEF Ect2 to the central spindle. *Dev Cell,* 12**,** 713-25.

PINES, J. (2006) Mitosis: a matter of getting rid of the right protein at the right time. *Trends Cell Biol,* 16**,** 55-63.

PLANAS-SILVA, M. D. & WEINBERG, R. A. (1997) The restriction point and control of cell proliferation. *Curr Opin Cell Biol,* 9**,** 768-72.

PREKERIS, R., HERNANDEZ, R. M., MAYHEW, M. W., WHITE, M. K. & TERRIAN, D. M. (1998) Molecular analysis of the interactions between protein kinase C-epsilon and filamentous actin. *J Biol Chem,* 273**,** 26790-8.

PREKERIS, R., MAYHEW, M. W., COOPER, J. B. & TERRIAN, D. M. (1996) Identification and localization of an actin-binding motif that is unique to the epsilon isoform of protein kinase C and participates in the regulation of synaptic function. *J Cell Biol,* 132**,** 77-90.

PREVOSTEL, C., ALVARO, V., DE BOISVILLIERS, F., MARTIN, A., JAFFIOL, C. & JOUBERT, D. (1995) The natural protein kinase C alpha mutant is present in human thyroid neoplasms. *Oncogene,* 11**,** 669-74.

PROSPERI, E., SCOVASSI, A. I., STIVALA, L. A. & BIANCHI, L. (1994) Proliferating cell nuclear antigen bound to DNA synthesis sites: phosphorylation and association with cyclin D1 and cyclin A. *Exp Cell Res,* 215**,** 257-62.

QI, ZH., SONG, M., WALLACE, MJ., WANG, D., NEWTON, PM., McMAHON, T., CHOU, WH., ZHANG, C., SHOKAT, KM. (2007) Protein kinase C epsilon regulates GABAA receptor sensitivity to ethanol and benzodiazepines through phosphorylation of gamma 2 subunits . *J Biol Chem,* 282**,** 33052-63.

QUITTAU-PREVOSTEL, C., DELAUNAY, N., COLLAZOS, A., VALLENTIN, A. & JOUBERT, D. (2004) Targeting of PKCalpha and epsilon in the pituitary: a highly regulated mechanism involving a GD(E)E motif of the V3 region. *J Cell Sci,* 117**,** 63-72.

RAPPAPORT, R. (1961) Experiments concerning the cleavage stimulus in sand dollar eggs. *J Exp Zool,* 148**,** 81-9.

RIEDER, C. L., SCHULTZ, A., COLE, R. & SLUDER, G. (1994) Anaphase onset in vertebrate somatic cells is controlled by a checkpoint that monitors sister kinetochore attachment to the spindle. *J Cell Biol,* 127**,** 1301-10.

RIEDL, J., CREVENNA, A. H., KESSENBROCK, K., YU, J. H., NEUKIRCHEN, D., BISTA, M., BRADKE, F., JENNE, D., HOLAK, T. A., WERB, Z., SIXT, M. & WEDLICH-SOLDNER, R. (2008) Lifeact: a versatile marker to visualize F-actin. *Nat Methods,* 5**,** 605-7.

ROMERO, S., LE CLAINCHE, C., DIDRY, D., EGILE, C., PANTALONI, D. & CARLIER, M. F. (2004) Formin is a processive motor that requires profilin to accelerate actin assembly and associated ATP hydrolysis. *Cell,* 119**,** 419-29.

ROSSE, C., LINCH, M., KERMORGANT, S., CAMERON, A. J., BOECKELER, K. & PARKER, P. J. (2010) PKC and the control of localized signal dynamics. *Nat Rev Mol Cell Biol,* 11**,** 103-12.

ROUILLER, I., XU, X. P., AMANN, K. J., EGILE, C., NICKELL, S., NICASTRO, D., LI, R., POLLARD, T. D., VOLKMANN, N. & HANEIN, D. (2008) The structural basis of actin filament branching by the Arp2/3 complex. *J Cell Biol,* 180**,** 887-95.

SANTOCANALE, C. & DIFFLEY, J. F. (1996) ORC- and Cdc6-dependent complexes at active and inactive chromosomal replication origins in Saccharomyces cerevisiae. *EMBO J,* 15**,** 6671-9.

SAUL, D., FABIAN, L., FORER, A. & BRILL, J. A. (2004) Continuous phosphatidylinositol metabolism is required for cleavage of crane fly spermatocytes. *J Cell Sci,* 117**,** 3887-96.

SAURIN, A. T., DURGAN, J., CAMERON, A. J., FAISAL, A., MARBER, M. S. & PARKER, P. J. (2008) The regulated assembly of a PKCepsilon complex controls the completion of cytokinesis. *Nat Cell Biol,* 10**,** 891-901.

SHARIF, TR. & SHARIF, M. (1999) Overexpression of protein kinase C epsilon in astroglial brain tumor derived cell lines and primary tumor samples. *Int J Oncol,* 15**,** 237-43.
SIMON, G. C., SCHONTEICH, E., WU, C. C., PIEKNY, A., EKIERT, D., YU, X., GOULD, G. W., GLOTZER, M. & PREKERIS, R. (2008) Sequential Cyk-4 binding to ECT2 and FIP3 regulates cleavage furrow ingression and abscission during cytokinesis. *EMBO J,* 27**,** 1791-803.
SKOUFIAS, D. A., ANDREASSEN, P. R., LACROIX, F. B., WILSON, L. & MARGOLIS, R. L. (2001) Mammalian mad2 and bub1/bubR1 recognize distinct spindle-attachment and kinetochore-tension checkpoints. *Proc Natl Acad Sci U S A,* 98**,** 4492-7.
SOMMA, M. P., FASULO, B., CENCI, G., CUNDARI, E. & GATTI, M. (2002) Molecular dissection of cytokinesis by RNA interference in Drosophila cultured cells. *Mol Biol Cell,* 13**,** 2448-60.
STEIGEMANN, P. & GERLICH, D. W. (2009a) An evolutionary conserved checkpoint controls abscission timing. *Cell Cycle,* 8**,** 1814-5.
STEIGEMANN, P. & GERLICH, D. W. (2009b) Cytokinetic abscission: cellular dynamics at the midbody. *Trends Cell Biol,* 19**,** 606-16.
STEIGEMANN, P., WURZENBERGER, C., SCHMITZ, M. H., HELD, M., GUIZETTI, J., MAAR, S. & GERLICH, D. W. (2009) Aurora B-mediated abscission checkpoint protects against tetraploidization. *Cell,* 136**,** 473-84.
STEINBERG, S. F. (2008) Structural basis of protein kinase C isoform function. *Physiol Rev,* 88**,** 1341-78.
SURYADINATA, R., SADOWSKI, M. & SARCEVIC, B. (2010) Control of cell cycle progression by phosphorylation of cyclin-dependent kinase (CDK) substrates. *Biosci Rep,* 30**,** 243-55.
SUZUKI, A., AKIMOTO, K. & OHNO, S. (2003) Protein kinase C lambda/iota (PKClambda/iota): a PKC isotype essential for the development of multicellular organisms. *J Biochem,* 133**,** 9-16.
SWAN, K. A., SEVERSON, A. F., CARTER, J. C., MARTIN, P. R., SCHNABEL, H., SCHNABEL, R. & BOWERMAN, B. (1998) cyk-1: a C. elegans FH gene required for a late step in embryonic cytokinesis. *J Cell Sci,* 111 (Pt 14)**,** 2017-27.
TAKEICHI, M. (1991) Cadherin cell adhesion receptors as a morphogenetic regulator. *Science,* 251**,** 1451-5.
TANAKA, T., KNAPP, D. & NASMYTH, K. (1997) Loading of an Mcm protein onto DNA replication origins is regulated by Cdc6p and CDKs. *Cell,* 90**,** 649-60.
TATSUMOTO, T., XIE, X., BLUMENTHAL, R., OKAMOTO, I. & MIKI, T. (1999) Human ECT2 is an exchange factor for Rho GTPases, phosphorylated in G2/M phases, and involved in cytokinesis. *J Cell Biol,* 147**,** 921-8.
TAYLOR, S. S. & MCKEON, F. (1997) Kinetochore localization of murine Bub1 is required for normal mitotic timing and checkpoint response to spindle damage. *Cell,* 89**,** 727-35.
TAYLOR, W. E. & YOUNG, E. T. (1990) cAMP-dependent phosphorylation and inactivation of yeast transcription factor ADR1 does not affect DNA binding. *Proc Natl Acad Sci U S A,* 87**,** 4098-102.

UHLMANN, F., LOTTSPEICH, F. & NASMYTH, K. (1999) Sister-chromatid separation at anaphase onset is promoted by cleavage of the cohesin subunit Scc1. *Nature,* 400**,** 37-42.
VARGA, A., CZIFRA, G., TALLAI, B., NEMETH, T., KOVACS, I., KOVACS, L., BIRO, T. (2004) Tumor grade-dependent alterations in the protein kinase C isoform pattern in urinary bladder carcinomas. *Eur Urol,* 46**,** 462-65.
VAVYLONIS, D., KOVAR, D. R., O'SHAUGHNESSY, B. & POLLARD, T. D. (2006) Model of formin-associated actin filament elongation. *Mol Cell,* 21**,** 455-66.
WALCZAK, C. E., CAI, S. & KHODJAKOV, A. (2010) Mechanisms of chromosome behaviour during mitosis. *Nat Rev Mol Cell Biol,* 11**,** 91-102.
WANG, Y. L. (2005) The mechanism of cortical ingression during early cytokinesis: thinking beyond the contractile ring hypothesis. *Trends Cell Biol,* 15**,** 581-8.
WATANABE, S., ANDO, Y., YASUDA, S., HOSOYA, H., WATANABE, N., ISHIZAKI, T. & NARUMIYA, S. (2008) mDia2 induces the actin scaffold for the contractile ring and stabilizes its position during cytokinesis in NIH 3T3 cells. *Mol Biol Cell,* 19**,** 2328-38.
WATANABE, S., OKAWA, K., MIKI, T., SAKAMOTO, S., MORINAGA, T., SEGAWA, K., ARAKAWA, T., KINOSHITA, M., ISHIZAKI, T. & NARUMIYA, S. (2010) Rho and anillin-dependent control of mDia2 localization and function in cytokinesis. *Mol Biol Cell,* 21**,** 3193-204.
WAY, K. J., CHOU, E. & KING, G. L. (2000) Identification of PKC-isoform-specific biological actions using pharmacological approaches. *Trends Pharmacol Sci,* 21**,** 181-7.
WILSON, G. M., FIELDING, A. B., SIMON, G. C., YU, X., ANDREWS, P. D., HAMES, R. S., FREY, A. M., PEDEN, A. A., GOULD, G. W. & PREKERIS, R. (2005) The FIP3-Rab11 protein complex regulates recycling endosome targeting to the cleavage furrow during late cytokinesis. *Mol Biol Cell,* 16**,** 849-60.
WOLFE, B. A., TAKAKI, T., PETRONCZKI, M. & GLOTZER, M. (2009) Polo-like kinase 1 directs assembly of the HsCyk-4 RhoGAP/Ect2 RhoGEF complex to initiate cleavage furrow formation. *PLoS Biol,* 7**,** e1000110.
WONG, R., HADJIYANNI, I., WEI, H. C., POLEVOY, G., MCBRIDE, R., SEM, K. P. & BRILL, J. A. (2005) PIP2 hydrolysis and calcium release are required for cytokinesis in Drosophila spermatocytes. *Curr Biol,* 15**,** 1401-6.
WOO, R. A. & POON, R. Y. (2003) Cyclin-dependent kinases and S phase control in mammalian cells. *Cell Cycle,* 2**,** 316-24.
XU, Y., MOSELEY, J. B., SAGOT, I., POY, F., PELLMAN, D., GOODE, B. L. & ECK, M. J. (2004) Crystal structures of a Formin Homology-2 domain reveal a tethered dimer architecture. *Cell,* 116**,** 711-23.
YAFFE, M. B., RITTINGER, K., VOLINIA, S., CARON, P. R., AITKEN, A., LEFFERS, H., GAMBLIN, S. J., SMERDON, S. J. & CANTLEY, L. C. (1997) The structural basis for 14-3-3:phosphopeptide binding specificity. *Cell,* 91**,** 961-71.
YAMANAKA, T., HORIKOSHI, Y., SUZUKI, A., SUGIYAMA, Y., KITAMURA, K., MANIWA, R., NAGAI, Y., YAMASHITA, A., HIROSE, T., ISHIKAWA, H. & OHNO, S. (2001) PAR-6 regulates aPKC activity in a novel way and

mediates cell-cell contact-induced formation of the epithelial junctional complex. *Genes Cells,* 6**,** 721-31.
YANG, Q., INOKI, K., IKENOUE, T. & GUAN, K. L. (2006) Identification of Sin1 as an essential TORC2 component required for complex formation and kinase activity. *Genes Dev,* 20**,** 2820-32.
YU, H. (2007) Cdc20: a WD40 activator for a cell cycle degradation machine. *Mol Cell,* 27**,** 3-16.
YUCE, O., PIEKNY, A. & GLOTZER, M. (2005) An ECT2-centralspindlin complex regulates the localization and function of RhoA. *J Cell Biol,* 170**,** 571-82.
ZENG, X. R., HAO, H., JIANG, Y. & LEE, M. Y. (1994) Regulation of human DNA polymerase delta during the cell cycle. *J Biol Chem,* 269**,** 24027-33.
ZHANG, H. S., POSTIGO, A. A. & DEAN, D. C. (1999) Active transcriptional repression by the Rb-E2F complex mediates G1 arrest triggered by p16INK4a, TGFbeta, and contact inhibition. *Cell,* 97**,** 53-61.
ZHANG, J., WANG, L., SCHWARTZ, J., BOND, R. W. & BISHOP, W. R. (1994) Phosphorylation of Thr642 is an early event in the processing of newly synthesized protein kinase C beta 1 and is essential for its activation. *J Biol Chem,* 269**,** 19578-84.
ZIEGLER, W. H., PAREKH, D. B., LE GOOD, J. A., WHELAN, R. D., KELLY, J. J., FRECH, M., HEMMINGS, B. A. & PARKER, P. J. (1999) Rapamycin-sensitive phosphorylation of PKC on a carboxy-terminal site by an atypical PKC complex. *Curr Biol,* 9**,** 522-9.